

T-3258

FREQUENCY RESPONSE OF A GEOPHONE
CLAMPED TO A BOREHOLE

by

Gregory R. Johnson

ProQuest Number: 10782835

All rights reserved

INFORMATION TO ALL USERS

The quality of this reproduction is dependent upon the quality of the copy submitted.

In the unlikely event that the author did not send a complete manuscript and there are missing pages, these will be noted. Also, if material had to be removed, a note will indicate the deletion.



ProQuest 10782835

Published by ProQuest LLC (2018). Copyright of the Dissertation is held by the Author.

All rights reserved.

This work is protected against unauthorized copying under Title 17, United States Code
Microform Edition © ProQuest LLC.

ProQuest LLC.
789 East Eisenhower Parkway
P.O. Box 1346
Ann Arbor, MI 48106 – 1346

T-3258

A thesis submitted to the Faculty and the Board of Trustees of the Colorado School of Mines in partial fulfillment of the requirements for the degree of Master of Science in Geophysics.

Golden, Colorado

Date 4/23/86

Signed: Gregory R. Johnson
Gregory R. Johnson.

Approved: J. E. White
J. E. White,
Thesis Advisor.

Golden, Colorado

Date 7/25/86

Approved: Phillip R. Romig
Phillip R. Romig,
Department Chairman,
Geophysics.

ABSTRACT

The theoretical response characteristics of a VSP tool-formation coupling are derived in terms of the impedance of the tool-formation contact for vertical displacement of the tool. The ratio of geophone motion to earth motion, defined as frequency response, is computed for a model of a tool in contact around the entire borehole circumference, and for the more realistic model of a tool in contact along a thin vertical strip. The effect of fluids in the borehole is also examined. Rigid rocks (dense sandstones and carbonates) exhibit flat frequency response curves for the frequencies of interest in a conventional VSP survey. Softer lithologies (such as shales) exhibit response curves which are not uniform over the 10 to 200 hz range, and could cause distortion of VSP data at higher frequencies.

TABLE OF CONTENTS

| | <u>PAGE</u> |
|---|-------------|
| ABSTRACT | iii |
| TABLE OF CONTENTS | iv |
| LIST OF FIGURES | vi |
| LIST OF TABLES | ix |
| ACKNOWLEDGEMENTS | x |
| I. Introduction | 1 |
| II. Mathematical Formulation for the frequency response of a geophone clamped to a borehole | 5 |
| II.1 Model of a VSP tool | 5 |
| II.2 Response in terms of impedances | 8 |
| - Geophone in an empty borehole | 8 |
| - Geophone in a fluid-filled borehole | 10 |
| III. Mathematical solution for the impedance of the tool-formation contact | 17 |
| III.1 Mathematical solution for Model 1 | 17 |
| III.2 Mathematical solution for Model 2 | 25 |
| IV. Numerical integration of the solutions | 32 |
| IV.1 Integration over finite range | 32 |
| IV.2 Sampling of the source functions | 36 |
| IV.3 Nature of source function P_{zr} | 39 |
| IV.4 Scaling of impedances | 47 |
| IV.5 Source function for Model 2 | 48 |

| | <u>PAGE</u> |
|---|-------------|
| V. Preliminary Calculations | 53 |
| - displacement as a function of frequency . . | 57 |
| VI. Results | 62 |
| VI.1 Frequency response curves - Model 1 . . . | 64 |
| VI.2 Frequency response curves - Model 2 . . | 73 |
| - Empty borehole | 73 |
| - Fluid-filled borehole | 77 |
| - Borehole coupling | 87 |
| VII. Conclusions | 97 |
| REFERENCES | 100 |
| Appendix A - Expressions for coefficients D_{11} - D_{22} . | 104 |
| Appendix B - Fourier cosine series for θ dependence of displacement | 106 |
| Appendix C - Computation of the displacement correction factors | 109 |
| Appendix D - Fortran code of program "FRVSP" | 113 |

LIST OF FIGURES

| <u>FIGURE</u> | <u>PAGE</u> |
|--|-------------|
| 2-1 Schematic of an actual VSP tool. Idealized geometry for Model 2 | 6 |
| 2-2 Assumed geometry for Model 1 | 7 |
| 4-1 Idealized stress distributions in spatial and wavenumber domains for uniform stress distribution | 40 |
| 4-2 Realizable uniform stress pattern | 41 |
| 4-3 Idealized stress distributions in spatial and wavenumber domains for constant displacement of the tool | 43 |
| 4-4 Realizable stress distribution for constant displacement of the tool | 44 |
| 4-5 Source function P_{zr} in time and frequency domain | 46 |
| 4-6 θ dependence of source function P_{zr} | 50 |
| 5-1 Model 1 - SS1: displacement along tool for uniform stress distribution | 55 |
| 5-2 Model 1 - SS1: displacement along tool for HAT stress distribution | 56 |
| 5-3 Model 1 - Soft Rock: time dependence of input (P_{zr}) and output (displacement) | 58 |
| 5-4 Model 2 - Soft Rock: real and imaginary parts of displacement in frequency domain | 60 |
| 6-1 Model 1 - SS1: frequency response for scaled and unscaled values of impedances | 65 |
| 6-2 Model 1 - Soft Rock: frequency response for scaled and unscaled values of impedances | 66 |

| <u>FIGURE</u> | <u>PAGE</u> |
|---|-------------|
| 6-3 Model 1: Frequency response in an empty borehole for two different lithologies, SS1 and the Soft Rock | 68 |
| 6-4 Model 1 - Soft Rock: frequency response for tools with different lengths in an empty borehole | 69 |
| 6-5 Model 1 - Soft Rock: frequency response for tools with different lengths in a Mud-filled borehole | 70 |
| 6-6 Model 1 - Soft Rock: frequency response for tools with different masses in an empty borehole | 71 |
| 6-7 Model 1 - Soft Rock: frequency response for tools with different masses in a mud-filled borehole | 72 |
| 6-8 Model 2: frequency response for tool in in empty borehole in the Soft Rock and SS2 lithologies | 74 |
| 6-9 Model 2 - Soft Rock: frequency response for tools of varying masses in an empty borehole | 75 |
| 6-10 Model 2 - Soft Rock: frequency response for tools of varying lengths in an empty borehole | 76 |
| 6-11 Model 2 - Pierre Shale: frequency response in an empty and mud-filled borehole | 78 |
| 6-12 Model 2: frequency response in a mud-filled borehole for the Soft Rock and SS2 | 79 |
| 6-13 Model 2: frequency response in a mud-filled borehole for Pierre Shale and Soft Rock | 80 |
| 6-14 Model 2 - Soft Rock: magnitude and phase response for tool in a mud-filled borehole . . | 82 |

| <u>FIGURE</u> | <u>PAGE</u> |
|---|-------------|
| 6-15 Model 2 - Soft Rock: frequency response for tools of varying masses in a mud-filled borehole | 83 |
| 6-16 Model 2 - Carbonate: frequency response for tools of varying masses in a mud-filled borehole | 84 |
| 6-17 Model 2 - Soft Rock: frequency response tools of varying lengths in a mud-filled borehole | 85 |
| 6-18 Model 2 - SS2: frequency response for tools of varying lengths in a mud-filled borehole | 86 |
| 6-19 Model 2 - Soft Rock: frequency response with and without borehole coupling | 88 |
| 6-20 Model 2 - SS2: frequency response with and without borehole coupling | 89 |
| 6-21 Model 2 - Soft Rock - Borehole coupling: magnitude and phase response | 90 |
| 6-22 Model 2 - SS2 - Borehole coupling: frequency response for tools of different masses | 93 |
| 6-23 Model 2 - Soft Rock - Borehole coupling: frequency response for tools of different masses | 94 |
| 6-24 Model 2 - Soft Rock - Borehole coupling: frequency response for tools of different lengths | 95 |

LIST OF TABLES

| <u>TABLE</u> | | <u>PAGE</u> |
|--------------|---|-------------|
| 5-1 | Properties of elastic media modeled in this thesis | 61 |

ACKNOWLEDGEMENTS

I would like to take this opportunity to thank Drs. J. E. White, J. K. Cohen, and G. H. Towle for serving on my committee. In particular, I wish to express my sincerest appreciation and gratitude to my advisor, Dr. J. E. White, for his guidance, suggestions, and numerous discussions, which were invaluable throughout the course of this study.

I would also like to thank Peter Kaczkowski for his time and patience in answering my many questions on the topic of computer programming.

Finally, I would like to express my gratitude to the Borehole Geophysics Project for the financial support I received during my graduate studies at the Colorado School of Mines.

I. INTRODUCTION

Vertical seismic profiling (VSP) has only recently evolved as a viable tool in the oil industry. In a vertical seismic profile, a seismic source is located on the surface of the earth, as it is in a conventional (or horizontal) seismic profile. However, in a vertical seismic profile the seismic signal is recorded by a geophone clamped to the wall of a borehole, rather than on the surface. This difference in geometry allows both upgoing and downgoing seismic events to be recorded, and can result in a better understanding of seismic wave propagation within the earth. This, in turn, can provide a valuable insight into the interpretation of conventional (or surface) seismic recordings.

In any attempt to record a signal, the effect of the recording instruments on the signal must be taken into account. In seismic exploration the geophone is the first link in this recording system. Assuming the geophone accurately reproduces ground motion, the phase and amplitude response of the (electrical) recording system can be removed, and the resulting signal is an accurate representation of the ground motion. However, if the geophone does not move with the earth, the ground motion cannot accurately be recorded. It is this problem of mechanical geophone coupling that will be studied in this

thesis.

Washburn and Wiley (1941) performed experiments on the effect of the placement of a conventional (or surface) geophone on its response characteristics. They determined that the geophone and the ground formed a resonant system, and conducted studies on the amplitude response of this system. Wolf (1944) modeled this geophone ground coupling as a damped oscillatory system. He developed a mathematical model of this system dependent upon the area of contact of the geophone with the earth, the mass of the geophone, and the elastic moduli of the earth.

Hoover and O'Brien (1980) computed theoretical and experimental response curves for the vertical response of a conventional geophone plant. They concluded that a lightweight geophone with a large earth contact exhibits a resonance peak well above the frequency of interest for seismic exploration, provided that the geophone is planted in well consolidated soil. Krohn's (1984) experimental results indicated that the response of a conventional geophone is independent of the geophone mass or diameter, but is strongly dependent on the firmness of the soil in which it is planted. These studies have shown that for a conventional geophone plant, the resonance peak is generally located outside of the desired bandwidth of

seismic data, and therefore there is minimal distortion due to the geophone-ground coupling.

In vertical seismic profiling, however, the seismic signal is recorded inside of a borehole, and the geophone must necessarily be able to withstand the high temperatures and pressures present in such a hostile environment. This problem is solved by housing the geophone in a massive, rigid tool which can be secured to the borehole wall. The question then arises as to whether such a tool will accurately reproduce ground motion in the surrounding medium.

Levin and Lynn (1958) conducted deep seismic surveys with wall coupled geophones. They found that the use of wall coupled geophones greatly attenuated the borehole tube waves. McDonal (1958) published experimental frequency response curves for a geophone hydraulically clamped to the formation. Measured resonance peaks varied from 1200 to 2000 hz in Pierre shale. White (1962) calculated the effect of radiation damping and pressure gradients in the mud column on the response characteristics of a geophone clamped to a borehole. He concluded that geophone motion is significantly affected by these factors. Wuenschel (1976) used a downhole tool which was hydraulically clamped to the borehole to obtain frequency response curves for the

tool-formation contact. A theoretical treatment of the tool-formation coupling was carried out by Beydoun (1981), for a tool in contact around the entire circumference of the hole. He concluded that a small tool mass and a large area of contact of the tool with the formation will result in a resonant peak outside of the desired bandwidth of the data.

In this study, the theoretical response characteristics of a VSP tool-formation coupling are computed. The system response is derived for vertical displacement of the tool. A tool in contact around the circumference of the hole is treated first, including the damping effects of low frequency tube waves. The more realistic assumption of contact along a vertical strip is also examined. Numerical results are given for tools of various lengths and masses clamped in five different lithologies: two sandstones, a carbonate, the Pierre Shale, and a "soft" formation (low compressional and shear wave velocities).

II. Mathematical Formulation for the Frequency Response of a Geophone Clamped to a Borehole

II.1 Model of a VSP tool

The objective of this study is to determine the frequency response of a vertical seismic profiling tool-formation coupling. This will be accomplished by developing a model of such a tool clamped to the wall of a borehole.

Figure 2-1 shows a schematic of a VSP tool in a borehole. A tool of mass M is in contact with the formation along a vertical strip of length L_0 and width w . Figure 2-2 illustrates the assumed geometry of the first model. The model has the same length L_0 and mass M as an actual tool, but it is in contact with the formation around the entire circumference of the borehole. This assumed geometry greatly simplifies the mathematics involved in solving for the impedance of the tool-formation coupling (discussed in section III), and is therefore treated first.

The second model is identical to the clamped geophone shown in Figure 2-1. The treatment of this more realistic geometry results in a much more complicated expression for the impedance of the tool-formation coupling.

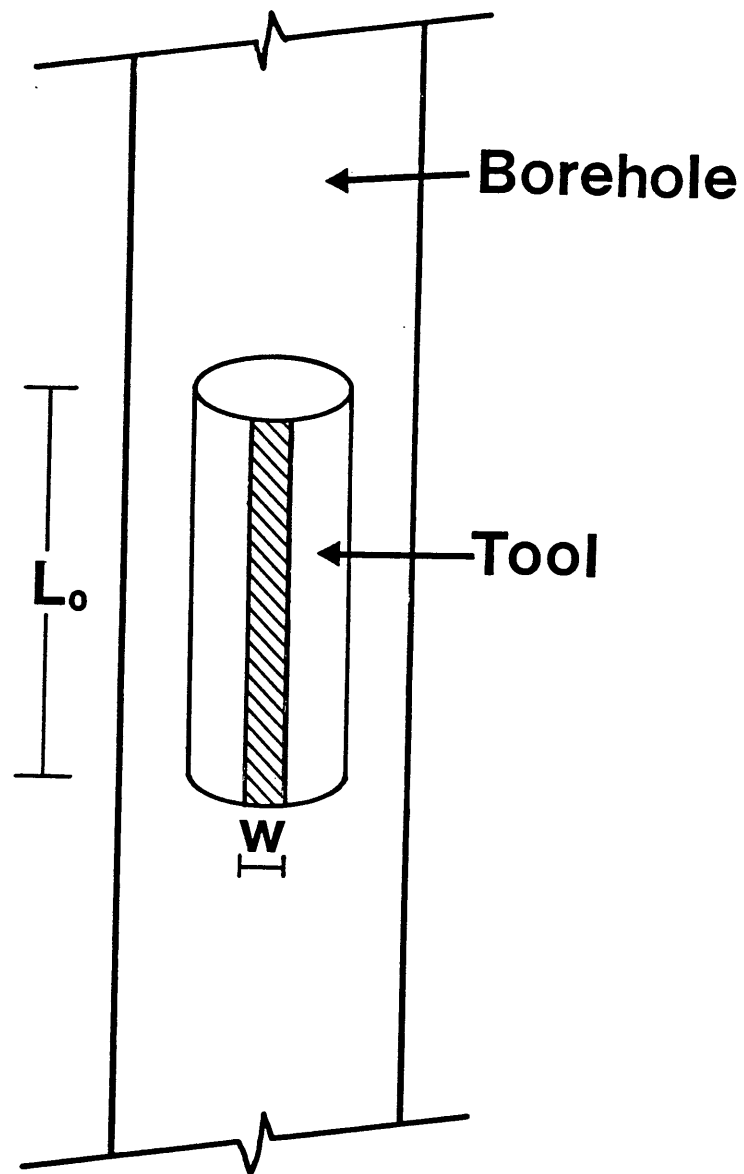


Figure 2-1.

Schematic of an actual V.S.P. tool of mass M , length L_0 , in contact with the formation over a width w . This is also the idealized geometry for Model 2.

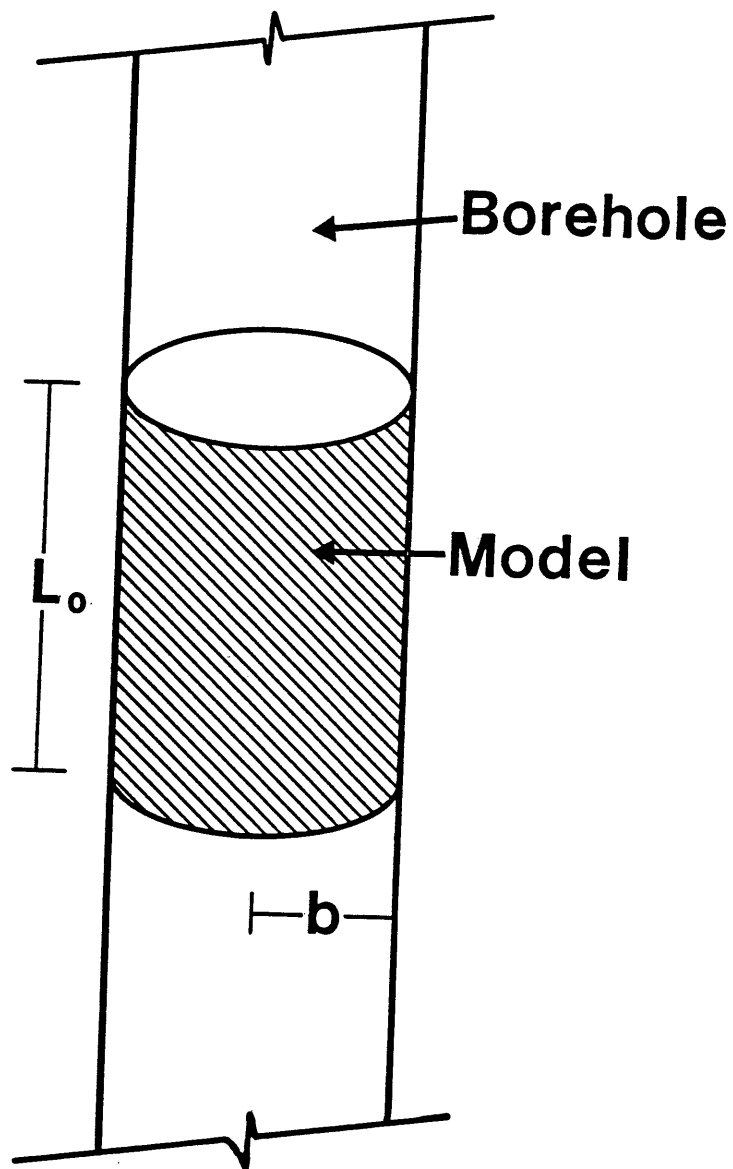


Figure 2-2

Assumed geometry for Model 1. A tool of mass M and length L_0 in contact around entire borehole circumference.

II.2 Response in Terms of Impedances

Geophone in an Empty Borehole

It seems well justified to model the geophone as a rigid body of mass M , small compared to all wavelengths. Over the area of contact with the formation, the particle velocity of the hole wall must be uniform and equal to that of the geophone, V_g . Integration of the stress which exists over the area of contact will yield the total force acting on the tool, F_s . With impedance defined as the ratio of force to velocity, we see that the wall impedance of the tool-formation coupling, Z_s , is given by:

$$Z_s = F_s / V_g. \quad (2-1)$$

Forces and particle velocity oscillate at angular frequency ω , and the quantities F_s and V_g are complex amplitudes multiplying $e^{i\omega t}$.

We are now faced with the problem of solving for the impedance of the tool-formation coupling due to a seismic wave in the surrounding formation. This is accomplished by use of the reciprocity relation stated by White (1960). This relation states that the coupling of a source and the coupling of a geophone to the surface of an inhomogeneous,

anisotropic, elastic medium are simply two aspects of the same situation. This can be exemplified in the following manner(after White (1960)): Assume that a rigid geophone is in contact with the formation over an area whose dimensions are small compared to wavelengths of interest. We are interested in the particle velocity of the geophone, V_g , due to the passage of a seismic wave which would create a particle velocity V_e if there were no geophone present. If the geophone were present, and if the motion of the geophone were somehow prevented, the seismic wave would exert a force, F_s , on the geophone. The ratio F_s/V_e is the impedance of the medium as a source acting through the area of contact with the tool. By use of the reciprocity relation, it is seen that this is the same impedance offered by the medium to a source acting through this same area of contact, and we therefore designate this the source impedance, Z_s . If the mechanical impedance of the geophone is Z_g , and no other forces act on the geophone, then the velocity of the geophone is:

$$V_g = \frac{F_s}{Z_g + Z_s} \quad (2-2)$$

Using $Z_s = F_s/V_e$ we find that:

$$V_g = \frac{V_e Z_s}{Z_g + Z_s} \quad (2-3)$$

In this terminology, the mechanical impedance due to the mass M of the geophone is $i\omega M$, and the velocity is then:

$$V_g = \frac{V_e Z_s}{i\omega M + Z_s} \quad (2-4)$$

If we define the frequency response of the tool-formation coupling as the ratio of geophone motion to earth motion when the geophone is not present, we see that:

$$\frac{V_g}{V_e} = \frac{Z_s}{i\omega M + Z_s} \quad (2-5)$$

Equation 2-5 governs the frequency response of a rigid tool clamped to the wall of an empty borehole.

Geophone in a Fluid-Filled Borehole

Additional considerations must be made if the geophone is in a fluid-filled borehole. The presence of the fluid will impede the motion of the geophone and cause a damping effect on its frequency response. We must also be concerned with the "borehole coupling" effect. Simply stated, this means that vertical motion of the earth due to the passage of a plane wave will set up pressures in the fluid, which will cause additional geophone motion. To accurately model the frequency response of a VSP tool, both of these effects must be taken into account.

We will first consider the impedance due to the presence of fluid in the borehole. As the geophone attempts to move with the surrounding medium due to the passage of a seismic wave, pressure waves (or tube waves) will be radiated in each direction within the fluid column. White (1983) gives the relation between pressure, P, and particle velocity, V, as:

$$P = \rho_f C_t V \quad (2-6)$$

where

ρ_f = density of the fluid

C_t = speed of tube waves in the borehole

C_t is given by:

$$C_t = [\rho_f (1/B + 1/\mu)]^{-1/2} \quad (2-7)$$

where

B = bulk modulus of the fluid, and

μ is the shear rigidity of the surrounding medium.

If it is assumed that the geophone blocks the borehole completely, the impedance due to the radiation of tube waves in each direction is given by :

$$Z_{f1} = 2\rho_f C_t \pi b^2 \quad (2-8)$$

If the tool does not completely block the borehole, we

simply substitute the area, A, that the tool occupies for πb^2 in the preceding discussion.

We see that the mechanical impedance of the geophone plus fluid is given by:

$$Z_g = i\omega M + 2\rho_f C_t A. \quad (2-9)$$

where A= area blocked by the geophone. This gives the velocity of a geophone clamped to the wall of a fluid-filled borehole as:

$$v_g = \frac{v_e Z_s}{i\omega M + 2\rho_f C_t A + Z_s}. \quad (2-10)$$

The ratio of geophone motion to earth motion is now given by

$$v_g/v_e = \frac{Z_s}{i\omega M + 2\rho_f C_t A + Z_s}. \quad (2-11)$$

There is one additional force acting on the geophone which must be considered. This is due to the " borehole coupling " effect, which refers to the pressure and axial motion created in a fluid-filled borehole as a result of elastic wave propagation in the surrounding medium. An

approximate theory of borehole coupling is treated by White (1983), under the assumption that all wavelengths are large compared with the borehole diameter. This is a valid assumption for the frequencies of interest in a vertical seismic profile.

If the vertical motion of the earth is due to the passage of a plane wave, then pressures set up in the fluid will act upon the geophone. White showed that the pressure generated in a fluid-filled borehole due to the passage of a plane compressional wave parallel to the borehole axis is:

$$P(z, \omega) e^{i\omega(t-z/\alpha)} = RN_0 e^{i\omega(t-z/\alpha)} \quad (2-12)$$

where

$$R = \frac{-\rho_f C_t^2 [1 - 2(\beta/\alpha)^2]}{\mu [1 - (C_t/\alpha)^2]} \quad (2-13)$$

β = speed of shear waves in the solid,

α = speed of compressional waves in the solid, and

$N_0 e^{i\omega(t-z/\alpha)}$ = stress in solid due to a seismic wave.

All other quantities are as defined earlier.

We will now make the assumption that the pressure gradient which exists in a fluid filled borehole with no geophone present is the same as that which exists when the

geophone is present. This is obviously an invalid assumption for Model 1, but is considered to be a good approximation for Model 2. Therefore, the borehole coupling effect will only be considered for Model 2.

Since the tool is short compared to the wavelengths of interest, the derivative of the pressure function with respect to the z axis, multiplied by the length of the tool L_0 , will yield the pressure difference across the tool. The short length of the tool also allows us to ignore the small phase delay due to the difference in time, Δt , of the pressure pulses acting on the opposite ends of the tool. The magnitude of the pressure gradient across the tool then becomes

$$-L_0 Ri\omega/\alpha N_0 \quad (2-14)$$

The force acting on the geophone due to the borehole coupling effect, F_{bc} , is simply

$$F_{bc} = -N_0 A L_0 Ri\omega/\alpha \quad (2-15)$$

where A is the area blocked off by the tool.

The velocity of the geophone due to this borehole coupling effect is given by the ratio of the borehole coupling force, F_{bc} , to the total impedance of the geophone, Z, which yields:

$$V_g = \frac{F_{bc}}{Z} = \frac{-(i\omega/\alpha)AL_0RN_0}{2A\rho_f C_t + Z_s + i\omega M}. \quad (2-16)$$

By adding the velocity of the geophone due to the motion of the borehole wall (given in equation 2-10) to the velocity due to the borehole coupling effect (given in equation 2-16) we find that:

$$V_g = \frac{-(i\omega/\alpha)AL_0RN_0 + V_e Z_s}{2A\rho_f C_t + Z_s + i\omega M}. \quad (2-17)$$

With the definition of geophone frequency response as the ratio of geophone motion to earth motion we have:

$$\frac{V_g}{V_e} = \frac{-(1/V_e)(i\omega/\alpha)AL_0RN_0 + Z_s}{2A\rho_f C_t + Z_s + i\omega M}. \quad (2-18)$$

The ratio of stress to particle velocity in an elastic medium is given by White (1983) as

$$N_0/V_e = -\rho/\alpha \quad (2-19)$$

Where ρ = density of the surrounding medium.

Equation (2-18) then becomes:

$$\frac{V_g}{V_e} = \frac{Z_s i\omega\rho AL_0R + Z_s}{2A\rho_f C_t + Z_s + i\omega M}. \quad (2-20)$$

The above expression yields the response of a clamped geophone in terms of a wall impedance Z_g . The following section provides a means of computing Z_g for both models discussed in section II.1.

III. Mathematical Solution for the Impedance of the Tool-Formation Contact.

We are now faced with the problem of solving for the impedance of the tool-formation contact. This will be accomplished by computing the impedance of the tool acting as a source through the area of contact with the formation. By applying the reciprocity relation, we know that this is the same impedance as that encountered by the formation acting as a source through this same area of contact with the tool. This impedance can then be entered into equations 2-5, 2-11, and 2-20 to compute the frequency response of the tool.

III.1 Mathematical Solution for Model 1

The following discussion is based on a paper by White (1984) .

Model 1, as seen in figure 2-2, is of a tool in positive contact around the entire circumference of the borehole. This assumed geometry greatly simplifies the mathematical treatment of the problem. Due to the axial symmetry of the problem, cylindrical coordinates (r, θ, z) will be used, where the z axis runs parallel to the borehole axis. For this first model, all quantities are

assumed independent of theta (θ), and the solution is therefore limited to waves with axial symmetry.

The wave equation will be solved by a Fourier inversion technique, for displacement in the z direction, designated u_z , and displacement in the r direction, designated u_r . Equations of motion in terms of these displacements are

$$(\lambda+2\mu)\left[\frac{\partial^2 u_r}{\partial r^2} + \frac{1}{r}\frac{\partial u_r}{\partial r} - \frac{u_r}{r^2}\right] + \frac{\mu\partial^2 u_r}{\partial z^2} + (\lambda+2\mu)\frac{\partial^2 u_z}{\partial r\partial z} = \frac{\rho\partial^2 u_r}{\partial t^2} \quad (3-1)$$

$$(\lambda+2\mu)\frac{\partial^2 u_z}{\partial z^2} + \mu\left[\frac{\partial^2 u_z}{\partial r^2} + \frac{1}{r}\frac{\partial u_z}{\partial r}\right] + (\lambda+\mu)\left[\frac{\partial^2 u_r}{\partial r\partial z} + \frac{1}{r}\frac{\partial u_r}{\partial z}\right] = \rho\frac{\partial^2 u_z}{\partial t^2} \quad (3-2)$$

where

λ = Lamé constant for the formation

ρ = density of the formation

μ = shear rigidity of the formation

t = time.

Displacements satisfying the equations of motion can be expressed in terms of a scalar potential ϕ and one component of a vector potential ψ :

$$\phi(r, z, t) = [1/(2\pi)^2] \int \int A(\ell, \omega) K_0(Mr) e^{i\ell z} e^{i\omega t} d\ell d\omega \quad (3-3)$$

$$\psi(r, z, t) = [1/(2\pi)^2] \int \int B(\ell, \omega) K_1(Kr) e^{i\ell z} e^{i\omega t} d\ell d\omega \quad (3-4)$$

where

$$M^2 = (\ell^2 - \omega^2/\alpha^2), \text{ and } \alpha^2 = (\lambda + 2\mu)/\rho \quad (3-5)$$

$$K^2 = (\ell^2 - \omega^2/\beta^2), \text{ and } \beta^2 = \mu/\rho \quad (3-6)$$

(M and K are either real or pure imaginary)

ℓ = axial wavenumber (z axis)

K_n = modified Bessel function of order n

A and B are coefficients which may be functions of ℓ and ω

All other variables are as defined earlier.

The potentials ϕ and ψ may exist together. and they represent a source on the borehole wall, radiating outward. The potentials are exponential functions of wavenumber ℓ and frequency ω . The entire solution to the problem is the sum of all possible solutions, and is expressed here as a double Fourier transform. It is important to recognize that every stress and displacement can be expressed as a double Fourier transform. We will adopt the convention that capital letters indicate a function in the transform (ℓ, ω) domain, and small letters in the temporal and spatial (z, t) domain. Thus, in the wavenumber-frequency domain we have:

$$\phi(r, \ell, \omega) = A(\ell, \omega)K_0(Mr) \quad (3-7)$$

$$\psi(r, \ell, \omega) = B(\ell, \omega)K_1(Kr) \quad (3-8)$$

The displacements u_r and u_z satisfy the equations of motion if they are derived from the potentials ϕ and ψ as follows:

$$u_r = \frac{\partial \phi}{\partial r} - \frac{\partial \psi}{\partial z} \quad (3-9) \quad u_z = \frac{\partial \phi}{\partial z} + \frac{\partial \psi}{\partial r} + \frac{\psi}{r} \quad (3-10)$$

By expressing stress and strains on the borehole wall in terms of displacements, White (1984) showed that

$$D_{11}A(\ell, \omega) + D_{12}B(\ell, \omega) = P_{rr} \quad (3-11)$$

$$D_{21}A(\ell, \omega) + D_{22}B(\ell, \omega) = P_{zr} \quad (3-12)$$

where

$$D_{11} = [(\lambda + 2\mu)M^2 - \lambda\ell^2]K_0(Mb) + (2\mu M/b)K_1(Mb) \quad (3-13)$$

$$D_{12} = 2\mu[i\ell K K_0(Kb) + (i\ell/b)K_1(Kb)] \quad (3-14)$$

$$D_{21} = -2i\ell M K_1(Mb) \quad (3-15)$$

$$D_{22} = (\ell^2 + K^2)K_1(Kb) \quad (3-16)$$

P_{rr} = normal stress in (ℓ, ω) domain

P_{zr} = tangential stress in (ℓ, ω) domain.

If the stresses P_{rr} and P_{zr} are known, or in this case, assumed, these equations can then be solved for the coefficients A and B. In this study, we will assume that the displacement of the tool is due to a shear stress acting parallel to the borehole axis, i.e. P_{zr} , and that the normal stress, P_{rr} , is zero. This yields:

$$D_{11}A(\ell, \omega) + D_{12}B(\ell, \omega) = 0 \quad (3-17)$$

$$D_{21}A(\ell, \omega) + D_{22}B(\ell, \omega) = P_{zr} \quad (3-18)$$

Solving for A and B yields:

$$A(\ell, \omega) = \frac{-P_{zr} D_{12}}{D_{11}D_{22} - D_{21}D_{12}} \quad (3-19)$$

$$B(\ell, \omega) = \frac{P_{zr} D_{11}}{D_{11}D_{22} - D_{21}D_{12}} \quad (3-20)$$

Once the coefficients A and B are known, the radial and axial displacements can be obtained from equations 3-9 and 3-10. In the transform domain, the displacements u_r and u_z become:

$$U_r(r, \ell, \omega) = -MA(\ell, \omega)W_1(Mr) - i\ell B(\ell, \omega)W_1(Kr) \quad (3-21)$$

$$U_z(r, \ell, \omega) = i\ell A(\ell, \omega) W_0(Mr) - KB(\ell, \omega) W_0(Kr) \quad (3-22)$$

where

$$W_1(Mr) = K_1(Mr) \text{ if } M \text{ is real, or} \quad (3-23)$$

$$W_1(Mr) = -\pi/2 [J_1(Mr) - iY_1(Mr)] \text{ if } M \text{ is pure imaginary,}$$

and

$$W_0(Mr) = K_0(Mr) \text{ if } M \text{ is real, or} \quad (3-24)$$

$$W_0(Mr) = -i\pi/2 [J_0(Mr) - iY_0(Mr)] \text{ if } M \text{ is pure imaginary,}$$

and similarly for Kr in place of Mr.

Here,

\bar{M} = imaginary part of M if M is pure imaginary

K_n = modified Bessel function of order n

J_n = Bessel function of the first kind of order n

Y_n = Bessel function of the second kind of order n

i = imaginary number $(-1)^{1/2}$.

To obtain the displacement in the temporal and spatial domain, we simply perform the integration as indicated below:

$$u_z(r, z, t) = [1/(2\pi)^2] \int_{-\infty}^{\infty} \int_{-\infty}^{\infty} U_z(r, \ell, \omega) e^{i\ell z} e^{i\omega t} d\ell d\omega \quad (3-25)$$

and similarly for u_r .

The source function P_{zr} and the method of numerical integration are discussed in section IV. We now turn our attention to the calculation of the impedance of the tool-formation contact.

We are interested in the impedance of the tool-formation contact as a function of frequency. If the integration indicated in equation 3-25 is only carried out in the wavenumber domain, the result will be $\bar{U}_z(r, z, \omega)$, where the bar indicates the result is in neither the (z, t) domain nor the (k, ω) domain. Though we have been designating \bar{U}_r as displacement, the program used to compute \bar{U}_r will give \bar{U}_r in units of displacement/force. A simple derivative in the frequency domain gives:

$$V = i\omega T \quad (3-26)$$

where

V = velocity

and T = displacement.

We also know that

$$\bar{U} = T/F_s. \quad (3-27)$$

Here, F_s is the force acting on the formation through the area of contact with the tool, and is obtained by integrating the stress pattern which exists over the area

of contact of the tool with the formation. By combining our definition of impedance given in equation 2-1, with equations 3-26 and 3-27, we find that the impedance of the tool-formation contact is given by

$$Z_g = 1/(i\omega\bar{U}) \quad (3-28)$$

This value of impedance can now be used to calculate the frequency response for our first model in an empty hole, and in a fluid-filled hole, as defined in equations 2-5 and 2-10, respectively.

III.2 Mathematical Solution for Model 2

The following discussion is based on a paper by Tongtaow (1982).

Model 2 is of a tool in positive contact with the borehole along a thin strip of width w and length L_0 , as shown in figure 2-1. We will again use cylindrical coordinates (r, θ, z) , but we can no longer assume that all quantities are independent of the azimuthal angle θ . This will result in more complicated expressions for the displacement functions.

Once again, the wave equation is solved by a Fourier inversion technique. We will solve for the three components of displacement u_r , u_z , and u_θ . With the inclusion of dependence on the azimuthal angle θ , the equations of motion in terms of particle displacement for an isotropic solid become:

$$\begin{aligned}
 (\lambda + 2\mu) \left[\frac{\partial^2 u_r}{\partial r^2} + \frac{1}{r} \frac{\partial u_r}{\partial r} - \frac{u_r}{r^2} - \frac{1}{r^2} \frac{\partial u_\theta}{\partial \theta} \right] + (\lambda + \mu) \left[-\frac{1}{r} \frac{\partial^2 u_\theta}{\partial r \partial \theta} + \frac{\partial^2 u_z}{\partial z \partial r} \right] \\
 + \mu \left[-\frac{1}{r^2} \frac{\partial^2 u_r}{\partial \theta^2} - \frac{1}{r^2} \frac{\partial u_\theta}{\partial \theta} + \frac{\partial^2 u_r}{\partial z^2} \right] = \rho \frac{\partial^2 u_r}{\partial t^2} \quad (3-29)
 \end{aligned}$$

$$\begin{aligned}
& (\lambda + 2\mu) \left[\frac{1}{r^2} \frac{\partial u_r}{\partial \theta} + \frac{1}{r^2} \frac{\partial^2 u_\theta}{\partial \theta^2} + \frac{1}{r} \frac{\partial^2 u_r}{\partial r \partial \theta} \right] + (\lambda + \mu) \left[-\frac{1}{r} \frac{\partial^2 u_z}{\partial r \partial \theta} \right] \\
& + \mu \left[\frac{\partial^2 u_\theta}{\partial r^2} + \frac{1}{r} \frac{\partial u_\theta}{\partial r} - \frac{u_\theta}{r^2} + \frac{1}{r^2} \frac{\partial u_r}{\partial \theta} - \frac{1}{r} \frac{\partial^2 u_r}{\partial r \partial \theta} + \frac{\partial^2 u_\theta}{\partial z^2} \right] = \rho \frac{\partial^2 u_\theta}{\partial t^2}
\end{aligned}
\tag{3-30}$$

$$\begin{aligned}
& (\lambda + 2\mu) \frac{\partial^2 u_z}{\partial z^2} + \lambda \left[\frac{\partial^2 u_r}{\partial z \partial r} + \frac{1}{r} \frac{\partial^2 u_\theta}{\partial z \partial \theta} + \frac{1}{r} \frac{\partial u_r}{\partial z} \right] \\
& + \mu \left[\frac{\partial^2 u_z}{\partial r^2} + \frac{1}{r} \frac{\partial u_z}{\partial r} + \frac{1}{r^2} \frac{\partial^2 u_z}{\partial \theta^2} + \frac{\partial^2 u_r}{\partial r \partial z} + \frac{1}{r} \frac{\partial u_r}{\partial z} + \frac{1}{r} \frac{\partial^2 u_\theta}{\partial \theta \partial z} \right] \\
& = \rho \frac{\partial^2 u_z}{\partial t^2}
\end{aligned}
\tag{3-31}$$

Three potentials, ϕ , χ , and γ are needed to solve these equations of motion. These potentials are given by:

$$\begin{aligned}
\phi(r, \theta, z, t) = \sum_{n=-\infty}^{\infty} \left[\frac{1}{(2\pi)^2} \right] \int_{-\infty}^{\infty} \int_{-\infty}^{\infty} A(l, \omega) K_n(Mr) e^{ilz} e^{i\omega t} \\
\cos(n\theta) dl d\omega
\end{aligned}
\tag{3-32}$$

$$\begin{aligned}
\chi(r, \theta, z, t) = \sum_{n=-\infty}^{\infty} \left[\frac{1}{(2\pi)^2} \right] \int_{-\infty}^{\infty} \int_{-\infty}^{\infty} C(l, \omega) K_n(Kr) e^{ilz} e^{i\omega t} \\
\sin(n\theta) dl d\omega
\end{aligned}
\tag{3-33}$$

$$\gamma(r, \theta, z, t) = \sum_{n=-\infty}^{\infty} \left[\frac{1}{(2\pi)^2} \right] \int_{-\infty}^{\infty} \int_{-\infty}^{\infty} B(\lambda, \omega) K_n(Mr) e^{i\lambda z} e^{i\omega t} \cos(n\theta) d\lambda d\omega \quad (3-34)$$

where

n is an integer or zero

A , B , and C are coefficients which may be functions of λ and ω .

All other variables are as defined earlier.

In this study, the summation with respect to n will be carried out from zero to ten. This will allow us to develop a model where the displacement of the tool is constant over its area of contact with the formation. This will be discussed in detail in section IV.

The three components of displacement satisfy the equations of motion if they are given by:

$$u_r = \frac{\partial \phi}{\partial r} + \frac{1}{r} \frac{\partial \chi}{\partial \theta} + \frac{\partial^2 \gamma}{\partial r \partial z} \quad (3-35)$$

$$u_\theta = \frac{1}{r} \frac{\partial \phi}{\partial \theta} - \frac{\partial \chi}{\partial r} + \frac{1}{r} \frac{\partial^2 \gamma}{\partial \theta \partial z} \quad (3-36)$$

$$u_z = \frac{\partial \phi}{\partial z} - \frac{\partial^2 \gamma}{\partial r^2} - \frac{1}{r} \frac{\partial \gamma}{\partial r} - \frac{1}{r^2} \frac{\partial^2 \gamma}{\partial \theta^2} \quad (3-37)$$

By expressing stresses and strains on the borehole wall in terms of displacements, Tongtaow (1982) showed that:

$$[D_{11}A(\ell, \omega) + D_{12}C(\ell, \omega) + D_{13}B(\ell, \omega)]\cos(n\theta) = P_{rr} \quad (3-38)$$

$$[D_{21}A(\ell, \omega) + D_{22}C(\ell, \omega) + D_{23}B(\ell, \omega)]\sin(n\theta) = P_{r\theta} \quad (3-39)$$

$$[D_{31}A(\ell, \omega) + D_{32}C(\ell, \omega) + D_{33}B(\ell, \omega)]\cos(n\theta) = P_{zr} \quad (3-40)$$

where

$P_{r\theta}$ is tangential stress in the theta direction

P_{rr} and P_{zr} are as defined in section III.1

The coefficients $D_{11} - D_{33}$ are lengthy expressions involving Bessel functions and are given in appendix A.

If the displacement of the geophone is due to a shear stress acting parallel to the borehole axis, (P_{zr}), and all other stresses are zero, we find that:

$$A(\ell, \omega) = \frac{P_{zr}(D_{12}D_{23} - D_{13}D_{22})}{\Delta} \quad (3-41)$$

$$B(\ell, \omega) = \frac{P_{zr}(D_{21}D_{13} - D_{11}D_{23})}{\Delta} \quad (3-42)$$

$$C(\lambda, \omega) = \frac{P_{zr} (D_{11}D_{22} - D_{12}D_{21})}{\Delta} \quad (3-43)$$

where

$$\Delta = D_{11}D_{22}D_{33} + D_{12}D_{23}D_{33} + D_{13}D_{21}D_{32} \\ - [D_{11}D_{32}D_{23} + D_{33}D_{12}D_{21} + D_{13}D_{22}D_{31}] \quad (3-44)$$

With the coefficients A, B, and C known, the displacements u_r , u_z , and u_θ can be obtained from equations 3-35 to 3-37. In the transform domain, we have:

$$U_r(r, \theta, \lambda, \omega) = \{ -M[W_{n-1}(Mb) + (n/Mb)W_n(Mb)]A(\lambda, \omega) + \\ (n/b)W_n(Kb)C(\lambda, \omega) - i\lambda K[W_{n-1}(Kb) + (n/Kb)W_n(Kb)]B(\lambda, \omega) \} \cos(n\theta) \quad (3-45)$$

$$U_\theta(r, \theta, \lambda, \omega) = \{ (-n/b)W_n(Mb)A(\lambda, \omega) + \\ K[W_{n-1}(Kb) + (n/Kb)W_n(Kb)]C(\lambda, \omega) - \\ (i\lambda n/b)W_n(Kb)B(\lambda, \omega) \} \sin(n\theta) \quad (3-46)$$

$$U_z(r, \theta, \lambda, \omega) = \{ i\lambda W_n(Mb)A(\lambda, \omega) - K^2 W_n(Kb)B(\lambda, \omega) \} \cos(n\theta) \quad (3-47)$$

The expressions for $W_{n-1}(\arg)$ and $W_n(\arg)$ are given in appendix A.

If the displacements are desired in the spatial and temporal domain, the summation and integration indicated below are performed.

$$u_z(r, \theta, z, t) = \sum_{n=-\infty}^{\infty} [1/(2\pi)^2] \int_{-\infty}^{\infty} \int_{-\infty}^{\infty} U_z e^{i\ell z} e^{i\omega t} d\ell d\omega \cos(n\theta) \quad (3-48)$$

and similarly for u_r and u_θ , except $\sin(n\theta)$ is substituted for $\cos(n\theta)$ in the case of u_θ .

We now wish to use the calculated value of U_z to determine the impedance of the tool-formation contact as a function of frequency. Integration over wavenumber ℓ and summation over n is performed, yielding $\bar{U}_z(r, \theta, z, \omega)$. Recall that the units on the computed value of \bar{U}_z are displacement/force. Following the same procedure discussed in section III.1, the impedance of the tool-formation contact, Z_s , is:

$$Z_s = 1/(i\omega \bar{U}_z) \quad (3-49)$$

We can now compute frequency response curves for our model of a geophone in contact with the formation along a thin strip of width w and length L_0 in an empty borehole

and in a fluid-filled borehole, by means of equations 2-5, 2-11, and 2-20. The source function, P_{zr} , and the method of numerical integration are discussed in the following section.

IV. Numerical Integration of the Solutions

IV.1 Integration over finite range

The solutions for displacement obtained in section III have limits of integration from $-\infty$ to $+\infty$. Therefore, to perform the integration digitally on a computer, the source function P_{zr} must be band limited in both frequency and wavenumber. The source function P_{zr} is chosen to be zero above some maximum value of axial wavenumber l_{max} , and if the displacement is desired in the time domain, P_{zr} must be zero outside some limited bandwidth in angular frequency ω . In this study, we are primarily interested in the displacement at the borehole wall as a function of frequency, or $\bar{U}_z(b, \theta, z, \omega)$. With a source that is band limited in wavenumber l , and omitting the integration over ω , equation (3-25) becomes

$$\bar{U}_z(b, z, \omega) = [1/(2\pi)] \int_{-l_{max}}^{l_{max}} U_z(b, l, \omega) e^{ilz} dl \quad (4-1)$$

for displacement at the borehole wall, where $r = b$.

This value for \bar{U}_z will be used in equation (3-28) to compute Z_g .

If the displacement is desired in the time domain, the source function must be band limited in angular frequency

ω , and this is expressed as:

$$u_z(b, z, t) = [1/(2\pi)^2] \int_{-\omega_{\max}}^{\omega_{\max}} \int_{-l_{\max}}^{l_{\max}} U_z(b, l, \omega) e^{ilz} e^{i\omega t} dl d\omega \quad (4-2)$$

The integration indicated in equation (3-48) can be curtailed in the same manner. However, the complete solutions for Model 2 necessitate a summation over the variable n from $-\infty$ to $+\infty$. This summation will be limited by using a source function which only consists of the terms from n equal zero to ten. With a source that is band limited in the axial wavenumber domain, and again omitting the integration over ω , equation (3-48) for Model 2 becomes:

$$\bar{U}_z(b, \theta, z, \omega) = \sum_{n=-10}^{10} [1/(2\pi)] \int_{-l_{\max}}^{l_{\max}} U_z(b, \theta, l, \omega) e^{ilz} dl \cos(n\theta) \quad (4-3)$$

This value of \bar{U}_z will be entered in equation (3-49) to compute the impedance of the tool-formation contact, Z_s .

For displacement in the time domain, we have:

$$U_z(b, \theta, z, t) = \sum_{n=10}^{10} [1/(2\pi)^2] \int_{-\omega_{\max}}^{\omega_{\max}} \int_{-l_{\max}}^{l_{\max}} U_z(b, \theta, l, \omega) e^{ilz} e^{i\omega t} dl d\omega \cos(n\theta) \quad (4-4)$$

The source function P_{zr} is the assumed pattern of tangential stress on the borehole wall. With our assumption that the tool is rigid, a stress pattern which results in a uniform displacement throughout the length of the tool is required. In the transform domain, the source function is expressed as

$$P_{zr} = -[Q/(2\pi b)]G(\lambda)F(\omega) \quad (4-5)$$

for Model 1, and

$$P_{zr} = -[Q/(2\pi b)]G(\lambda)F(\omega)\cos(n\theta) \quad (4-6)$$

for Model 2.

Q has the units of force, and is the magnitude of the force; $G(\lambda)$ is the source function in the wavenumber domain; $F(\omega)$ is the source function in the frequency domain. The displacement U_z is an even function of axial wavenumber λ for both Model 1 and 2. The source function $G(\lambda)$, discussed in section IV.3, is also an even function of λ , and the integration over wavenumber in equations (4-1) and (4-2) can therefore be written as

$$U_z(b, z, \omega) = [2/(2\pi)] \int_0^{\lambda_{\max}} U_z(b, \lambda, \omega) \cos(\lambda z) d\lambda \quad (4-7)$$

and

$$u_z(b, z, t) = [2/(2\pi)^2] \int_{-\omega_{\max}}^{\omega_{\max}} \int_0^{\ell_{\max}} U_z(b, \ell, \omega) \cos(\ell z) e^{i\omega t} d\ell d\omega$$

(4-8)

Equations (4-3) and (4-4) can be modified in the same manner.

IV.2 Sampling of the source functions

To perform the integration indicated in the preceding discussion on a digital computer, the functions must be computed at discrete values $k\Delta l$ and $I\Delta\omega$. This is achieved by multiplying the source function P_{zr} by the Dirac fences

$$k=-\alpha \sum^{\alpha} \delta(l - k\Delta l)\Delta l \quad (4-9)$$

and

$$I=-\alpha \sum^{\alpha} \delta(\omega - I\Delta\omega)\Delta\omega \quad (4-10)$$

The Fourier transforms of these functions are given by White(1983) as

$$k=-\alpha \sum^{\alpha} \delta(z - 2\pi k/\Delta l) \quad (4-11)$$

and

$$I=-\alpha \sum^{\alpha} \delta(t - 2\pi I/\Delta\omega) \quad (4-12)$$

Multiplication of the source by the Dirac fences in the wavenumber-frequency domain corresponds to convolution in the time and space domain with the Fourier transforms of these functions, given by equations (4-11) and (4-12). The effect of this sampling process is to add an infinite

array of "ghost" sources spaced at $2\pi/\Delta l$ along the z axis, and repeating in time at the rate $2\pi/\Delta\omega$.

Since the source function is band limited in wavenumber and frequency, the summation from $-\infty$ to $+\infty$ in equations (4-9) and (4-10) becomes

$$k=-k_{\max} \sum^k_{k_{\max}} \delta(l - k\Delta l)\Delta l \quad (4-13)$$

$$I=-I_{\max} \sum^I_{I_{\max}} \delta(\omega - I\Delta\omega)\Delta\omega \quad (4-14)$$

After multiplying by the Dirac fences, and band limiting the source functions, the integration in equations (4-1) and (4-3) becomes

$$\begin{aligned} \bar{U}_z(b, z, \omega) &= (\Delta l/2\pi) U_z(b, 0, \omega) + \\ & (\Delta l/\pi) \sum_{k=1}^{k_{\max}} U_z(b, k\Delta l, \omega) \cos(k\Delta l z) \end{aligned} \quad (4-15)$$

For Model 1, and

$$\begin{aligned} \bar{U}_z(b, \theta, z, \omega) &= \sum_{n=-10}^{10} \{ (\Delta l/2\pi) U_z(b, n, 0, \omega) + \\ & (\Delta l/\pi) \sum_{k=1}^{k_{\max}} U_z(b, n, k\Delta l, \omega) \cos(k\Delta l z) \} \cos(n\theta) \end{aligned} \quad (4-16)$$

for Model 2.

The numerical integration indicated above is used to compute the impedance of the tool-formation contact as a function of frequency. For displacements in the time domain, the displacements must be entirely real to have any physical meaning. This necessitates that the source and solutions have symmetric (even) real parts and anti-symmetric (odd) imaginary parts in the frequency domain. Therefore, the solutions need only be computed for the positive values of frequency, and the negative values set equal to the complex conjugate of the positive values. When these Fourier coefficients are transformed to the time domain, the result is a physically realizable (i.e., entirely real) function of time.

The numerical integration is accomplished by summation over wavenumber k at each frequency, as shown in equations (4-15) and (4-16). The inverse transform to the time domain, which corresponds to summation over frequency ω , is performed by a Fast Fourier Transform program.

IV.3 Nature of source function P_{zr}

To solve for the displacements, the tangential stress on the borehole wall, P_{zr} , must be specified. Equation (4-5) gives the source function in the transform domain as the product of $G(\lambda)$ and $F(\omega)$. The desired stress pattern will ideally result in constant displacement throughout the length of the tool.

The initial spatial stress distribution used was a boxcar, assuming that the stress across the tool is constant. The representation of a boxcar in the transform domain is the sinc function, defined by:

$$G(\lambda) = \{ \sin(\pi\lambda/\lambda_0) \} / (\pi\lambda/\lambda_0) \text{ for } |\lambda| < \lambda_{\max} \quad (4-17)$$

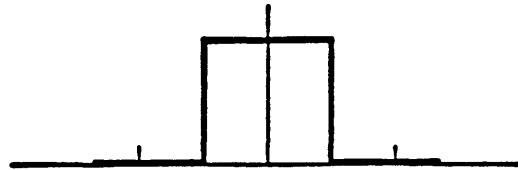
where

$$\lambda_0 = 2\pi/L_0$$

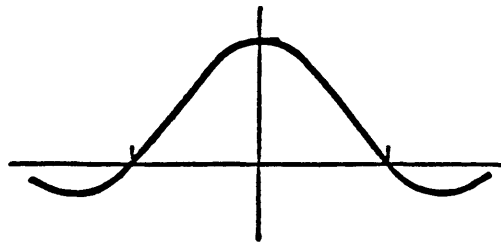
L_0 = length of the geophone.

$G(\lambda)$ is normalized to make the area under $g(z)$ equal to unity.

Idealized stress distributions in the wavenumber and spatial domains are shown in Figure 4-1. As a result of summation over a finite range of wavenumber λ , the idealized spatial stress pattern (boxcar) was achieved



Stress distribution $g(z)$ in spatial domain.



Stress distribution $G(\ell)$ in wavenumber domain.

Figure 4-1

Idealized stress distributions for boxcar and sinc function in the spatial and wavenumber domains, respectively.

Stress along Tool

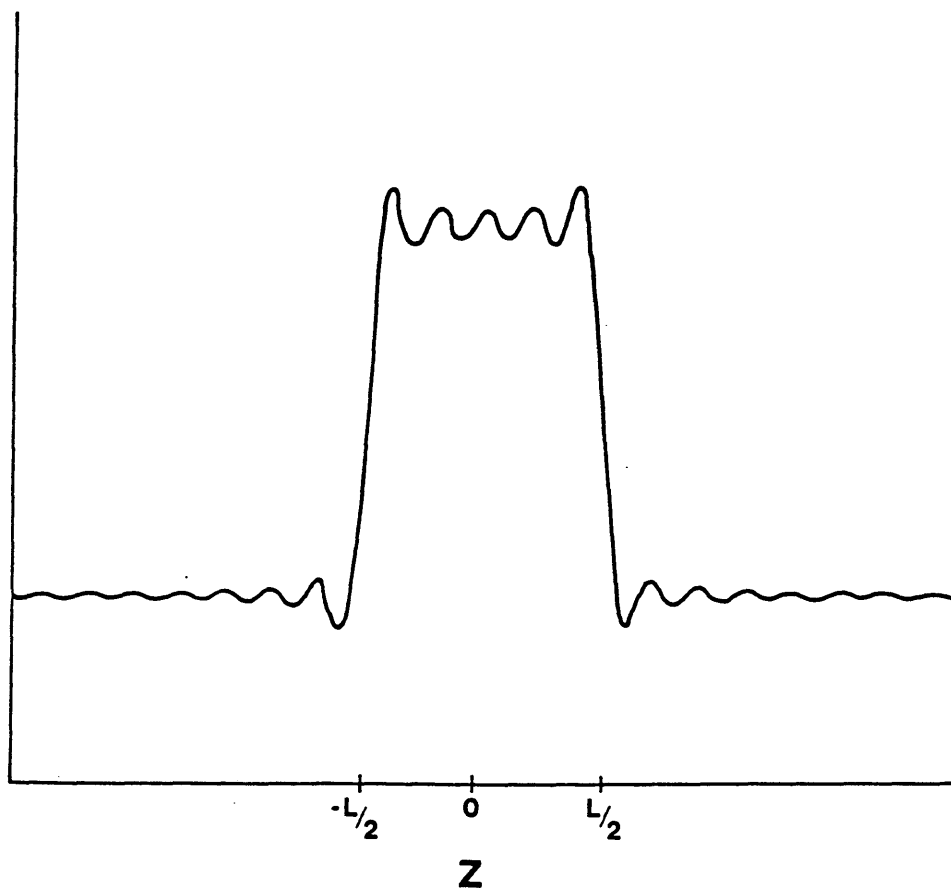


Figure 4-2

Actual spatial stress distribution obtained for boxcar.

only approximately, as seen in figure 4-2.

It was found that this stress pattern did not produce constant displacements throughout the length of the tool, and thus invalidated the assumption that the tool be rigid. The displacements were greater near the center of the tool, and tapered off at both ends. Thus it seemed logical that a stress pattern which reaches a maximum at the ends of the tool and a minimum in the center would produce a more constant displacement throughout the length of the tool.

The idealized stress patterns that were chosen are shown in figure 4-3. Once again, $G(\xi)$ is normalized to make the area under $g(z)$ equal to one. The analytical expression for $G(\xi)$ is

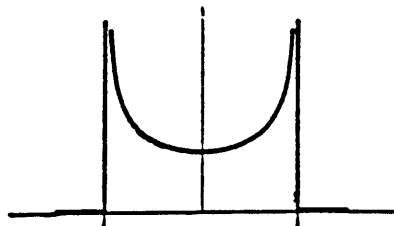
$$G(\xi) = J_0\{ (L_0/2)\xi \} \quad \text{for } |\xi| < \xi_{\max} \quad (4-18)$$

where

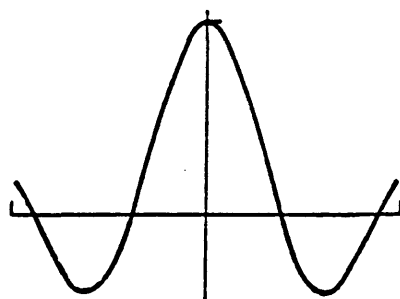
$$J_0 = \text{Bessel function of zero order.}$$

Figure 4-4 shows the actual stress pattern in the spatial domain. As in the previous example, the idealized spatial stress pattern is achieved only approximately, due to the finite range in wavenumber ξ .

When computing the impedance of the tool-formation contact as a function of frequency, the summation over ω is



Stress distribution $g(z)$ in spatial domain.



Stress distribution $G(\lambda)$ in wavenumber domain.

Figure 4-3

Idealized stress distributions in spatial and wavenumber domain for higher at ends (HAT) stress pattern.

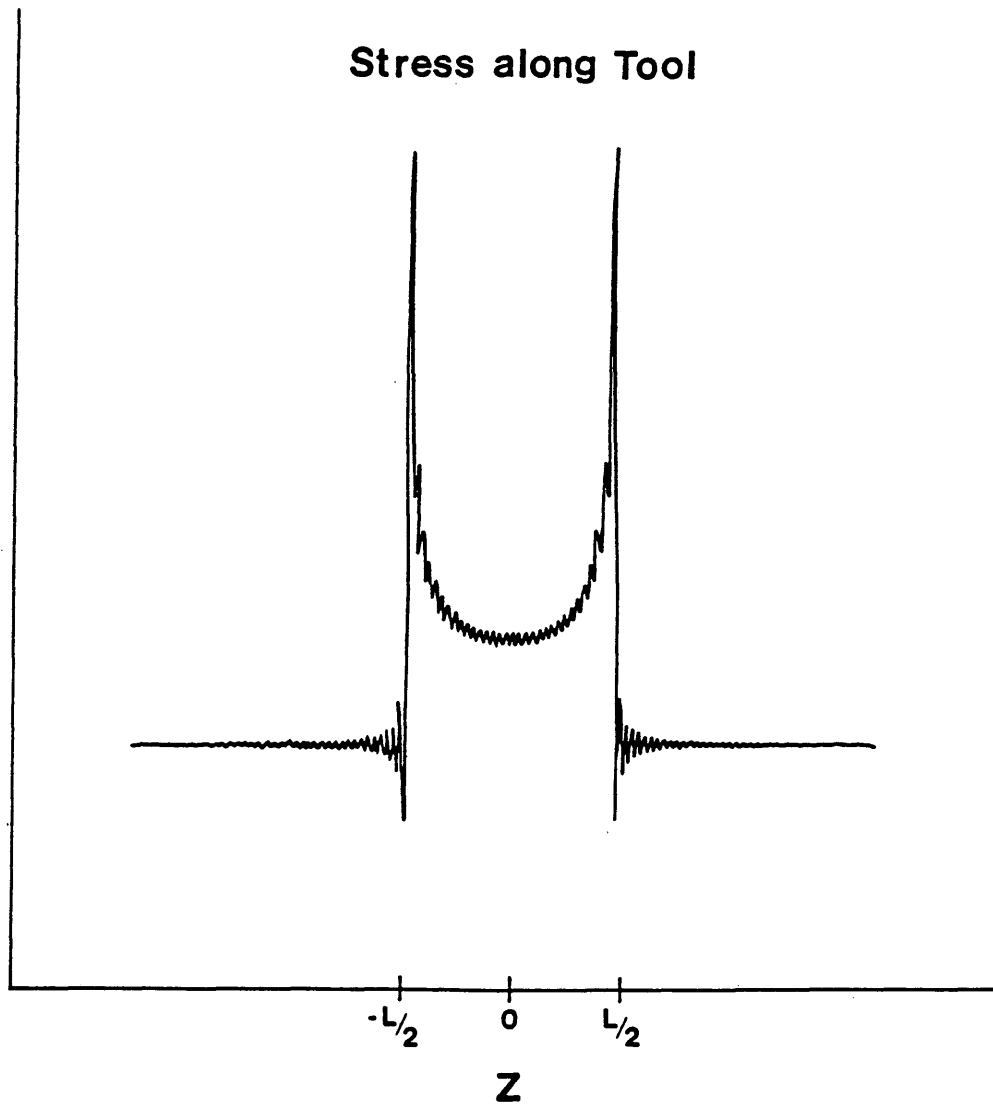


Figure 4-4

Actual spatial stress pattern obtained for higher at ends
(HAT) stress pattern.

omitted, and $F(\omega)$ is set equal to unity. However, when the response of the tool is computed in the time domain, $F(\omega)$ will be defined as

$$F(\omega) = \frac{\pi^2 \sin\{ \pi(\omega - \omega_0)/\omega_c \}}{2\omega_c [\text{Si}(\pi)] \pi\{(\omega - \omega_0)/\omega_c\}} \quad \text{for } (\omega_0 - \omega_c) < \omega < (\omega_0 + \omega_c)$$

(4-19)

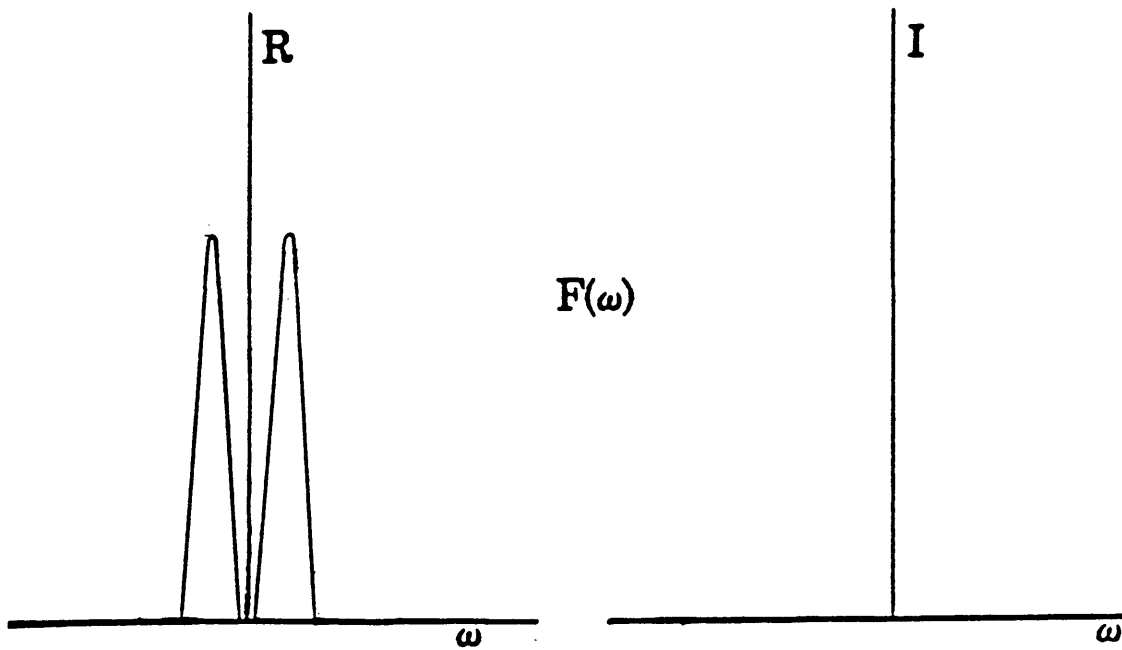
For reference, $\text{Si}(\pi) \approx 1.8516$

This source function is an even function of frequency and is normalized to make the peak at $t = 0$ unity. The source function as a function of time and frequency is shown in Figure 4-5.

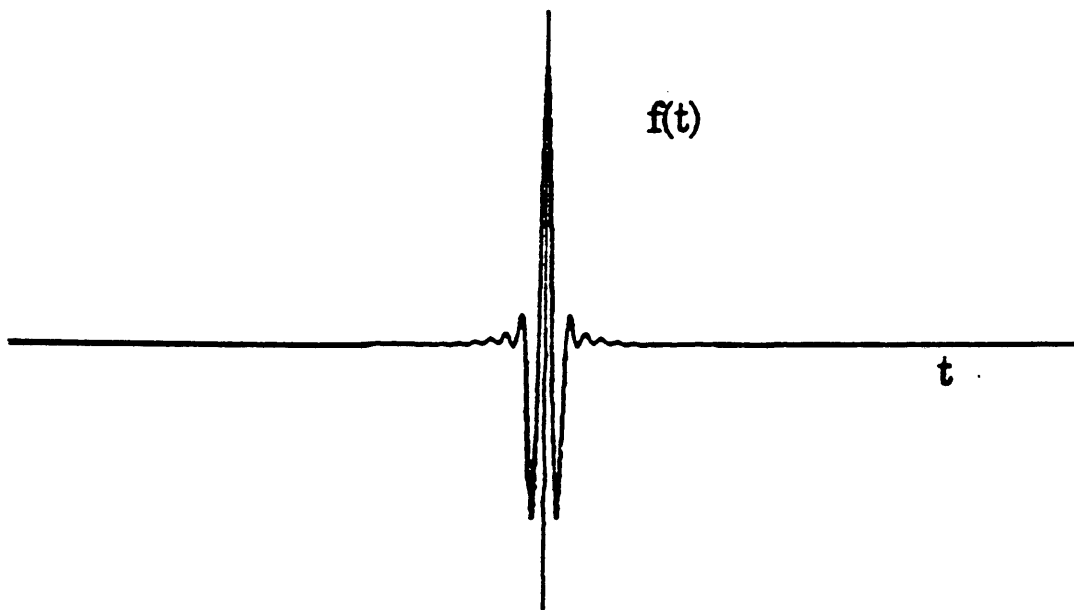
For Model 1, the tangential stress in the time domain is

$$p_{zr}(b, z, t) = -Q[g(z)f(t)]/(2\pi b) \quad (4-20)$$

$g(z)$ is normalized so that the area under the curve is unity, and it has units of meter⁻¹. $f(t)$ is dimensionless and has a peak of unity at $t=0$. Thus, Q has the units of force, and is the magnitude of the force.



Source function in the frequency domain.



Source function in the time domain.

Figure 4-5

Source function as a function of time and frequency.

IV.4 Scaling of Impedances

Frequency response curves for Model 1 were found to exhibit very mild resonant peaks at unreasonably large frequencies. This can probably be attributed to the overly simplified geometry of the model, in that the tool is in contact around the entire borehole circumference. To make an attempt at correcting for this simplified geometry, the assumption is made that the impedance of the tool-formation contact is proportional to the area of contact of the tool with the formation. With the length and mass of the tool unchanged, the calculated impedance is scaled by the factor $w/(2\pi b)$, and the frequency response curves are computed with this scaled value of impedance. The validity of this assumption can be evaluated by comparing frequency response curves computed with this scaled impedance to those computed with Model 2 (tool in contact along thin vertical strip).

IV.5 Source function for Model 2

The source term for Model 2 is identical to that of Model 1, except that it is multiplied by the term $\cos(n\theta)$. This dependence on azimuthal angle (θ) makes it possible to develop a model of a tool in contact with the formation over a length L_0 and along a thin vertical strip of width w .

In order to model the tool shown in figure 2-1, the displacement of the tool must be constant over the length L_0 and width w of the tool. Equation (4-18) describes a stress pattern which results in uniform displacement along the z axis. The method of obtaining uniform displacements over a strip of width w is now discussed.

For a typical borehole radius of ten centimeters and a tool radius of five centimeters, a width of contact w of six centimeters is not unreasonable. The desired displacement is uniform over the angle w/b radians. For the dimensions just mentioned this is .6 radians, or approximately 34.4 degrees.

As mentioned in the previous section, the summation over the variable n will only be carried out from n equal zero to ten. This is a purely economic constraint, since the computer time required to compute the displacements is directly proportional to the variable n .

The actual theta dependence of displacement is approximated by computing the Fourier cosine series of the idealized displacement for n equal zero to ten. The Fourier coefficients are computed in Appendix B for a contact width w of six centimeters, and a borehole radius of ten centimeters. With summation over the variable n limited to ten terms, the uniform displacement over a strip of width w is only approximately achieved, as figure 4-6 shows. The objective now is to modify the input, tangential stress P_{zr} , so that the resulting displacement as a function of theta, is given by figure 4-7. This will be accomplished in the following manner:

- 1.) The response to the normalized zero phase wavelet shown in figure 4-6, with $\omega_0 = 40 \cdot 2\pi$, $\omega_c = 30 \cdot 2\pi$, and $G(\lambda)$ as described by equation (4-18), is computed for n equal zero to ten. The summation over the variable n is not performed.

- 2.) The displacements are then normalized to the n equal zero term. That is, the displacement at n is expressed as a constant, $\epsilon(n)$, times the displacement at n equal zero. $\epsilon(n)$ is computed for each value of n .

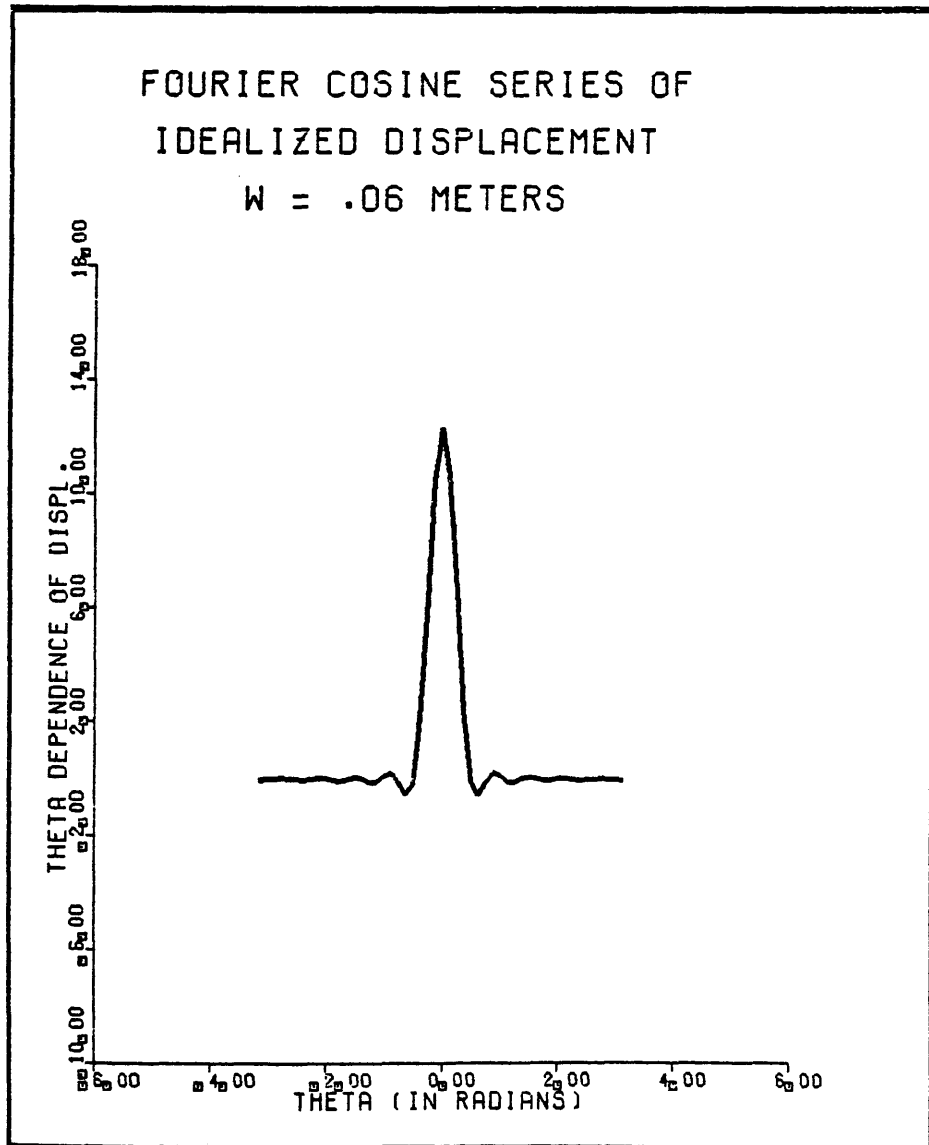


Figure 4-6

Theta dependence of displacement.

3.) To obtain the desired displacement as a function of theta, the relative magnitudes of the displacements for each value of n must be the same as the normalized Fourier coefficients computed in Appendix B. This is accomplished by multiplying the source term, P_{zr} , by a displacement correction factor, $dcf(n)$, for each value of n. The displacement correction factors are calculated by setting the normalized Fourier coefficients, $nfc(n)$, equal to the relative magnitudes of the displacements, $\epsilon(n)$, times the displacement correction factor, $dcf(n)$, for each value of n. This yields

$$dcf(n) = nfc(n) / \epsilon(n) \quad (4-21)$$

In this manner, a displacement correction factor is determined for each value of n. When the source P_{zr} is multiplied by the displacement correction factor for each value of n, a displacement whose theta dependence is shown in figure 4-6 results. The source function P_{zr} given in equation (4-6) then becomes

$$P_{zr} = -[Q/(2\pi b)]G(\ell)F(\omega)\cos(n\theta)dcf(n) \quad (4-22)$$

and the summation over the variable n in equation (4-16) from $n = -10$ to 10 , can be changed to a summation from $n =$

0 to 10. An example of the computation of the displacement correction factors is given in Appendix C.

The effect of multiplying the source by these displacement correction factors will now be considered. The force acting on the tool is given by the integration of the area under the stress curve in the time and space domain. The integration of the stress pattern (p_{zr}) over the range zero to 2π will equal zero for n greater than zero. Thus only the n equal zero term contributes to the force acting on the tool. This term is the same as the source term used for Model 1, and is normalized, as shown in section IV.3.

This pattern of spatial displacement approximates that of a source in contact with the formation over a length L_0 and width w . Thus, the values of displacement computed in this manner will be entered into equation (3-49) and the resulting impedance will be used to calculate frequency response curves for Model 2.

V. Preliminary Calculations

Before calculating the frequency response curves, some preliminary calculations were performed. The first of these involved determining if the displacement of the tool is constant over its length. This is required to validate the assumption that the tool is rigid.

As mentioned previously, the initial spatial stress distribution used was a boxcar, assuming a constant stress across the tool. However, it was determined that this did not produce uniform displacement along the tool. The stress pattern whose spatial distribution, $g(z)$, is seen in Figure 4-4, provided a much more uniform displacement at different points along the tool's length. This stress pattern will be referred to as the higher at ends (or HAT) stress pattern.

The magnitude of the displacements (in time) was computed at several points along the tool for Model 1, using the boxcar and HAT spatial source distributions. The response to the zero phase, 10 to 70 hz wavelet represented in the transform domain by (4-19) was calculated, and the peak displacements (at $t=0$) were compared. The length of the tool was one meter, and displacements were computed at $z = 0, 0.1, 0.25, 0.35, \text{ and } 0.5$ meters, where $z = 0$

represents the center of the tool, and $z = 0.5$ is at the end of the tool. The displacement u_z is an even function of z , and therefore need only be computed for positive values of z .

The calculated displacements are represented schematically in Figures 5-1 and 5-2, for the boxcar and HAT stress patterns, respectively. The tool was assumed to be in contact with a formation whose properties are defined as follows:

$$\alpha = 4000 \text{ m/s}$$

$$\beta = 2300 \text{ m/s}$$

$$\rho = 2600 \text{ kg/m}^3$$

The average displacement for the boxcar stress pattern was 2.07×10^{-11} m/newton, while the HAT stress distribution gave an average displacement of 1.94×10^{-11} m/newton. Notice that the standard deviation (represented in the figures by S.D.) for the HAT stress pattern is approximately one-fifth of that for the uniform stress distribution. Therefore, the assumption that the tool is rigid is much more plausible for the HAT stress pattern, and this is the spatial stress distribution along the z axis that will be used throughout this thesis.

Displacement across Tool

S.D. = 0.34

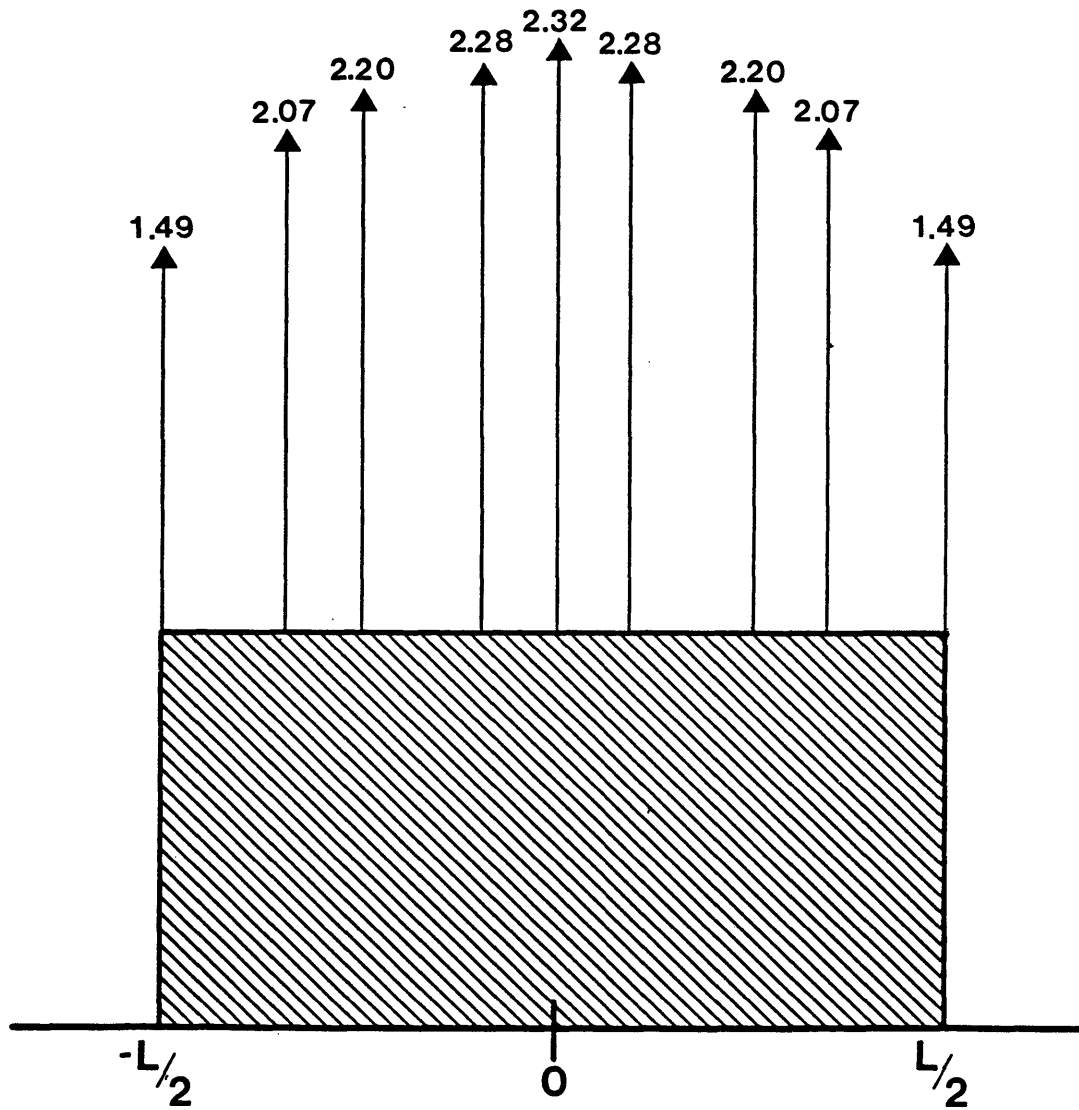


Figure 5-1

Displacements along the tool for boxcar stress pattern.

(Computed in SS1, $L_0 = 3$ m.).

Displacement across Tool

S.D. = 0.07

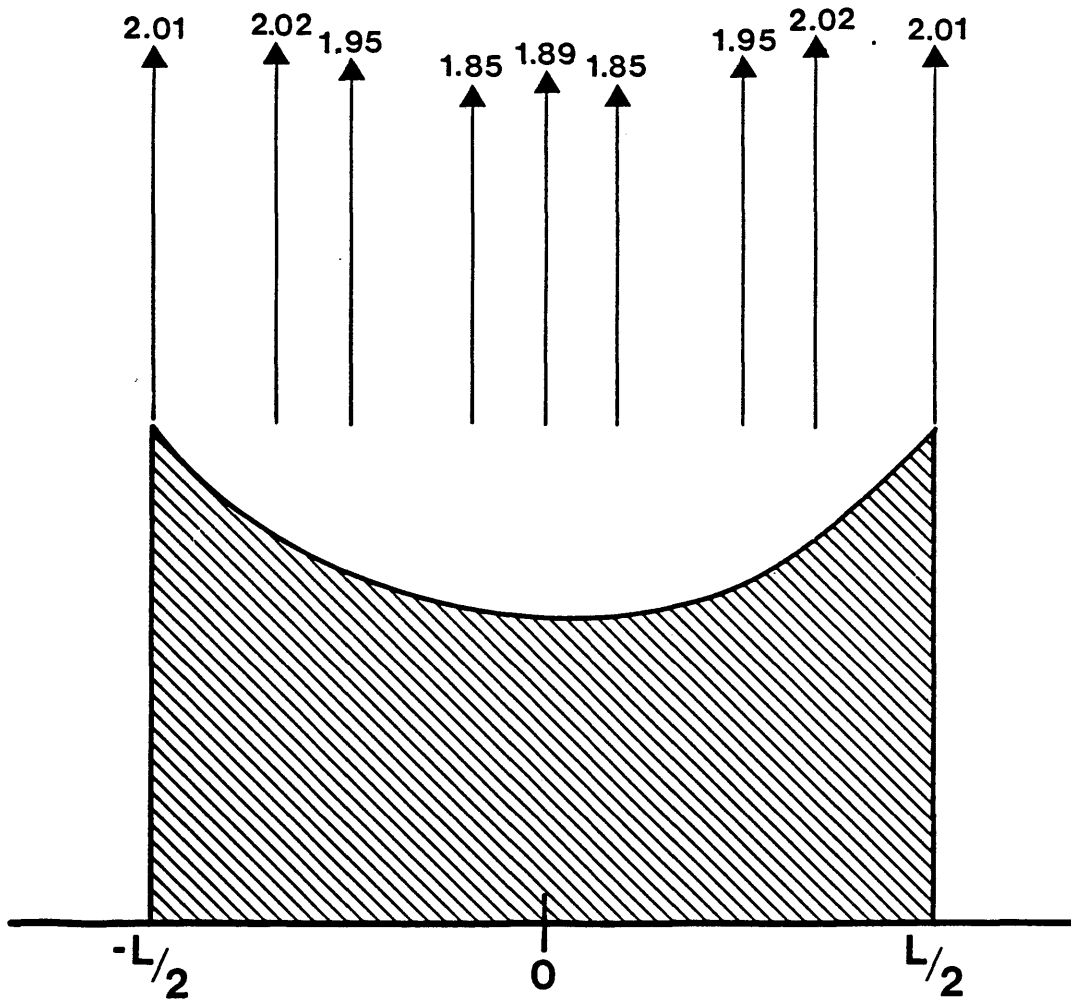


Figure 5-2

Displacements along the tool for higher at ends (HAT)
stress pattern. (computed in SS1, $L_0 = 3$ m.)

Displacement as a function of frequency

The initial investigation involved determining if the coupling of the tool to the formation yielded an output (displacement/force) that was independent of frequency. Examples are taken from both Model 1 and Model 2.

If the displacement/force of the tool-formation contact is independent of frequency, and if a transient stress pattern is applied as input, this same waveform will be reproduced as the displacement of the tool. Figure 5-3 shows the input and output waveforms, corresponding to the time dependence of the stress pattern and the displacement of the tool, respectively. These plots were run for Model 1 (tool in contact around entire circumference of the borehole). Visually, the waveforms are identical. The input wavelet is the 10 to 70 hz, zero phase wavelet described previously. By comparing the displacements in the frequency domain, it was found that the axial displacement varied by only ten percent in the 10 to 70 hz range. Thus, a spring constant was determined for this coupling. Spring constants were on the order of 10^{10} newtons/m, with higher values for rigid rocks (dense sandstones) and lower values for softer rocks (such as shales).

For Model 2 (tool in contact along a thin vertical

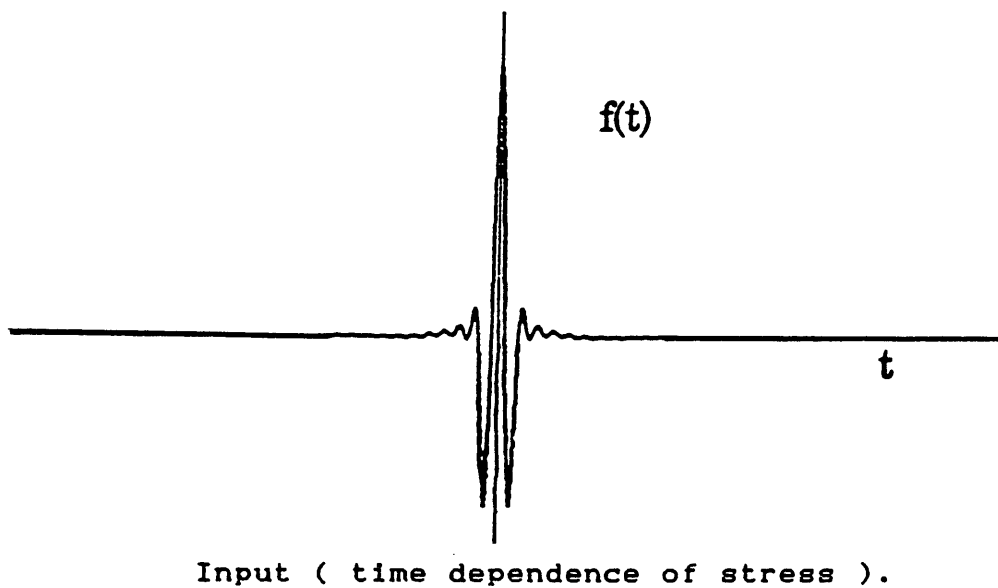
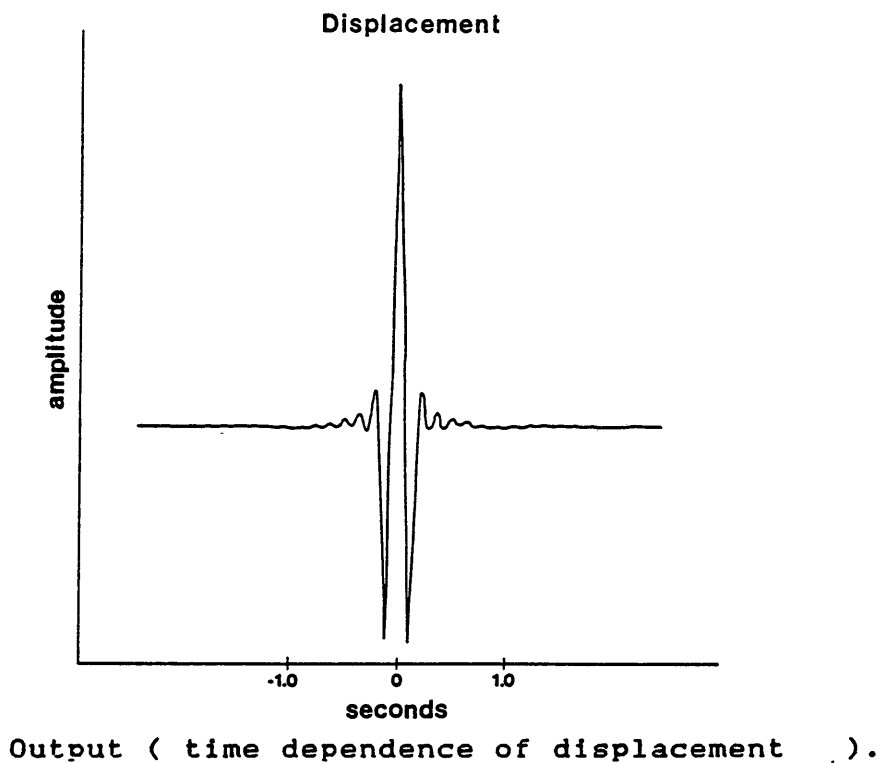


Figure 5-3

Input (time dependence of stress) and output (time dependence of displacement) for Soft Rock, $L_0 = 3$ m.

strip), the real and imaginary parts of displacement are plotted as a function of frequency in Figure 5-4. The properties of the surrounding formation are those of the soft rock, and are given in Table 5-1. It is seen that both the real and imaginary parts are nearly constant, indicating that the output (displacement/force) is independent of frequency. The presence of the imaginary part represents radiation of energy away from the tool into the surrounding formation, and is found to increase with frequency.

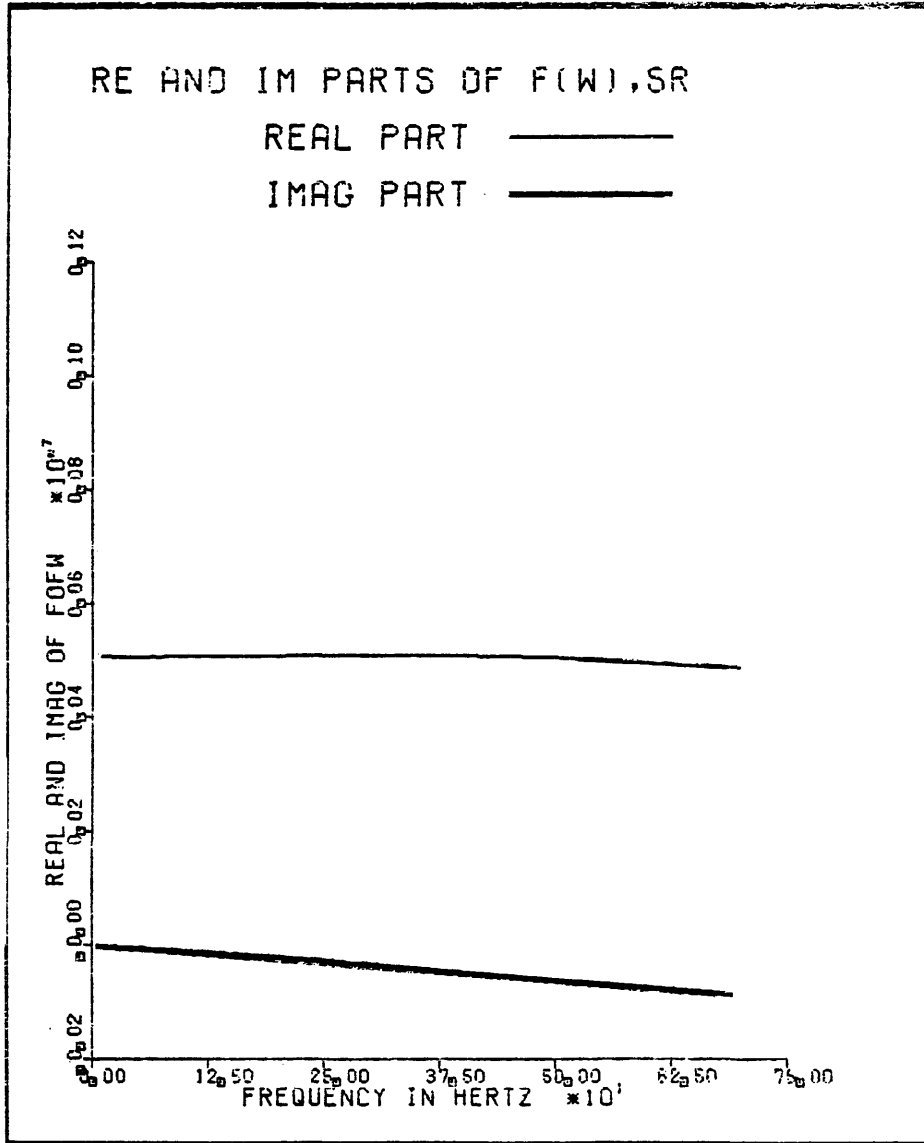


Figure 5-4

Real and Imaginary parts of $F(\omega)$ for a 3 m tool in the Soft Rock (Model 2).

Properties of elastic media modelled in this thesis.

| | ρ | α | β | λ | μ |
|------------------|--------|----------|---------|-----------|-------|
| Soft Rock | 1900 | 1900 | 572 | 0.562 | 0.062 |
| Sandstone1 (SS1) | 2600 | 4000 | 2300 | 1.41 | 1.38 |
| Sandstone2 (SS2) | 2400 | 4000 | 2300 | 1.30 | 1.27 |
| Carbonate | 2500 | 4900 | 2600 | 2.62 | 1.69 |
| Pierre Shale | 2100 | 2250 | 860 | 0.752 | 0.155 |
| Drilling Mud | 1500 | 1650 | 0 | 0.408 | 0 |

density is in kg/m^3 ,

velocity in m/sec

elastic constants are 10^{10} Newtons/ m^2 .

Table 5-1

VI. Results

The solutions for displacement were written in Fortran code and entered into a digital computer. The programs were initially executed on a DEC10 computer, and the final versions were run on a Gould 9750 computer.

With the boundary conditions applied (tool excited by a shear stress P_{zr} ; all other stresses zero), the amplitudes of the potentials are determined, and the displacements computed. The summation over wavenumber λ is performed at each angular frequency ω to obtain the Fourier coefficient for that frequency. This is repeated for $n = 0$ to ten (for Model 2) and the resulting Fourier coefficients are summed over n at each frequency. The spectra can then be transformed to the time domain by means of a Fast Fourier Transform.

In computing the frequency response of the tool, there is no need to transform to the time domain. Therefore, the function $F(\omega)$, which corresponds to a time transient $f(t)$ in the time domain, will be set equal to unity. The program output will then be in the frequency domain, and is suitable for computing frequency response curves.

The Fortran code of the programs written for this thesis is listed in Appendix D.

Properties of the lithologies and fluids in the borehole for which frequency response curves were computed are listed in Table 5-1.

All frequency response curves are for tools in a ten centimeter hole, and are computed from the displacement at $z = 0$, the center of the tool. The magnitude of the force Q is unity for all curves. For Model 2, the width w is constant, and is equal to .06 meters (6 cm.s). The ratio of tool length to mass varies from 15 kg/m to 30 kg/m. These dimensions and mass to length ratios are consistent with VSP tools currently in use.

In seismic exploration the primary interest lies in the frequency range from 10 to 120 hz. In this study frequency response curves will be computed over the range from 10 to 1000 hz, with the objective to determine the response curves for tools of varying masses and lengths clamped in different lithologies.

VI.1 Frequency response curves - Model 1

Model 1 is depicted in Figure 2-2, a simplified model of a tool in contact with the formation around the entire circumference of the borehole. This is equivalent to the $n = 0$ case for Model 2 (no θ dependence). The ratio of geophone motion to earth motion, which has been defined as frequency response, is seen in figure 6-1 for a 90 kg, 3 m tool in an empty borehole. The response of the tool in this lithology (SS1) is quite flat when using the unscaled value of impedance. In the same figure, the response is compared to that obtained when the scaled value of impedance (discussed in section IV.4) is used. The scaling width is 5 cm.s. The response to the scaled value of impedance is much more reasonable. The response of this same tool to the soft rock is shown in figure 6-2. Once again, the response is nearly uniform over all frequencies for the unscaled value of impedance , with a mild peak near 1200 hz. When the response is computed with the scaled value of impedance, the curve exhibits a resonance peak close to 200 hz.

These examples illustrate that the use of a scaled impedance results in frequency response curves which are much more plausible. This lends credence to the assumption that the impedance is indeed proportional to the area of

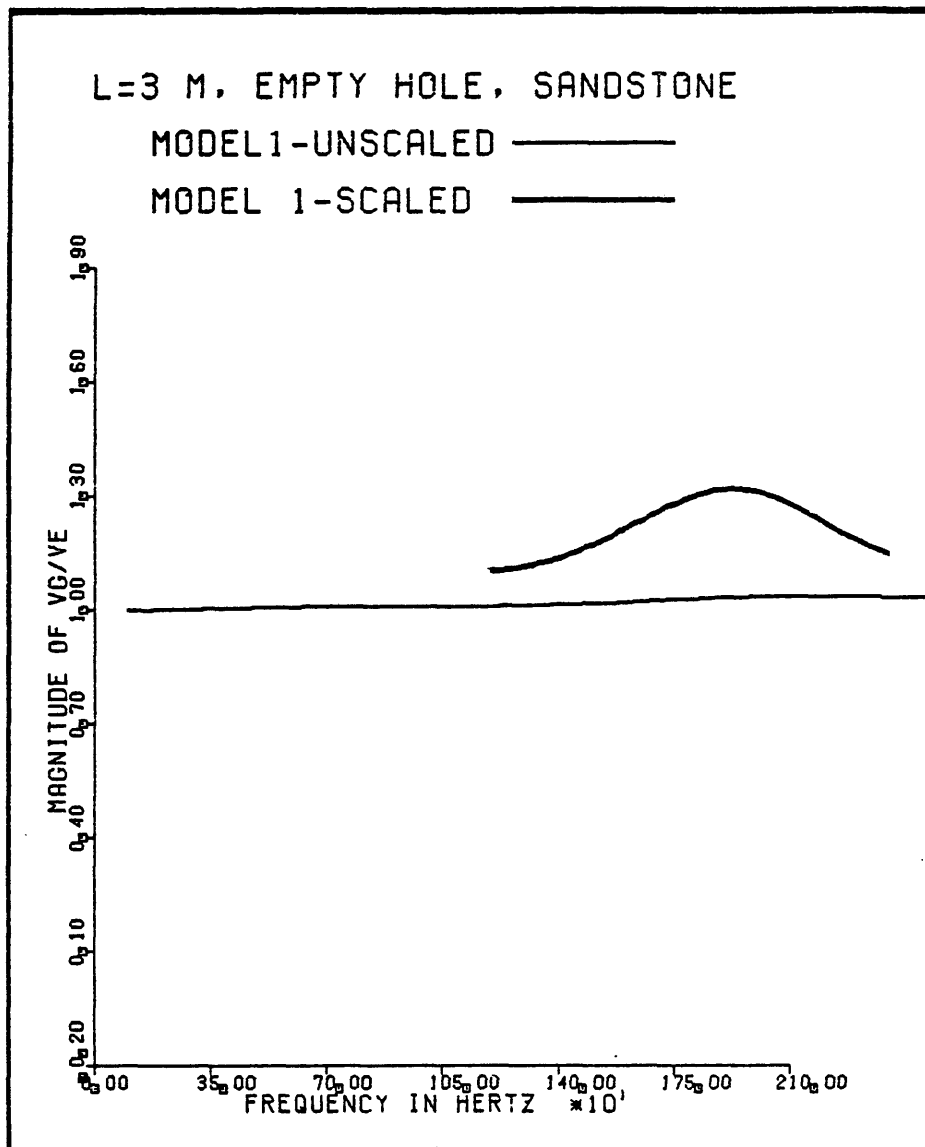


Figure 6-1

Frequency response for Model 1. 90 kg, 3 m tool clamped in an empty borehole in the SS1 lithology. Comparison of response curves computed with scaled and unscaled values of impedance.

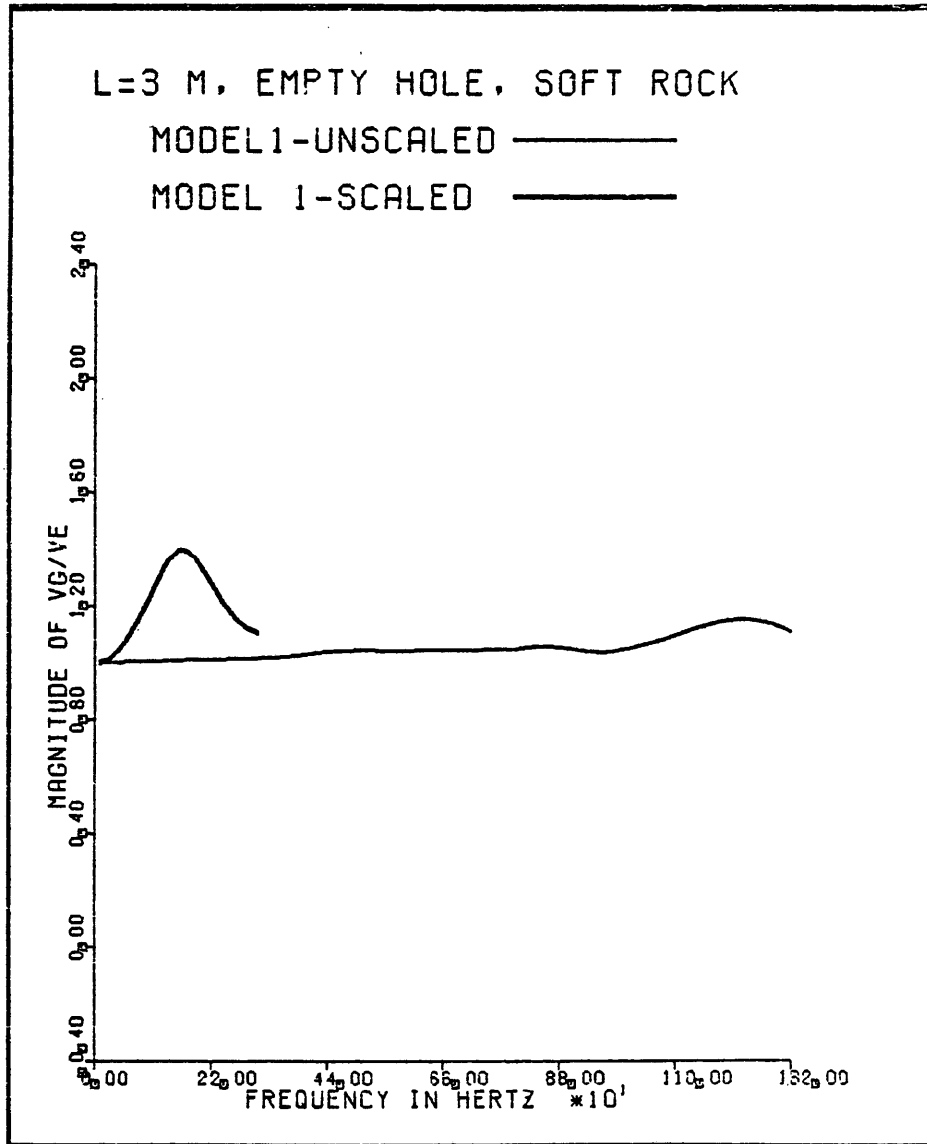


Figure 6-2

Frequency response for Model 1. 90 kg, 3 m tool clamped in an empty borehole in the Soft Rock. Comparison of response curves computed with scaled and unscaled values of impedance.

contact of the tool with the formation. Therefore, the remainder of the curves for Model 1 will be calculated with scaled values of impedance, with scaling width $w = .02$ m.

The frequency response of a 3 meter, 90 kg tool in different lithologies is seen in figure 6-3. The coupling of the rigid tool to the formation is strongly dependent on the properties of the formation. The resonance peak occurs at higher frequencies in "stiffer" lithologies (i.e., rocks with high densities, and large values of shear and compressional wave speeds). Response curves for tools with varying lengths, but constant ratios of mass/length, show that the resonant peaks move to higher frequencies as the tool's length decreases (see Figure 6-4). When the borehole is fluid-filled, the damping of the tool's vibrations severely attenuates the high frequency response of the tool, as seen in Figure 6-5. The damping effect is greater for the smaller tools.

The effect of varying the mass of the tool is seen in Figures 6-6 and 6-7, for a 1 meter tool in empty and mud filled boreholes, respectively. In an empty hole, the resonance peak for the lighter tool occurs at a higher frequency than that of the heavier tool. When the borehole is mud-filled, the response of both tools is severely damped, and neither tool exhibits a resonance peak.

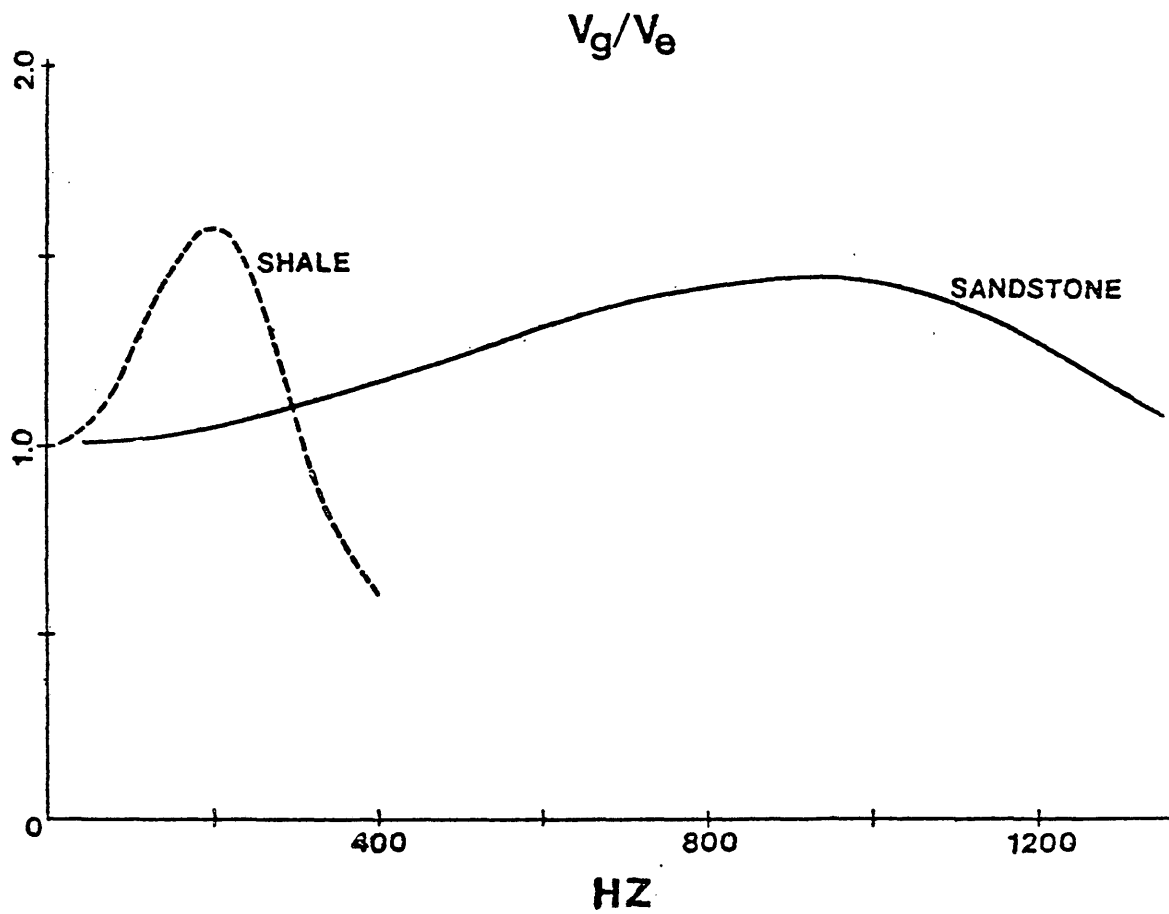


Figure 6-3

Frequency response for Model 1. Response for a 3 m, 90 kg tool in an empty borehole clamped in two different lithologies, SSl and the Soft Rock.

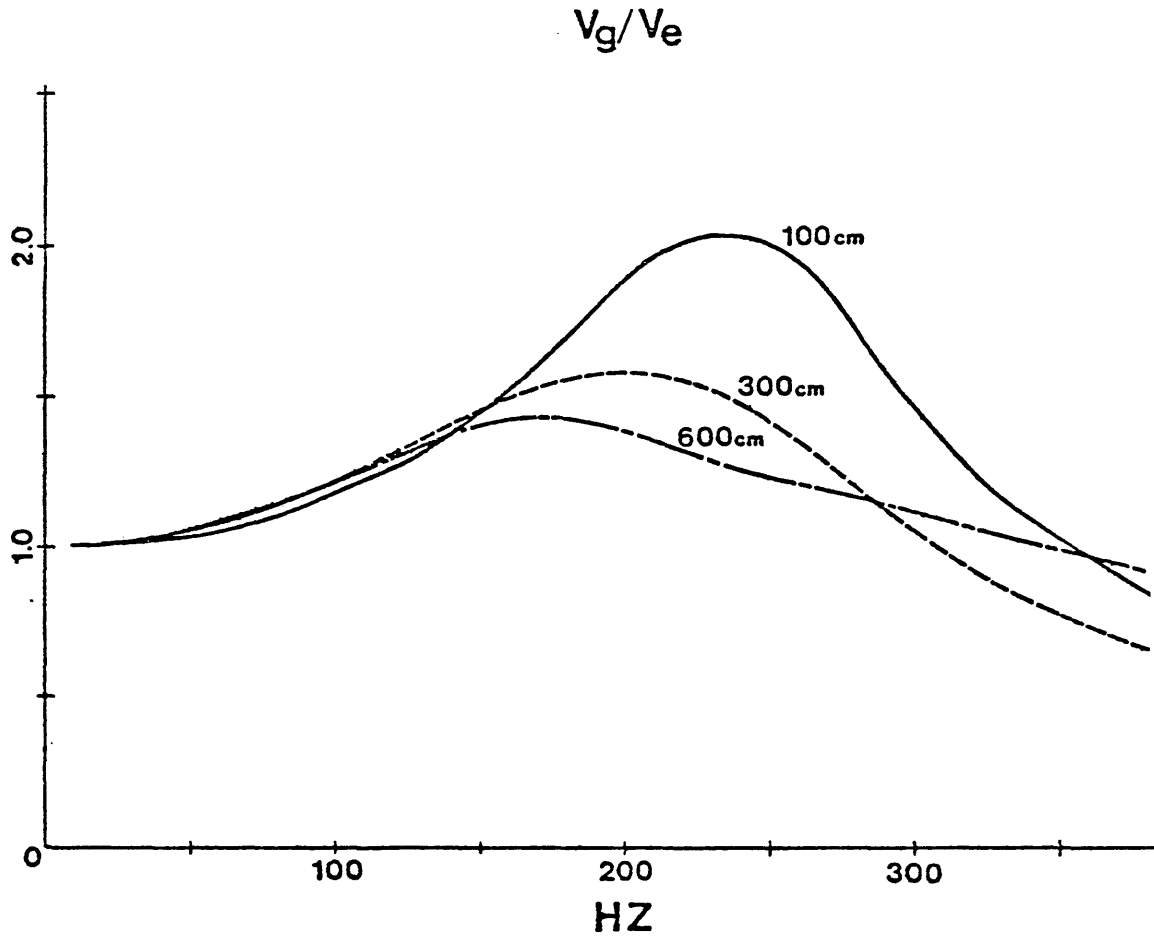


Figure 6-4

Frequency response for Model 1. Response curves for tools in the same lithology (Soft Rock) but with varying lengths, in an empty borehole. The mass/length ratio is constant for each tool and is 30 kg/m.

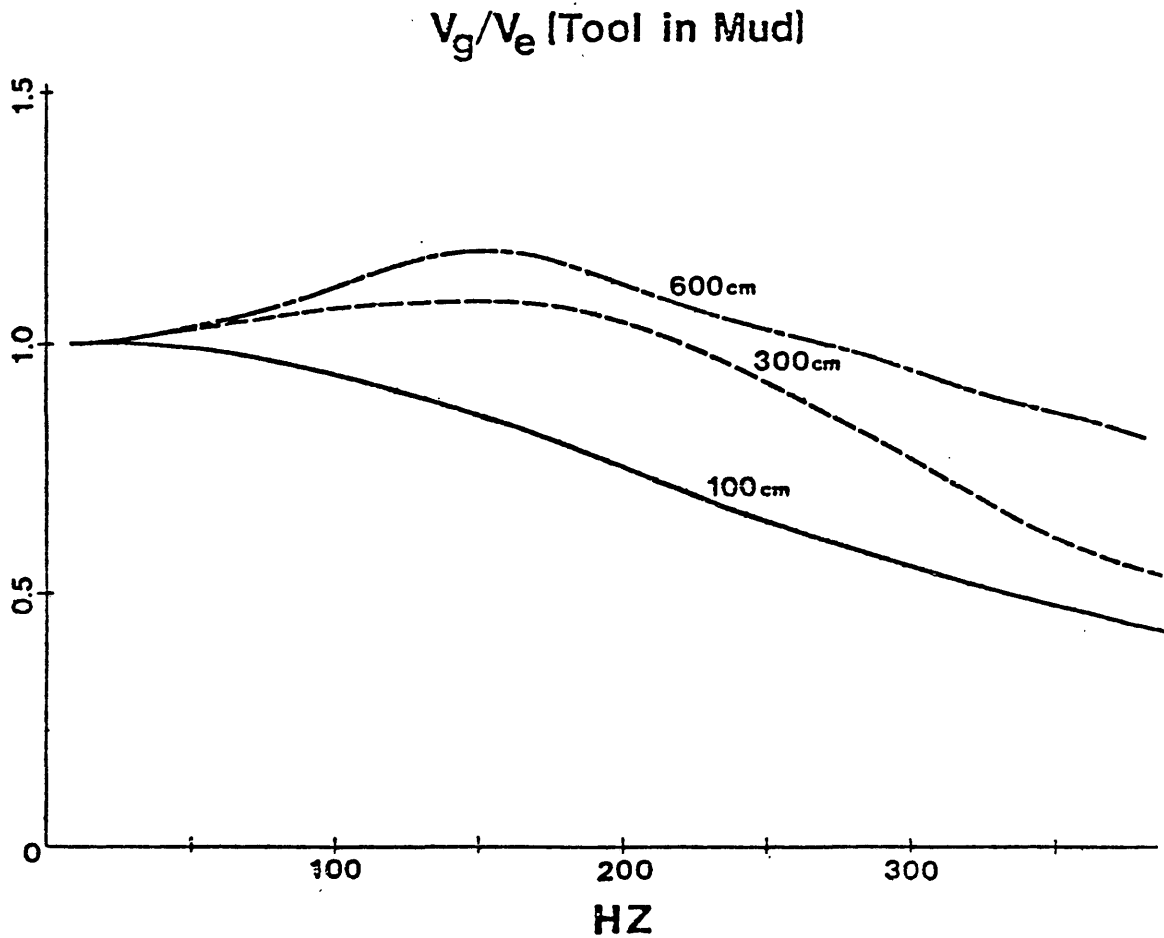


Figure 6-5

Frequency response for Model 1. Response curves for tools in the same lithology (Soft Rock) but with varying lengths, in a mud-filled borehole. The mass/length ratio is constant for each tool and is 30 kg/m.

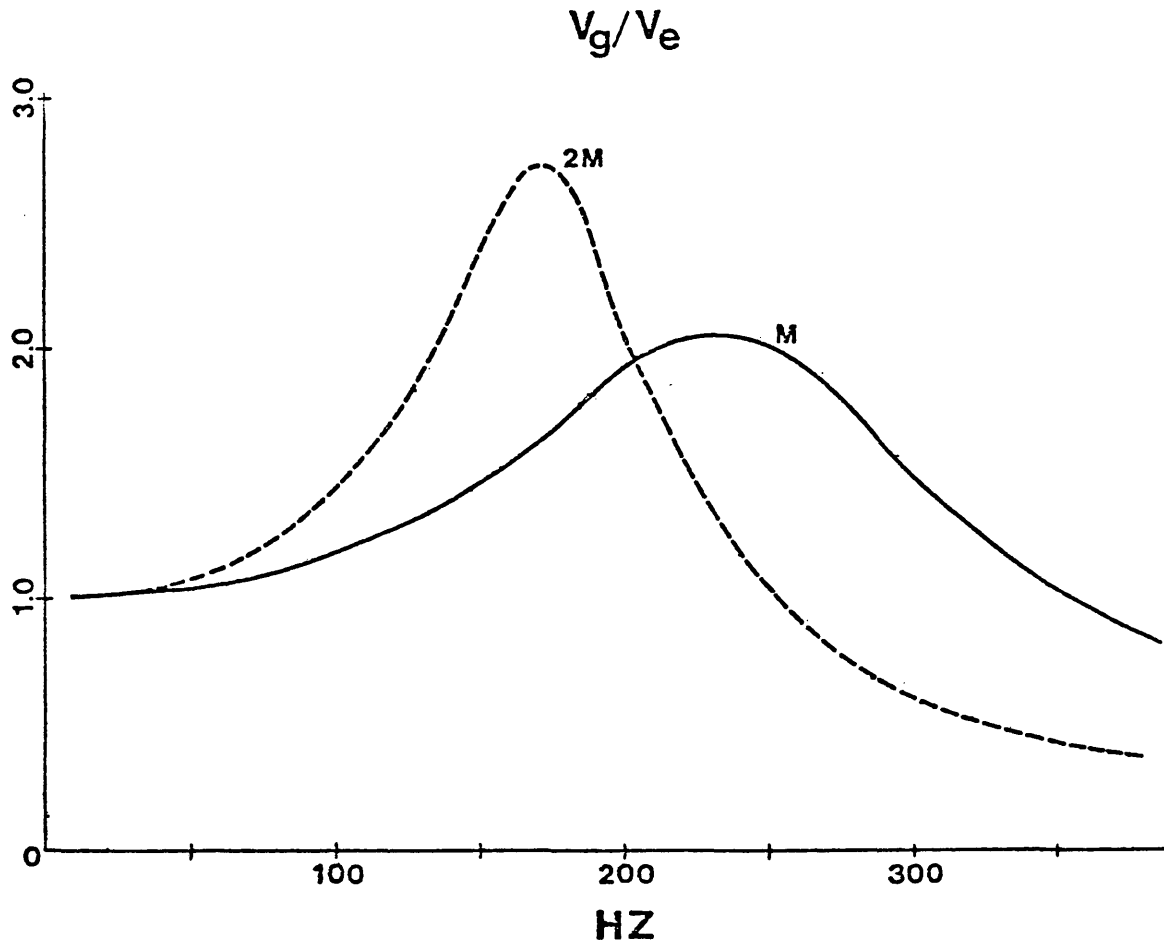


Figure 6-6

Frequency response for Model 1. Effect of tool mass on response in empty borehole in the Soft Rock.

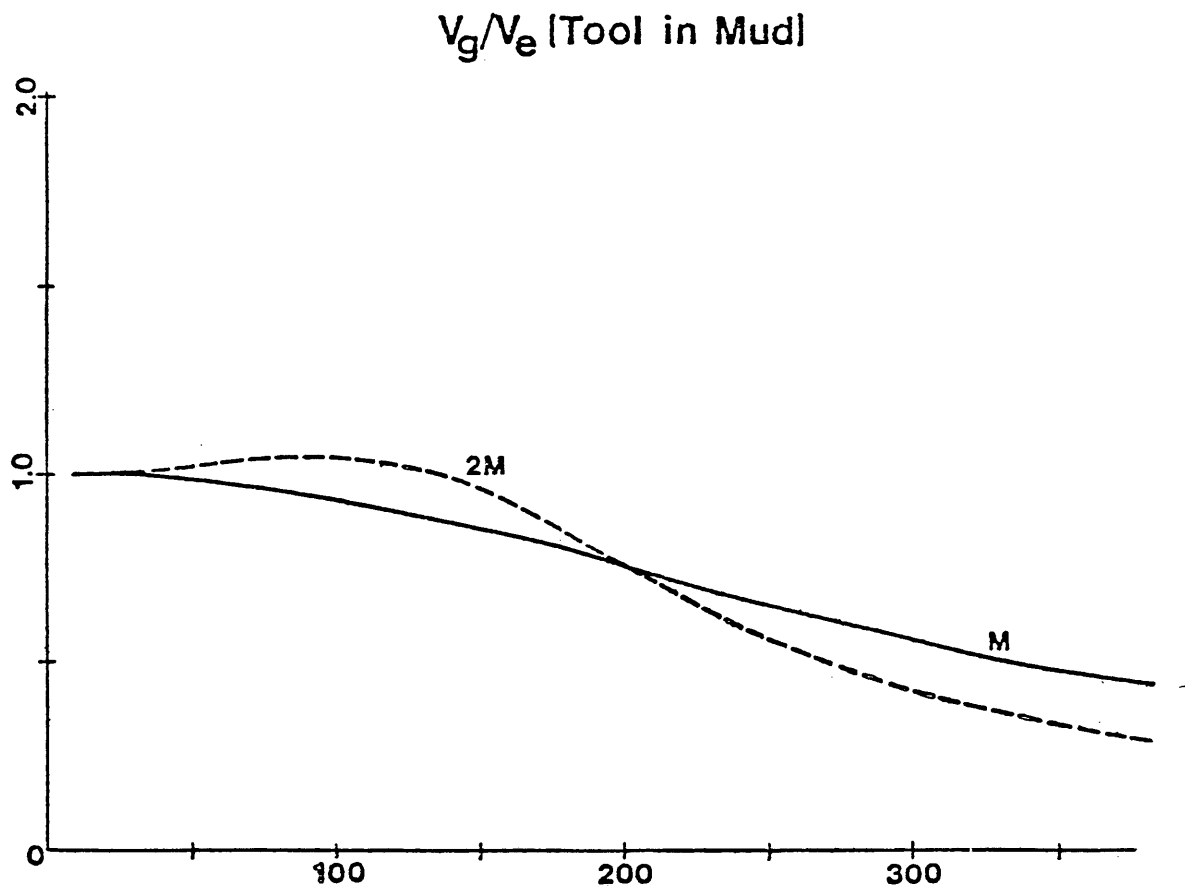


Figure 6-7

Frequency response for Model 1. Effect of tool mass on response in mud-filled borehole in the Soft Rock.

VI. Frequency response curves - Model 2

Empty borehole

Frequency response curves for Model 2, which more closely approximates the coupling of an actual VSP tool, are now discussed. Figure 6-8 shows the response of a 3 meter, 90 kg tool in an empty hole for two different lithologies, the soft rock and sandstone #2 (SS2). The resonance peaks for the two rocks are the same amplitude, but the peak for the more rigid sandstone is located at a much higher frequency. Figure 6-10 shows the effect of varying the mass of the tool. The lighter mass causes the amplitude of the peak to decrease and move to a higher frequency. The effect of varying the length of the tool is seen in Figure 6-11 for two tools with the same mass/length ratio (30 kg/meter). The resonance peak decreases in magnitude and moves to a higher frequency for the shorter tool length. The drop in amplitude is greater than that due to a change in mass but the shift in frequency of the resonance peak is less pronounced.

These results are compared to those obtained with the scaled impedances for Model 1. Figures 6-3 and 6-8 exhibit the same qualitative behavior for tools in different lithologies, but the magnitude of the resonance peaks and

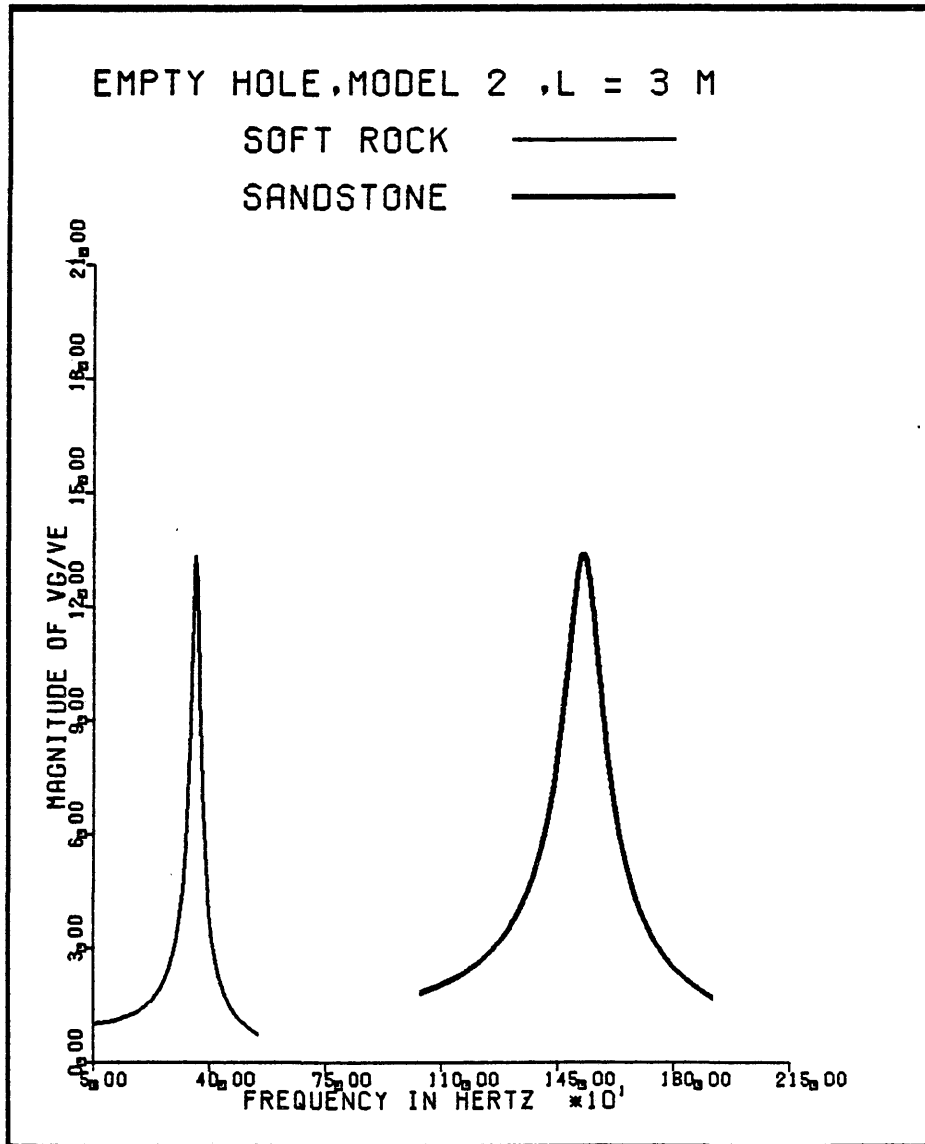


Figure 6-8

Frequency response for Model 2. Comparison of response for a 3 m, 90 kg, tool in an empty hole for the Soft Rock and SS2 lithologies.

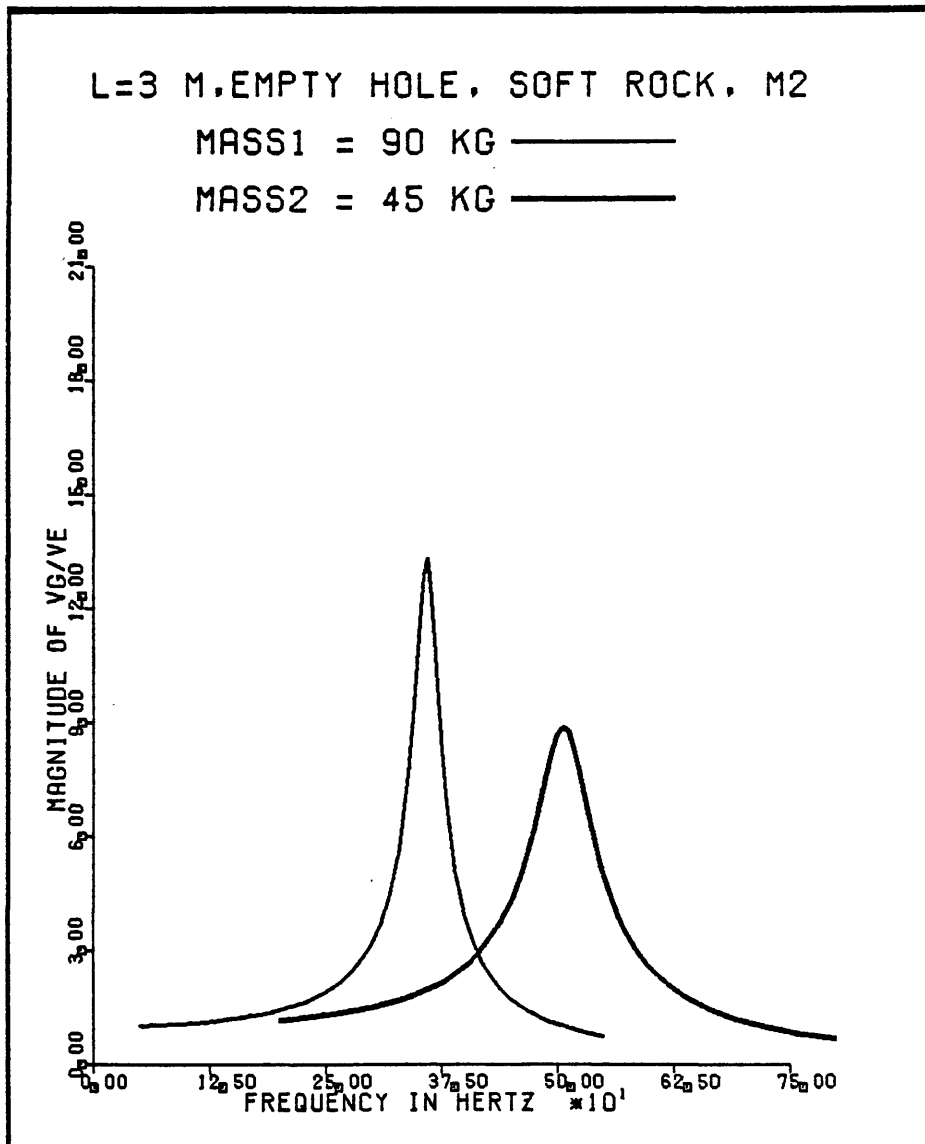


Figure 6-9

Frequency response for Model 2. Effect of varying the mass on the response of a 3 m tool in the Soft Rock (empty hole).

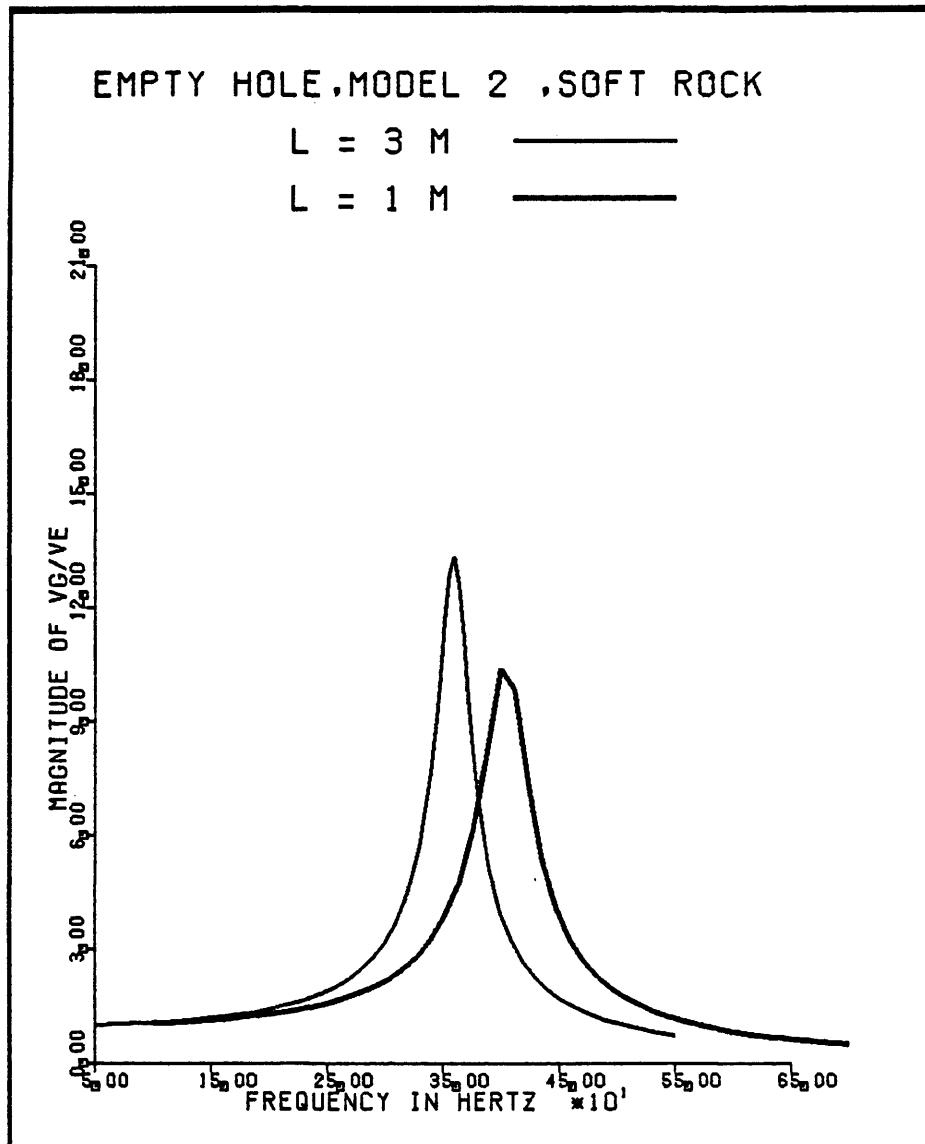


Figure 6-10

Frequency response for Model 2. Effect of varying the length of the tool in an empty borehole. The lithology is the Soft Rock, L_0 is 3 m, and mass/length = 30kg/m.

the frequencies at which they occur are not equivalent. The effect of varying the mass of the tool is, once again, qualitatively the same. Figures 6-6 and 6-9 show that for both models the lighter tool has a resonance peak which decreases in amplitude and occurs at a higher frequency. When the length of the tool is decreased, the resonance peak moves to a higher frequency for both models, but the effect on the amplitude, however, is not the same. The magnitude of the resonance peak increases for a shorter tool in Model 1, while it decreases for Model 2.

Fluid-filled borehole

The effect of tube wave radiation into the borehole on the response curves for model 2 is now examined. The response is computed for a borehole containing a typical drilling mud whose properties are listed in Table 5-1. Figures 6-11 to 6-13 show the effect of the drilling mud on the response of the tool. In all cases, the effect of the fluid was to decrease the amplitude of the resonant peak by about 50 % below the value for an empty borehole, with no change in the frequency at which the peak occurs. The response to a water filled borehole is almost identical, and therefore only the response to a mud filled borehole is shown in this thesis.

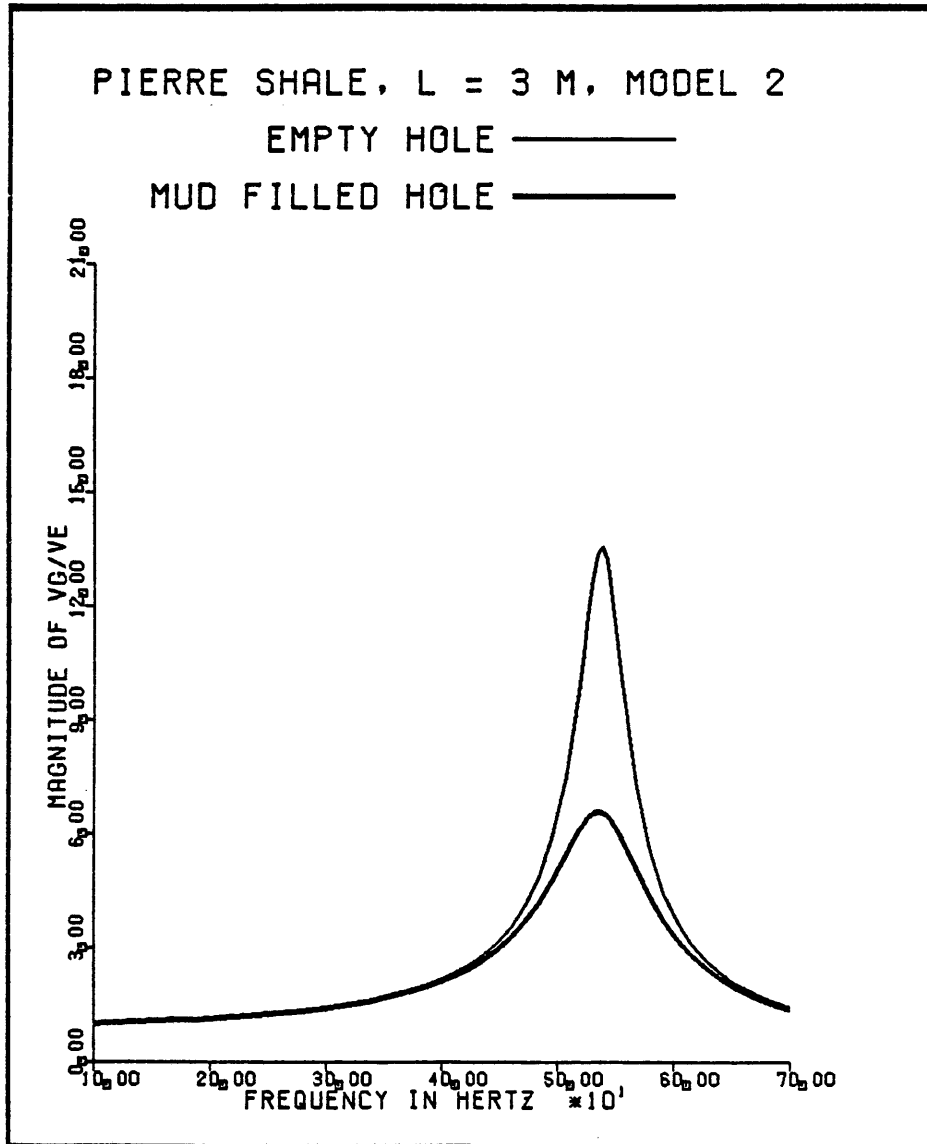


Figure 6-11

Frequency response for Model 2. 3 m, 90 kg tool in Pierre Shale. Empty and mud-filled borehole.

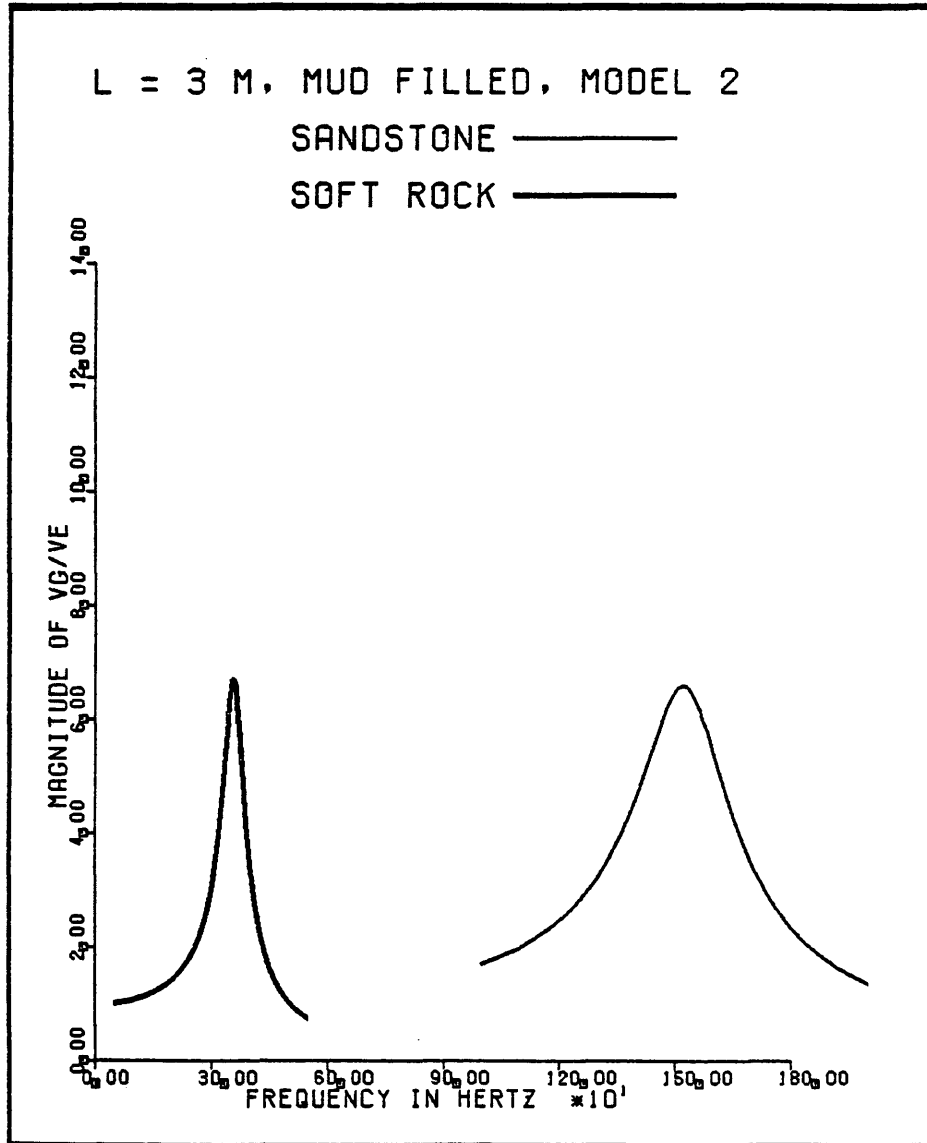


Figure 6-12

Frequency response for Model 2. Comparison of response to a 3 m, 90 kg tool in the Soft Rock and SS2 (mud-filled hole).

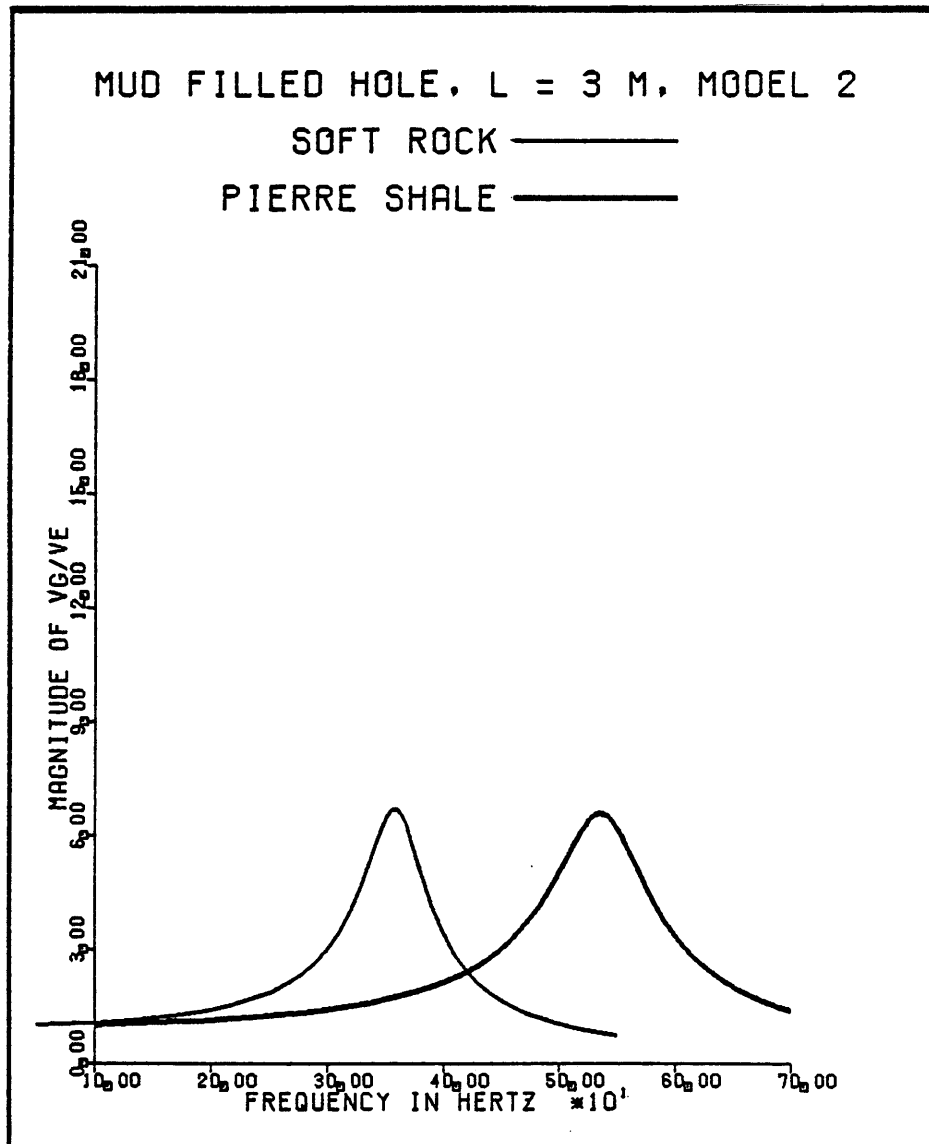


Figure 6-13

Frequency response for Model 2, mud-filled borehole. Response of a 3 m, 90 kg tool in Pierre Shale and the Soft Rock.

The phase response for the frequency response curves in Models 1 and 2 are identical, and are typified by Figure 6-14. The magnitude and phase response shown in this figure are for a 3 m, 90 kg tool in the soft rock. The phase starts out at zero (in phase), begins to drop as the resonance peak is approached, and levels off at $-\pi$ for the higher frequencies (180 degrees out of phase). This is the expected phase response for a resonant system, and was identical for both empty and mud filled boreholes in Models 1 and 2.

Figures 6-15 and 6-16 show the effect of varying the mass of the tool when it is clamped in a fluid filled borehole. The effect is the same as that observed in an empty hole, a lower magnitude of the resonant peak occurring at a higher frequency. The effect of varying the tool's length in the soft rock and SS2 is seen in Figures 6-17 and 6-18, respectively. The shorter tool's response decreases in amplitude and the resonant peak shifts to a higher frequency, the same effect observed in an empty borehole.

The damping affect of the fluid is much more severe for Model 1 than for Model 2. This is a direct result of the geometry assumed for Model 1. The tool is assumed to block the entire area of the borehole in Model 1. In model 2, the

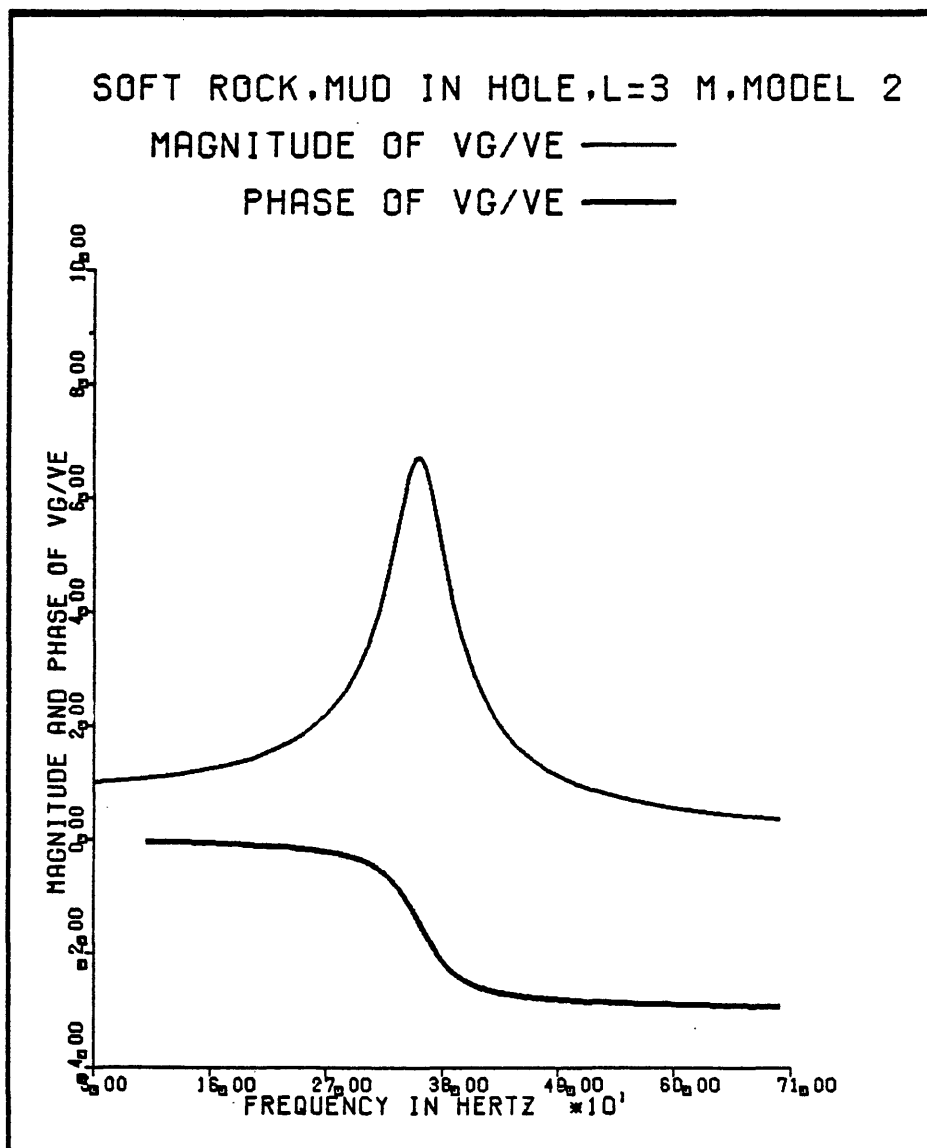


Figure 6-14

Magnitude and phase response for Model 2. 3 m, 90 kg tool clamped in a mud-filled borehole. Lithology is the Soft Rock.

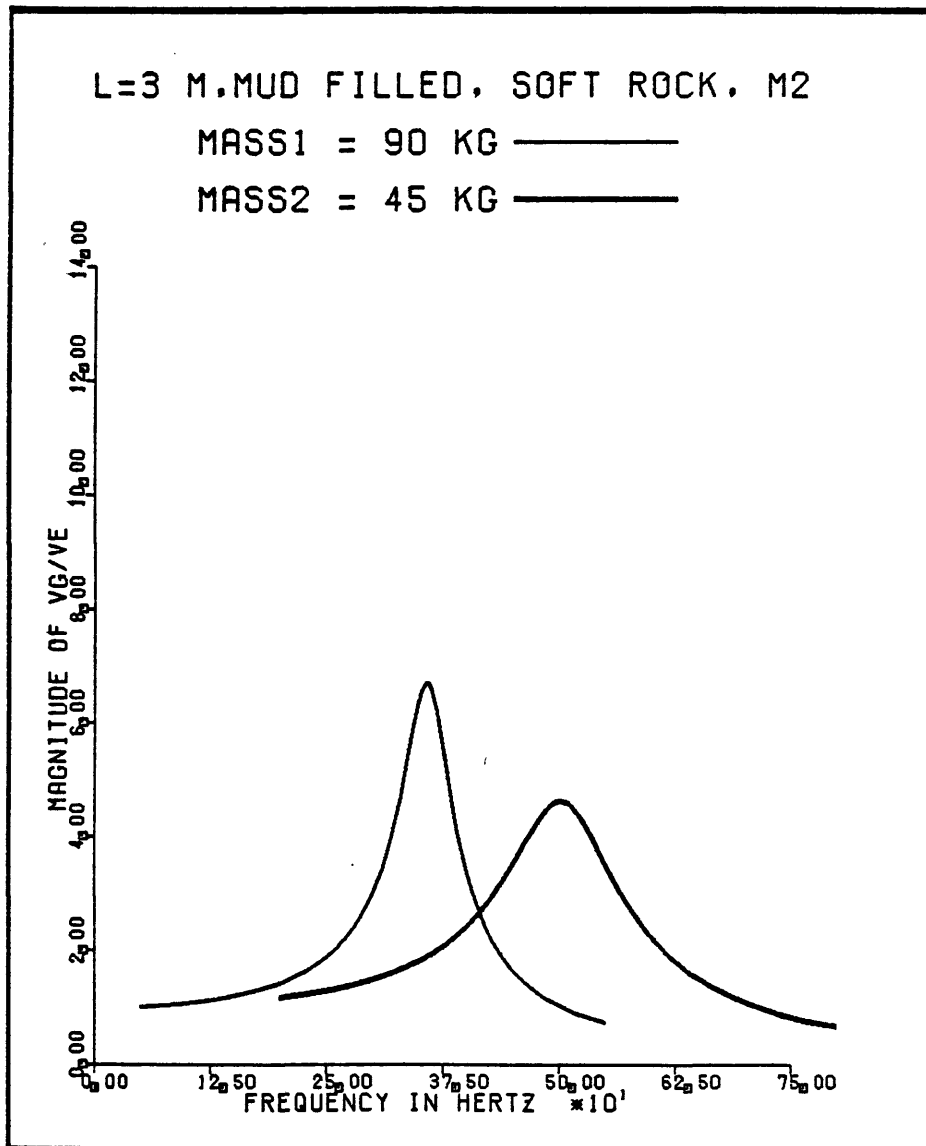


Figure 6-15

Frequency response for Model 2. Effect of varying the mass of a 3 m tool in a mud-filled borehole. The lithology is the Soft Rock.

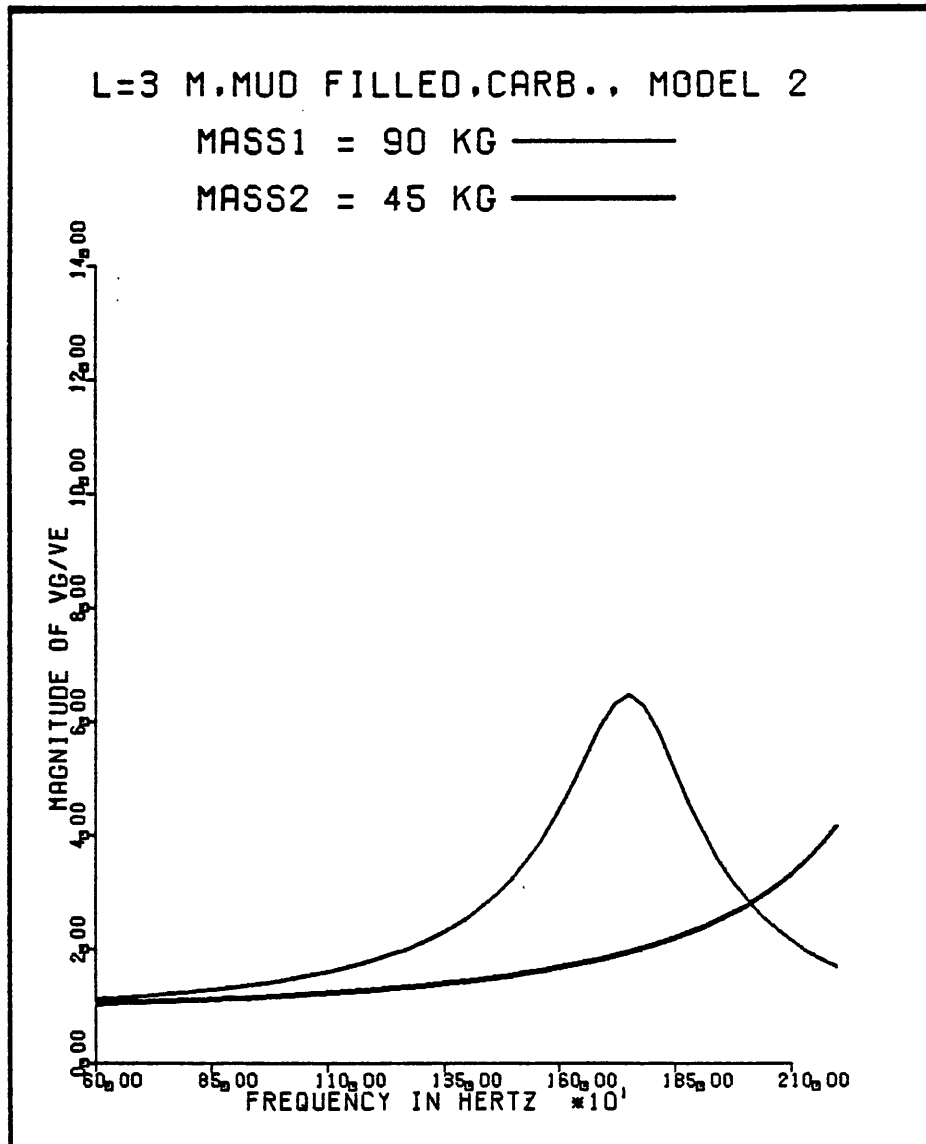


Figure 6-16

Frequency response for Model 2. Effect of varying the mass of a 3 m tool in a mud-filled borehole. The lithology is a Carbonate.

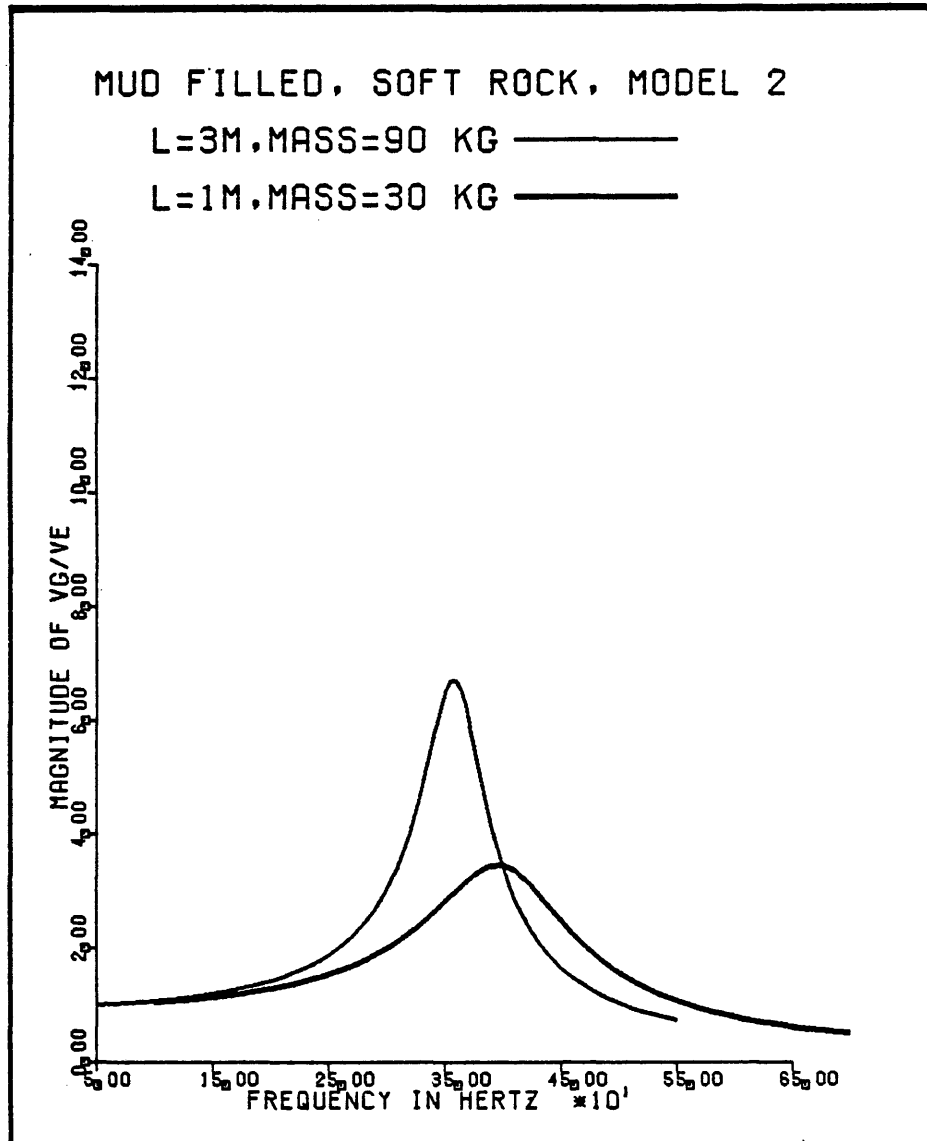


Figure 6-17

Frequency response for Model 2. Effect of varying the tool's length in a mud-filled borehole (Soft Rock).

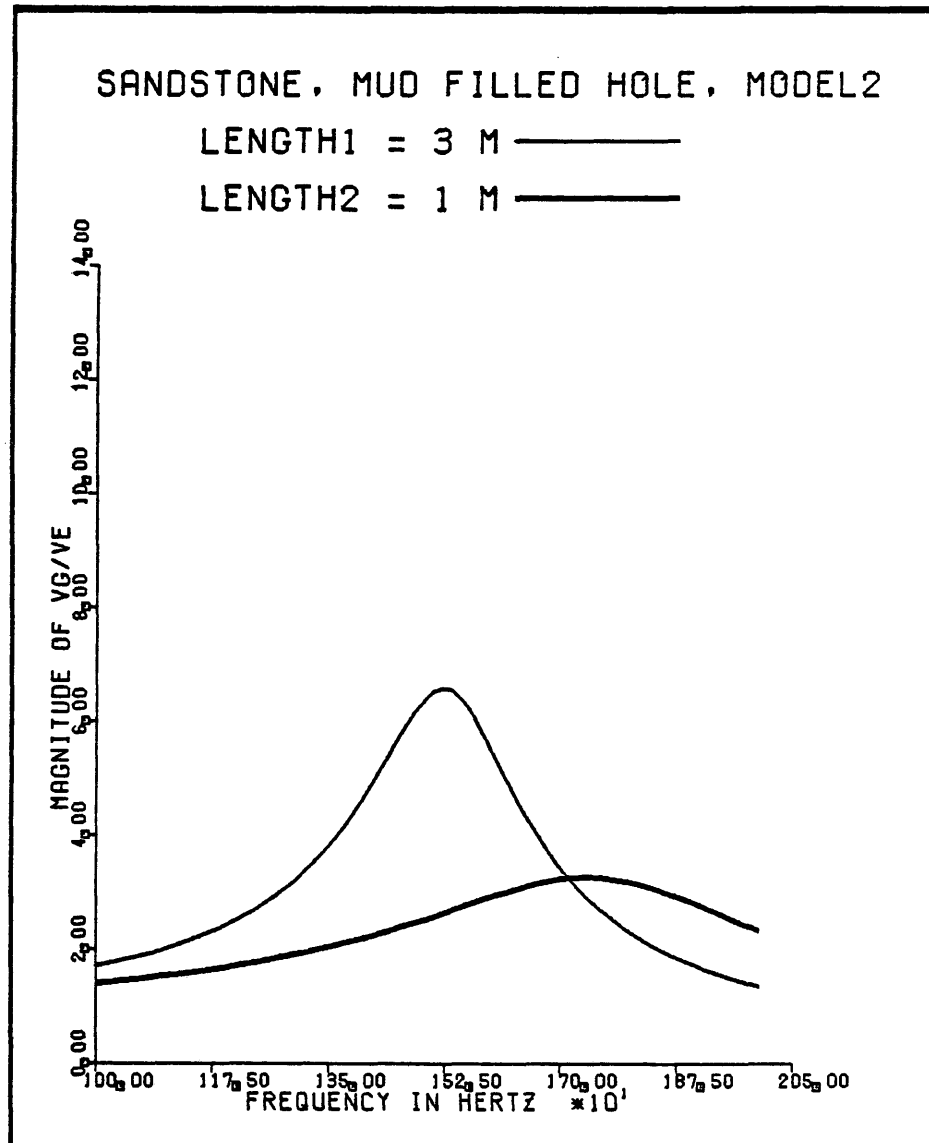


Figure 6-18

Frequency response for Model 2. Effect of varying the tool's length in a mud-filled borehole (SS2 lithology).

radius of the tool is taken to be .05 meters. Thus the damping, which is assumed to be proportional to the area occupied by the geophone, is much less for Model 2.

Borehole coupling

The last effect to be considered is the borehole coupling effect. The borehole coupling force is of opposite sign of that imparted to the geophone as a result of earth motion. The effect is found to depend on frequency, with the force increasing for higher frequencies.

Figures 6-19 and 6-20 show frequency response curves for the soft rock and SS2, respectively. The effect of the borehole coupling force is quite pronounced. The inclusion of the borehole coupling force results in resonance peaks which are significantly decreased in amplitude. The response curve is also seen to drop below unity before the resonant peak, which has not been observed in any previous response curves.

When analyzing the effect of the borehole coupling force, it is instructive to examine the phase response of the tool's motion when this force is included. Figure 6-21 shows the magnitude and phase response of the tool when the borehole coupling force is applied to the tool. There are two important differences between this plot and that of

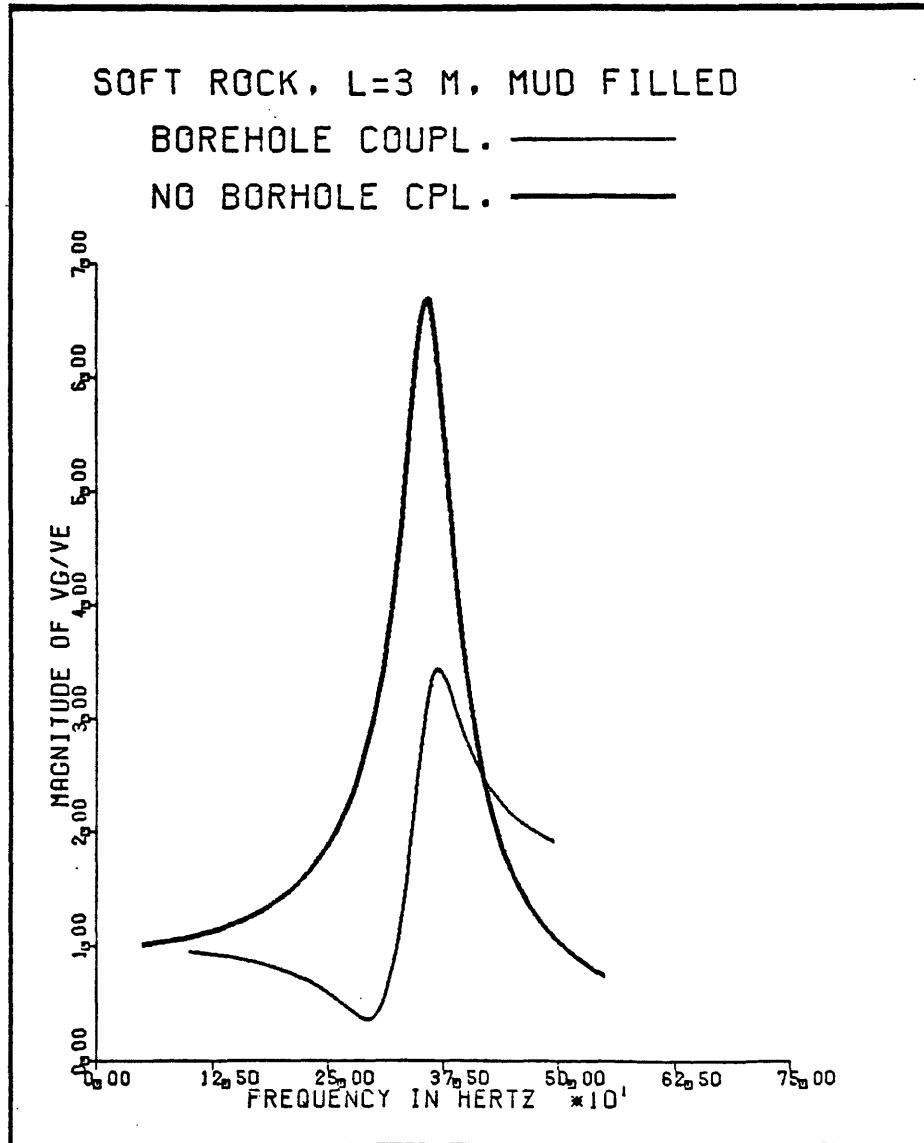


Figure 6-19

Frequency response for Model 2 with borehole coupling. 3 m,
90 kg tool in mud-filled borehole (Soft Rock).

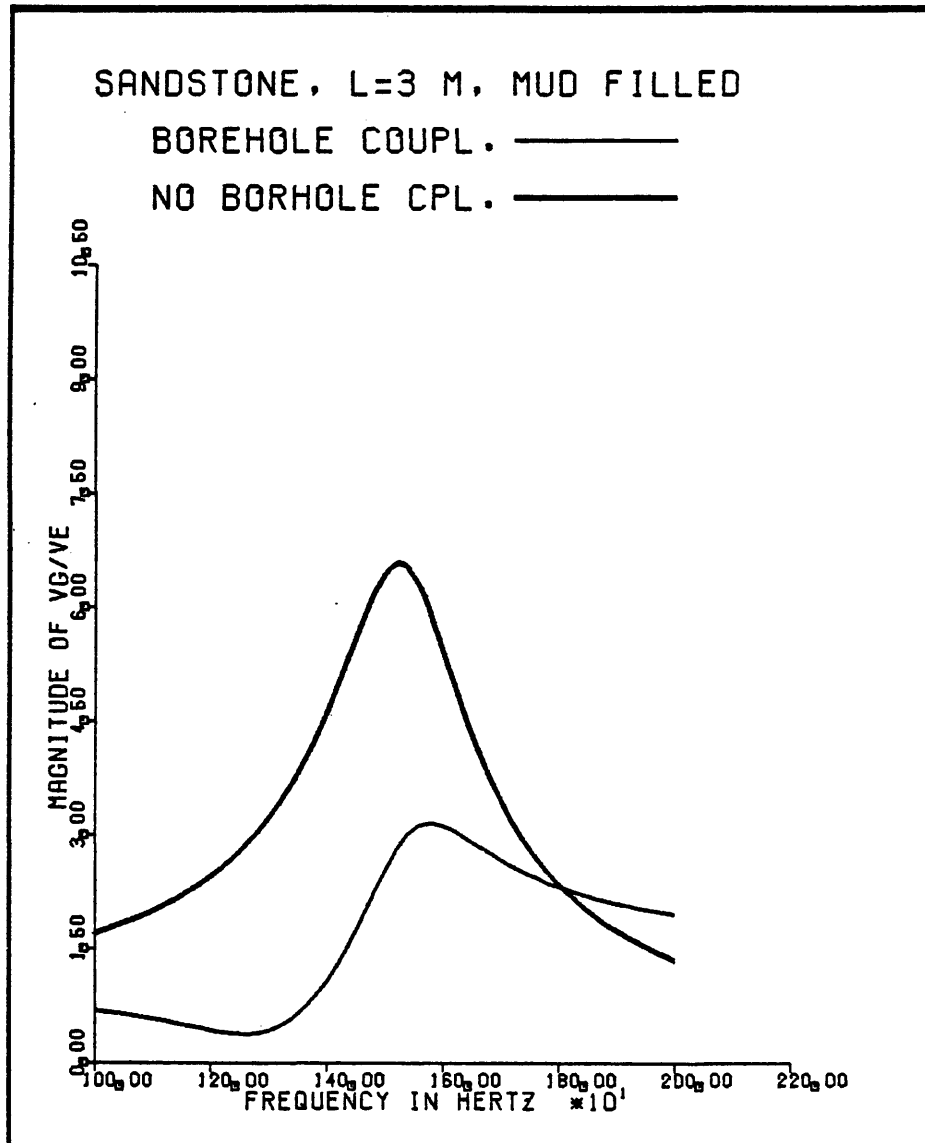


Figure 6-20

Frequency response for Model 2 with borehole coupling. 3 m,
90 kg tool in mud-filled borehole (SS2).

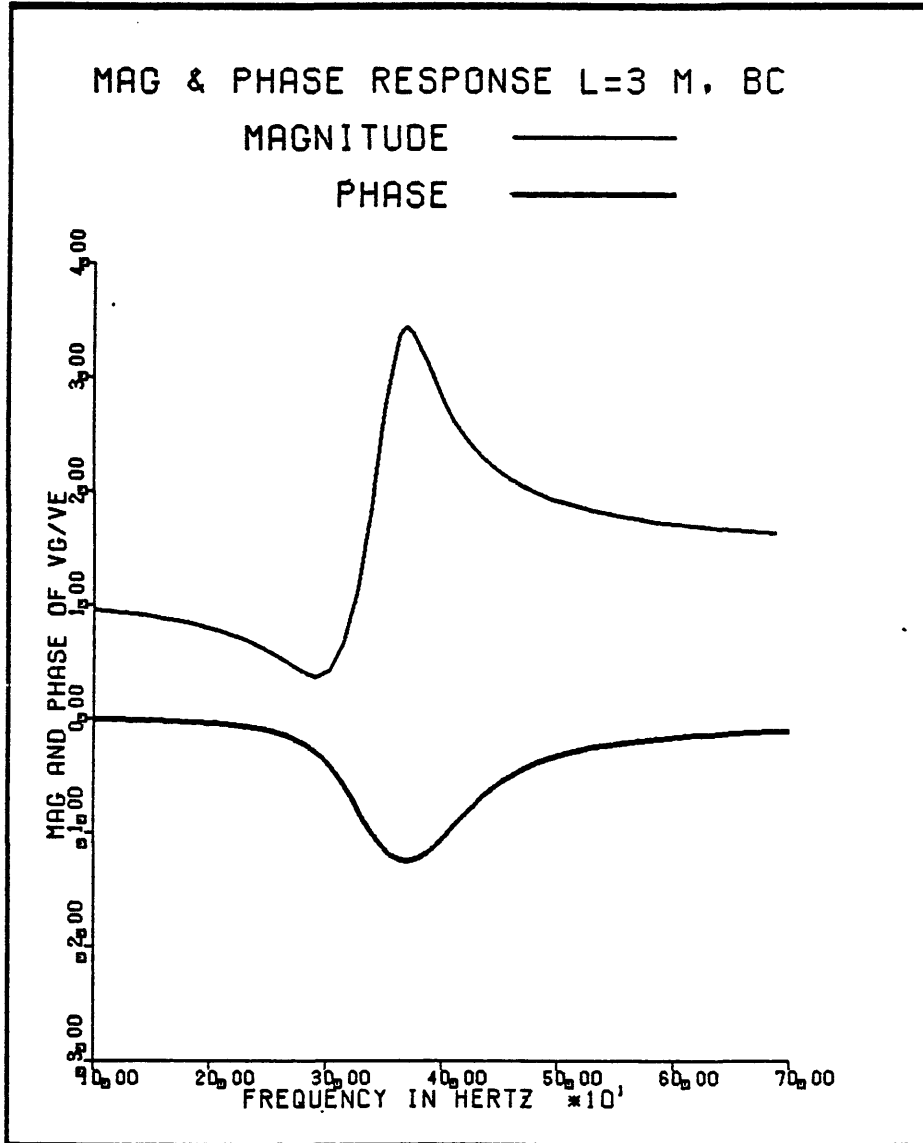


Figure 6-21

Magnitude and phase response for Model 2 with borehole coupling. 3 m, 90 kg tool in Soft Rock (mud-filled).

Figure 6-14, which shows the phase and magnitude response for an identical tool without the borehole coupling force. First, the phase does not go to $-\pi$ (180 degrees out of phase) for high frequencies, but returns to zero after passing through a minimum near the resonant frequency. Second, the magnitude of the frequency response does not drop below unity for high frequencies, but is seen to approach a constant value. Both these effects are accounted for by examining the borehole coupling force as a function of frequency. The motion of the geophone due to the borehole coupling force is always in phase with the earth motion. Since our frequency response curves are defined as the ratio of geophone motion to earth motion, this results in a constant phase of zero for the motion due to the borehole coupling force. The phase response of the geophone's motion due to it's contact with the borehole is seen in Figure 6-14. When we include the effect of borehole coupling, the motion of the geophone is then zero phase for the lower frequencies (both forces in phase with earth motion at low frequencies). However, at higher frequencies the phase response will be determined by the relative magnitudes of the two forces. As the frequency increases, the frequency-dependent borehole coupling force increases, and this term dominates. The resulting phase response is a

constant phase of zero for high frequencies. Near the resonant peak, the two forces are approximately the same magnitude, and a mixed phase response results.

The magnitude of the frequency response at high frequencies approaches a constant value. This is a result of the frequency dependence of the borehole coupling force. When the borehole coupling force was computed, the assumption was made in computing the pressure difference across the tool, that the tool was small compared to all wavelengths in the surrounding medium. As the wavelengths in the solid approach the tool's length (at high frequencies), this assumption is no longer valid, and the tool's response is no longer accurately described by equation 4-20. Therefore, the response curves involving the borehole coupling force are only valid in the low frequency range.

With this in mind, the response was computed for tools of varying masses in Figures 6-22 and 6-23, with the inclusion of the borehole coupling force. The resonant peak occurs at higher frequencies and exhibits a greater magnitude for the lighter tools. In all previous results, the magnitude of the resonant peak moved to a higher frequency for the lighter tool, but was always found to decrease. This is possibly due to the magnitude of the

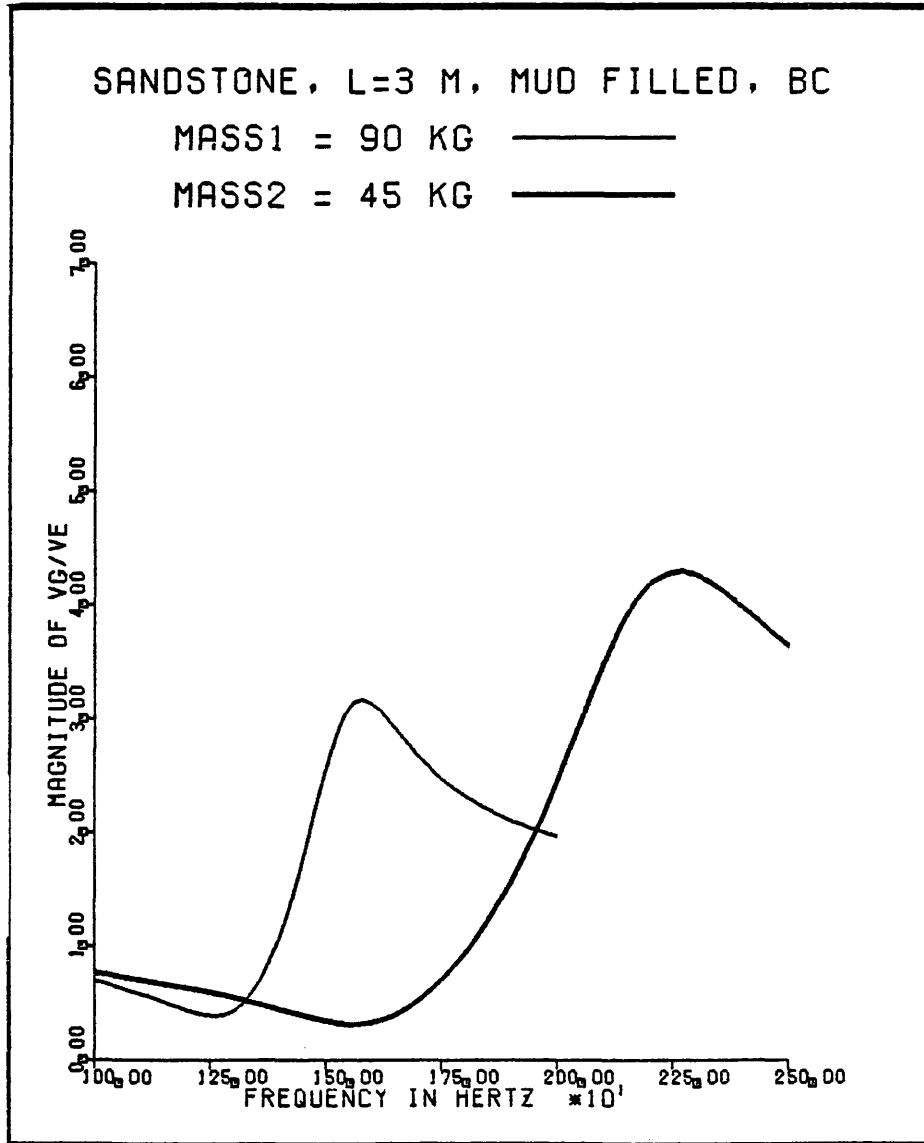


Figure 6-22

Frequency response for Model 2 with borehole coupling.
 Effect of varying the mass of a 3 m tool in SS2.

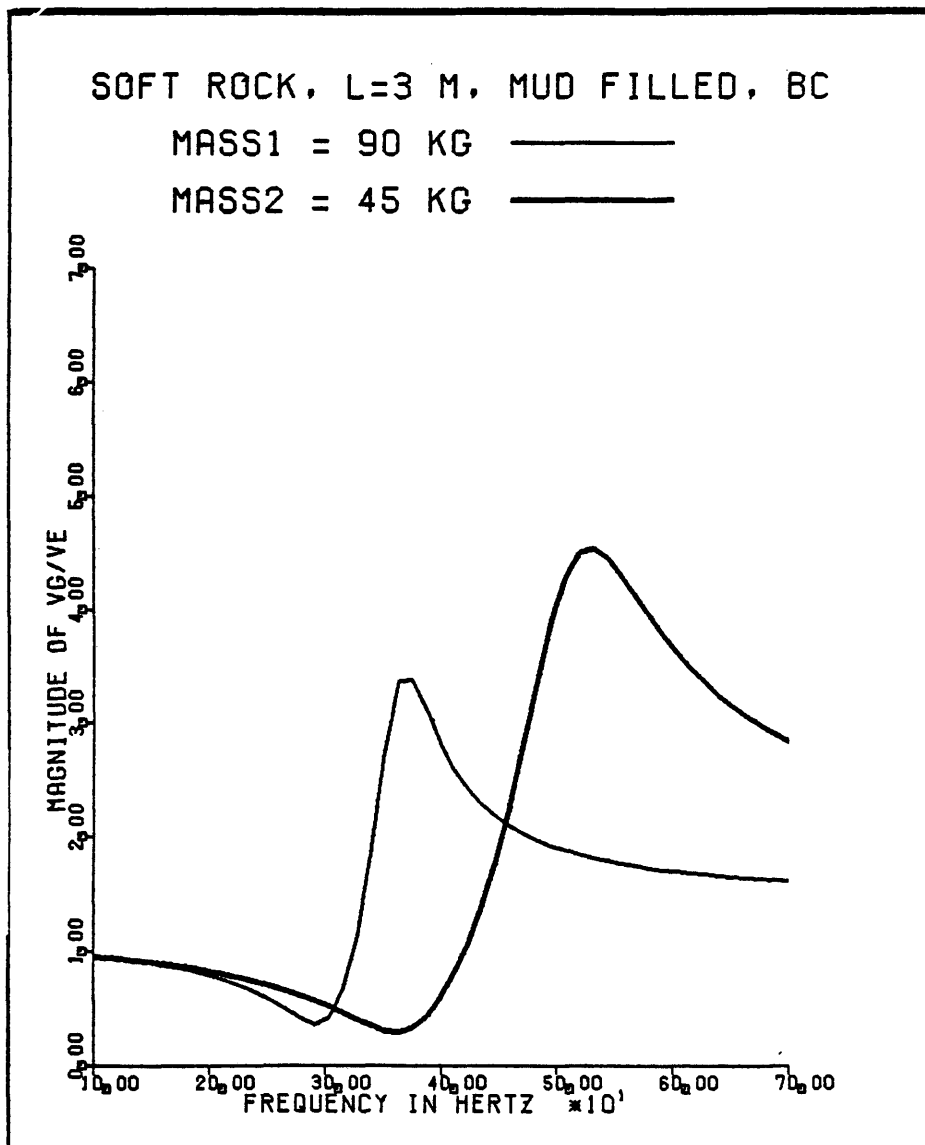


Figure 6-23

Frequency response for Model 2 with borehole coupling.
Effect of varying the mass of a 3 m tool in the Soft Rock.

borehole coupling force, as computed by equation 4-20, being larger than it actually should be. The results for tools of different lengths are plotted in Figure 6-24. The resonant peak decreases and shifts to a higher frequency for the shorter tool, the same effect as observed in figures 6-17 and 6-18.

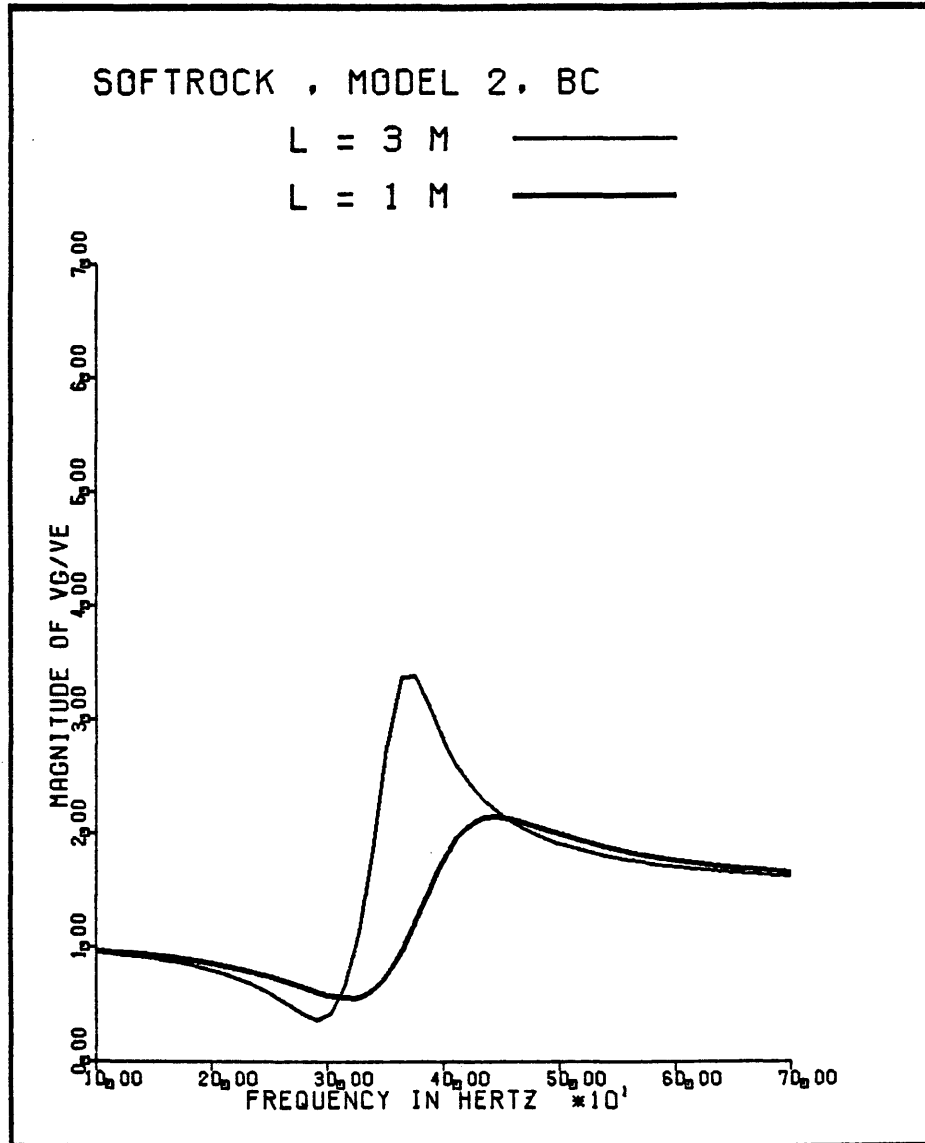


Figure 6-24

Frequency response for Model 2 with borehole coupling.
Effect of varying the length of the tool in the Soft Rock.

VII. Conclusions

1.) Rigid rocks (dense sandstones and shales) exhibit flat frequency responses for the frequencies of interest in a conventional VSP survey. The resonant peaks occur in the range 1500 - 2000 hz. Softer lithologies (such as shales) exhibit resonances in the 300 - 500 hz. range, and could therefore cause high frequency distortion to contaminate VSP data.

2.) The assumption for Model 1 that the impedance is proportional to the area of contact with the formation is reasonable, though not exact. Response curves computed for Model 1 with scaled impedances compare qualitatively with those obtained with Model 2.

3.) The magnitude of displacement is nearly constant as a function of frequency. Thus, the geophone-formation coupling can be modelled as a simple stiffness. However, the magnitude of the imaginary part of the impedance does increase slightly for higher frequencies and represents radiation of energy into the solid.

4.) Resonance peaks for Model 2 exhibit greater magnitudes than those for Model 1. Damping was extreme for Model 1, and the effect of fluid on the tool's

response is more plausible for Model 2. Model 2 is considered to give more realistic results than the simplified geometry and assumptions used for Model 1.

The following conclusions are based on data from Model 2 only.

5.) Lighter tools exhibit resonance peaks at higher frequencies and flatter response curves at lower frequencies than those for heavier tools. The magnitude of the resonant peak increases in magnitude when the borehole coupling force is not included, and decreases when it is included.

6.) Resonance peaks for shorter tools occur at slightly higher frequencies, and exhibit smaller amplitudes than those for longer tools (for tools with the same mass per unit length).

7.) The phase response for Model 2 with no borehole coupling starts at zero for low frequencies, goes through a transition region near the resonance, and is 180 degrees out of phase at high frequencies. The magnitude starts at unity, climbs to resonance amplitudes ranging from 3 to 13, and then approaches zero for high frequencies.

8.) When the borehole coupling force is included, the phase angle of the response curve goes through a minimum near resonance. At both low and high frequencies the phase angle is zero. The magnitude of V_g/V_e starts at unity, decreases to a minimum just before the resonance peak, and approaches a constant value at high frequencies. The resonance peak is of lower amplitude than the response computed without the borehole coupling force. The magnitude of V_g/V_e for a tool in the soft rock (shale) is down by approximately 50% at 250 hz, and could therefore result in a loss of high frequency content of VSP data. Response curves which include the borehole coupling effect are not valid at high frequencies, but are considered to yield the best results for low frequencies.

REFERENCES

Abramowitz, M., and Stegun, I. A., 1964, Handbook of Mathematical Functions, Washington, D.C.: U. S. Government Printing Office.

Balch, A. H., and Lee, M. W., Vertical seismic profiling: Techniques, applications, and case histories: Boston, International Human Resources Development Corporation.

Beydoun, W. B., 1984, Seismic tool-formation coupling in boreholes; Vertical seismic profiling, Part B.: London, Geophysical Press.

Bracewell, R. N., 1978, The Fourier Transform and it's applications: New York, Mcgraw Hill.

Hardage, B. A., 1983, Vertical seismic profiling, Part A: Principles: London, Geophysical Press.

Hoover, G. M., and O'Brien, J. T., 1980, The influence of the planted geophone on seismic land data: Geophysics, v. 45, pp. 1239-1253.

Krohn, C. E., 1984, Geophone ground coupling: Geophysics, v. 49, pp. 722-731.

Levin, F. K., and Lynn, R. D., 1958, Deep hole geophone studies: Geophysics, v. 23, pp. 639-664.

McDonal, F. J., Angona, F. A., Mills, R. L., Sengbush, R. L., Van Nostrand, R. G., and White, J. E., 1958, Attenuation of shear and compressional waves in Pierre Shale: Geophysics, v. 23, pp. 421-439.

O'Neill, P. V., 1983, Advanced engineering mathematics: Belmont, CA., Wadsworth Publishing Company.

Tongtaow, C., 1980, Transient response of an acoustic logging tool in transversely isotropic media: Golden, Colorado School of Mines, M. Sc. thesis T-2424.

Tongtaow, C., 1982, Wave propagation along a cylindrical bore in a transversely isotropic medium, Golden, Colorado School of Mines PhD. thesis T-2682.

Washburn, H. and Wiley, H., 1941, The effect of the placement of a seismometer on it's response

characteristics: *Geophysics*, v. 6, pp. 116-131.

White, J. E., 1984, Computed waveforms in transversely isotropic media I: Line source and vertical point force: *Colorado School of Mines Quarterly*, v. 79, no. 2, pp. 33-60.

White, J. E., 1960, Use of reciprocity theorem for computation of low frequency radiation patterns: *Geophysics*, v. 25, pp. 613-624.

White, J. E., 1962, Elastic waves along a cylindrical bore: *Geophysics*, v. 27, pp. 327-333.

White, J. E., 1984, *Underground sound - application of seismic waves*, New York, Elsevier Science.

White, J. E., and Zechman, R. E., 1968, Computed response of an acoustic logging tool: *Geophysics* v. 33, pp. 302-310.

Wolf, A., 1944, The equation of motion of a geophone on the surface of an elastic earth: *Geophysics*, v. 9, pp. 29-35.

Wuenschel, P. C., 1976, The vertical array in reflection seismology - some experimental studies: *Geophysics*, v. 41, pp. 219-232.

Appendix A

Expressions for coefficients $D_{11} - D_{33}$

Tongtaow (1982) derived solutions for wave propagation in transversely isotropic media in terms of the displacement potentials ϕ , χ , and γ given in equations 3-32 to 3-34. These expressions were reduced to those seen in section III.2 for isotropic media. The coefficients $D_{11} - D_{33}$ seen in equations 3-38 to 3-40 are given by

$$D_{11} = [(\lambda + 2\mu)M^2 - \lambda k^2]W_n(Mb) + (2\mu M/b)Y_2(Mb) \quad (A-1)$$

$$D_{12} = -2\mu n K^2 Y_3(Kb) \quad (A-2)$$

$$D_{13} = 2\mu i k K^2 W_n(Kb) + (2k K i / b) Y_2(Kb) \quad (A-3)$$

$$D_{21} = (2\mu n M/b) Y_4(Mb) \quad (A-4)$$

$$D_{22} = \mu K^2 Y_5(Kb) \quad (A-5)$$

$$D_{23} = (2\mu n K i / b) Y_4(Kb) \quad (A-6)$$

$$D_{31} = -2\mu M i k Y_1(Mb) \quad (A-7)$$

$$D_{32} = (\mu i k n / b) W_n(Kb) \quad (A-8)$$

$$D_{33} = \mu K(\ell^2 + K^2)Y_1(Kb) \quad (A-9)$$

Where

$$Y_1(X) = W_n(X) + (n/X)W_n(X) \quad (A-10)$$

$$Y_2(X) = n(n+1)W_n(X)/X + W_{n-1}(X) \quad (A-11)$$

$$Y_3(X) = (n+1)W_n(X)/X^2 + W_{n-1}(X)/X^2 \quad (A-12)$$

$$Y_4(X) = W_{n-1}(X) + (n+1)W_n(X)/X \quad (A-13)$$

$$Y_5(X) = 2W_{n-1}(X)/X + [1 + 2n(n+1)W_n(X)/X^2] \quad (A-14)$$

(from Tongtaow (1982))

and

$$W_n(X) = K_n(X) \quad \text{for } X \text{ real, or}$$

$$W_n(X) = (i\pi/2)[\cos(n\pi/2) + i\sin(n\pi/2)][-1(-1)^n][J_n(\bar{X}) - iY_n(\bar{X})] \quad (A-15)$$

(From Abramowitz (1964)).

for \bar{X} = imaginary part of X when X is pure imaginary.

and similarly for W_{n-1} , with n replaced by $n-1$.

Appendix B

Fourier cosine series for θ dependence of displacement

A constant displacement over a width of 0.6 radians is the idealized theta dependence of the displacement of the tool. This is accomplished by representing the idealized displacement as a Fourier series consisting of the terms from n equal zero to ten. O'Neil (1983) defines the Fourier series of a function on an interval $-L \leq x \leq L$ as

$$a_0/2 + \sum_{n=1}^{\infty} a_n \cos(n\pi x/L) + b_n \sin(n\pi x/L) \quad (B-1)$$

where

$$a_n = (1/L) \int_{-L}^L f(x) \cos(n\pi x/L) dx \quad (B-2)$$

$$b_n = (1/L) \int_{-L}^L f(x) \sin(n\pi x/L) dx \quad (B-3)$$

and

$$a_0 = (1/L) \int_{-L}^L f(x) dx \quad (B-4)$$

The numbers a_0 , a_n , and b_n are the Fourier Coefficients of $f(x)$ on $[-L, L]$.

We are interested in the interval from $-\pi$ to π , and $f(\theta)$ is given by

$$f(\theta) = \begin{cases} H & \text{for } -.3 < \theta < .3 \\ 0 & \text{at all other points.} \end{cases} \quad (\text{B-5})$$

The Fourier Coefficients are now computed for $f(\theta)$. Equation (B-3) is an integral of an odd function over symmetric limits, and is therefore zero for all b_n terms. For a_0 , we find

$$a_0 = (1/\pi) \int_{-.3}^{.3} H d\theta = .6H/\pi \quad (\text{B-6})$$

Solving for a_n yields

$$a_n = (1/\pi) \int_{-.3}^{.3} H \cos(n\theta) d\theta = 2H \sin(.3n)/(n\pi) \quad (\text{B-7})$$

From which the coefficients a_1 to a_{10} can be determined.

The first term in the desired Fourier series is $a_0/2$. A normalized Fourier series will be computed by dividing each term by $a_0/2$. This yields the normalized Fourier coefficients as

$$\text{nfc}(0) = 1$$

$$\text{nfc}(1) = 1.97$$

$$\text{nfc}(2) = 1.88$$

$$\text{nfc}(3) = 1.74$$

$$\text{nfc}(4) = 1.55$$

$$\text{nfc}(5) = 1.33$$

$$\text{nfc}(6) = 1.08$$

$$\text{nfc}(7) = 0.82$$

$$\text{nfc}(8) = 0.56$$

$$\text{nfc}(9) = 0.32$$

$$\text{nfc}(10) = 0.09$$

These coefficients are then used to compute the displacement correction factors, $\text{dcf}(n)$, discussed in Appendix C.

Appendix C

Computation of the displacement correction factors

The following is an example of the computation of the displacement correction factors, which will result in a θ dependence of displacement as seen in Figure 4-6. The example will be for a 3 meter tool in the Carbonate lithology.

1.) The response to the normalized, 10 to 70 hz, zero phase wavelet described by equation (4-18) is computed for n equal zero to ten, with the summation over n omitted. The peak displacement (at $t = 0$) is determined for each value of n, and is listed below.

| n | Magnitude of displacement (10^{-12} m/newton) |
|----|---|
| 0 | 7.58 |
| 1 | 2.18 |
| 2 | 1.12 |
| 3 | 0.76 |
| 4 | 0.57 |
| 5 | 0.46 |
| 6 | 0.38 |
| 7 | 0.33 |
| 8 | 0.29 |
| 9 | 0.26 |
| 10 | 0.23 |

2.) These values are then normalized to the n equal zero term; that is, they are expressed as a constant, $\epsilon(n)$, times the displacement at n equal zero, yielding

| n | $\epsilon(n)$ |
|-----|---------------|
| 0 | 1 |
| 1 | 0.288 |
| 2 | 0.148 |
| 3 | 0.100 |
| 4 | 0.075 |
| 5 | 0.061 |
| 6 | 0.050 |
| 7 | 0.044 |
| 8 | 0.038 |
| 9 | 0.034 |
| 10 | 0.030 |

3.) To obtain the desired displacement as a function of θ , the relative magnitudes of displacement for each value of n must be the same as the normalized Fourier coefficients computed in Appendix B. This yields

$$dcf(n) = nfc(n)/\epsilon(n) \quad (C-1)$$

The displacement correction factors are then computed at each value of n . For a 3 meter tool in the Carbonate

lithology, the displacement correction factors are

| n | dcf(n) |
|----|--------|
| 0 | 1 |
| 1 | 6.84 |
| 2 | 12.7 |
| 3 | 17.4 |
| 4 | 20.7 |
| 5 | 21.8 |
| 6 | 21.6 |
| 7 | 18.6 |
| 8 | 14.7 |
| 9 | 9.4 |
| 10 | 3.1 |

Multiplying the source term (P_{zr}) by these displacement correction factors will yield the displacement whose θ dependence is shown in Figure 4-7. This is accomplished by multiplying the source term in equation (4- 6) by the displacement correction factor for each value of n. P_{zr} is then given by

$$P_{zr} = -[Q/(2\pi b)]G(\lambda)F(\omega)\cos(n\theta)dcf(n) \quad (C-2)$$

With the inclusion of the displacement correction factors, the summation over n in equation (4-16) from -10

to 10, can be replaced by a summation from n equal 0 to 10.

Appendix D

Fortran code of program "FRVSP"

```

*****
C
C   This program will compute the frequency response
C
C   of a geophone clamped to a borehole. The response
C
C   of the tool to a time transient f(t) can also be
C
C   computed.
C
C   WRITTEN BY GREGORY R. JOHNSON, JANUARY, 1986.
C
C       ALL UNITS ARE IN THE M.K.S. SYSTEM
C
C*****
C
C Variable declarations and definitions
C
C Compressional wave speed in medium
C
C       REAL ALPHA
C
C Shear wave speed in medium
C
C       REAL BETA
C
C Density of medium
C
C       REAL RHO
C
C Lamé constant
C
C       REAL LAMDA
C
C Shear modulus
C
C       REAL MU
C
C Borehole radius
C
C       REAL BOR RAD

```

C pi=3.14159265

REAL PI

C Length of source (or geophone)

REAL Z0

C Coordinate at which displacement is computed

REAL Z

C Wavenumber corresponding to sourcelength Z0

REAL L0

C Axial wavenumber

REAL L

C Angular frequency

REAL W

C Center angular frequency for computations

REAL W0

C 1/2 width of angular frequency for computations

REAL WC

C Center frequency (in hertz) for computations

REAL F0

C 1/2 width of frequency (in hertz) for computations

REAL FC

C Limit on summation over wavenumber L

REAL LMAX

C Lower limit of angular frequency = W0 - WC

REAL WMIN

C Upper limit of angular frequency = $\omega_0 + \omega_c$

REAL WMAX

C Incremental step in frequency (hertz)

REAL DELTAF

C Incremental step in angular frequency

REAL DELTAW

C Incremental step in wavenumber

REAL DELTAL

C Maximum time to which the displ.'s are plotted

REAL TMAX

C M squared

DOUBLE PRECISION M2

C K squared

DOUBLE PRECISION K2

C Values of $G(L)$ for specific L and L_0

REAL GOFL

C Values of $F(W)$ for specific W, ω_0 , and ω_c

REAL FOFW

C IM. part of rad. displ. in time dom. = $I_r(b,z,t)$

REAL URTIM

C Real part of rad. displ. in time dom. = $R_r(b,z,t)$

REAL URTRE

C IM part of tan. displ. in time dom. = $I_z(b,z,t)$

REAL UZTIM

C Real part of tan. displ. in time dom. = $Rz(b,z,t)$
REAL UZTRE

C Real part of angular displ. in time domain = $Rt(b,z,t)$
REAL UTTRE

C imag part of angular displ. in time domain = $It(b,z,t)$
REAL UTTIM

C Real part of rad. displ. in freq dom = $Rr(b,z,w)$
REAL AURWRE(256)

C Real part of rad displ in freq dom = $Rr(b,z,w)$
REAL URWREA(256)

C IM part of rad displ in freq dom = $Ir(b,z,w)$
REAL AURWIM(256)

C IM part of rad displ in freq dom = $Ir(b,z,w)$
REAL URWIMA(256)

C Real part of tan displ in freq dom = $Rz(b,z,w)$
REAL AUZWRE(256)

C Real part of tan displ in freq dom = $Rz(b,z,w)$
REAL UZWREA(256)

C IM part of tan displ in freq dom = $Iz(b,z,w)$
REAL AUZWIM(256)

C IM part of tan displ in freq dom = $Iz(b,z,w)$
REAL UZWIMA(256)

C IM part of angular displ. in the freq. domain = $It(b,z,w)$
REAL AUTWIM(256)

C Real part of angular displ. in freq. domain = $Rt(b,z,w)$
REAL AUTWRE(256)

C Real part of angular displ. in freq. domain = $Rt(b,z,w)$
REAL UTWREA(256)

C IM part of angular displ. in the freq. domain = $It(b,z,w)$
REAL UTWIMA(256)

C Density of mud
REAL RM

C Density of water
REAL RW

C Speed of tube waves in water
REAL CTW

C Speed of tube waves in mud
REAL CTM

C Mass of geophone in kilograms
REAL MASS

C the imaginary number $I = (0,1)$
COMPLEX I

C Tangential displacement used to calculate frequency resp.
COMPLEX R

C VG/VE (empty hole)
COMPLEX VGVE

C VG/VE (empty hole) mass=M/2
COMPLEX VGVE2

C VG/VE (water-filled borehole)

COMPLEX VGVEW

C VG/VE (water-filled borehole) mass=M/2

COMPLEX VGVEW2

C VG/VE (mud-filled borehole)

COMPLEX VGVEM

C VG/VE (mud-filled borehole) mass=M/2

COMPLEX VGVEM2

C VG/VE (water-filled borehole) with borehole coupling

COMPLEX VGVEWB

C VG/VE (water-filled hole) mass=M/2 with borehole coupling

COMPLEX VGVEWB2

C VG/VE (mud-filled borehole) with borehole coupling

COMPLEX VGVEMB

C VG/VE (mud-filled hole) mass=M/2 with borehole coupling

COMPLEX VGVEMB2

C M (pure imaginary or real)

DOUBLE COMPLEX MC

C K (pure imaginary or real)

DOUBLE COMPLEX KC

C Coefficient A used in solving for displacements

DOUBLE COMPLEX A

C Coefficient B used in solving for displacements

DOUBLE COMPLEX B

C Coefficient C used in solving for displacements

DOUBLE COMPLEX C

C Complex radial displacement = $U_r(b, l, w)$

COMPLEX UROFL

C Complex tangential displacement = $U_z(b, l, w)$

COMPLEX UZOFL

C Complex angular displacement = $U_t(b, l, w)$

COMPLEX UTOFL

C Bessel functions $W_0(Kb)$ to $W_{10}(Kb)$

DOUBLE COMPLEX WKB(12)

C Bessel functions $W_0(Mb)$ to $W_{10}(Mb)$

DOUBLE COMPLEX WMB(12)

C $MC \cdot BOR \text{ RAD} = MB$

DOUBLE COMPLEX MB

C $KC \cdot BOR \text{ RAD} = KB$

DOUBLE COMPLEX KB

C complex radial displacement in frequency domain

COMPLEX URSUMW(256,12)

C complex tangential displacement in frequency domain

COMPLEX UZSUMW(256,12)

C complex angular displacement in frequency domain

COMPLEX UTSUMW(256,12)

C complex angular displacement in the frequency domain

COMPLEX UTOFW

C complex radial displacement in the frequency domain

COMPLEX UROFW

C complex tangential displacement in the frequency domain

COMPLEX UZOFW

C Amplitude of the borehole coupling force

REAL AMPBC

C Lower limit for frequency (in hertz)

REAL FMIN

C Upper limit for frequency (in hertz)

REAL FMAX

C Source term Pzr

REAL SOURCE

C Angle at which the freq. response is computed (radians)

REAL THETA

C Frequency in hertz

REAL F

C Used to determine DELTAL = LO/XX

REAL XX

C Incremental step in time for transient response of tool

REAL DELTAT

C Time (in seconds)

REAL T

C Area that the tool occupies

REAL AREA

C Displacement correction factors

REAL DCF(12)

C Order of Bessel functions and theta dependence

INTEGER N

C Maximum summation over the variable N

INTEGER NMAX

C Integer used for Bessel function arrays

INTEGER NPLUS1

C Integer used for Bessel function arrays

INTEGER NPLUS2

C Number of terms used for FFT (must be power of 2)

INTEGER SS

C Counter for arrays as a function of frequency

INTEGER K

C Counter used for the inverse FFT to the time domain

INTEGER E

C Variable used to initiate a transform to time domain

INTEGER TD

C NMAX, ZO, and Z are input by the user.

WRITE(6,*) 'input nmax'

READ(5,*) NMAX

WRITE(6,*) 'NMAX=',NMAX

WRITE(6,*) 'INPUT ZO'

READ(5,*)ZO

```
WRITE(6,*)'ZO=',ZO
WRITE(6,*)'INPUT Z'
READ(5,*)Z
WRITE(6,*)'Z=',Z
```

C A 1 is entered if the response to a time transient
C is desired. If the frequency response is desired
C any other integer is entered.

```
WRITE(6,*) 'If the response is desired in the time'
WRITE(6,*) 'domain, enter a 1. If the frequency'
WRITE(6,*) 'response is desired, enter any other #'
READ(5,*) TD
```

C The displacement correction factors are read from 'corfact'

```
OPEN (UNIT=57,FILE='CORFACT')
REWIND 57
DO 38 J=1,NMAX+1
    READ(57,*) DCF(J)
```

38 CONTINUE

C Initialization of parameters

```
PI=3.14159265
FO=40.00
FC=30.00
DELTAW=4*PI
DELTAF=2.0
I=(0.0,1.0)
```

```
LO=2*PI/ZO
LMAX=5*LO
RHO=2600
ALPHA=4000
BETA=2300
BOR RAD=0.1
XX=27.395217
DELTAL=LO/XX
K=0
MASS=90
THETA=0.0
AREA= .0113
```

C Subroutine PARAM is called which displays current

C parameter values and allows the user to change them.

```
* CALL PARAM(FO,FC,BOR RAD,RHO,ALPHA,BETA
,DELTAL,DELTA F,THETA,MASS,AREA)
```

```
WO=2*PI*FO
WC=2*PI*FC
WMIN=WO-WC
WMAX=WO+WC
FMIN=FO-FC
FMAX=FO+FC
DELTAW=2*PI*DELTA F
MU=(BETA**2)*RHO
LAMDA=(ALPHA**2)*RHO-2*MU
```

C The formatted output file is opened

```
OPEN ( UNIT=10, FILE='output')
REWIND 10
```

C The title page for the data printout is now printed

```
CALL TITLE(ZO,Z,ALPHA,BETA,RHO,DELTAL,DELTA
* ,FO,FC,BOR RAD,LAMDA,MU,XX,THETA)
```

C CALCULATE $U_r(b,z,w)$ and $U_z(b,z,w)$

```
DO 555 N=0,NMAX
    NPLUS1=N+1
    NPLUS2=N+2
```

C The titles for the data output tables are printed out.

```
    * WRITE(10,106)'These values are for the n=',N,'
      case'
106   FORMAT('1',36X,A,I2,A)
    * WRITE(10,110)'FREQUENCY', 'Ur(b,z,w)', 'Uz(b,z,w)'
      , 'Ut(b,z,w)'
110   FORMAT(A,14X,A10,31X,A,30X,A)
    * WRITE(10,120)' (in hertz)', 'REAL', 'IMAG', 'REAL',
      'IMAG', 'REAL', 'IMAG'
120   FORMAT(A,8X,A,13X,A,17X,A,13X,A,17X,A,13X,A)
      WRITE(10, 30)
30    FORMAT('0')
      W=WMIN
      DO 10 F=FMIN,FMAX,DELTA
          K=K+1
          J=0
          UROFW=0
```

```

      UZOFW=0
      UTOFW=0
C   Calculate f(w)
      IF ( TD .EQ. 1 ) THEN
          CALL COFOFW(W,WO,WC,FOFW)
      ELSE
          FOFW = 1.0
      ENDIF
C   Calculate  $U_r(b,1,w)$  and  $U_z(b,1,w)$ . then sum on L to get
C    $U_r(b,z,w)$  and  $U_z(b,z,w)$ .
      DO 20 L=0,LMAX,DELTAL
C   Compute MC and KC and determine if they are real or imag..
          CALL MKTEST(L,W,ALPHA,BETA,M2,MC,K2,KC,DELTAL)
C   Calculate G(L)
          CALL COGOFL(L,LO,GOFL,ZO)
C   Compute bessel functions WMB(N) and WMB(N-1)
          MB=MC*BOR RAD
          CALL WMBN(MB,PI,I,N,WMB)
C   Compute Bessel functions WKB(N) and WKB(N-1)
          KB=KC*BOR RAD
          CALL WKBN(KB,PI,I,N,WKB)
C   Compute coef's A, B and C used to calculate  $U_r(b,1,w)$ ,
C    $U_t(b,1,w)$  &  $U_z(b,1,w)$ 
          CALL ABC(LAMDA,MU,BOR RAD,L,W,MC,M2,MB,KC,K2,

```

```

*          KB,FOFW,GOFL,WMB,WKB,A,B,C,I,PI,N,THETA,
*          SOURCE,F,DCF)

C  Compute Ur(b,l,w) , Ut(b,l,w) and Uz(b,l,w)

          CALL CURZTL(L,MC,M2,MB,KC,K2,KB,WMB,WKB,UROFL
*          ,UZOFL,UTOFL,I,N,NPLUS1,NPLUS2,THETA,BORRAD,
*          A,B,C)

C  Sum on L to give Ur(b,z,w), Uz(b,z,w) and Ut(b,z,w)

          CALL SUM(PI,DELTA,UROFL,UZOFL,UTOFL,I,Z,L,
*          UROFW,UZOFW,UTOFW)

20      CONTINUE

C  Summation over the variable N is performed

          CALL SUMN(N,UROFW,UZOFW,UTOFW,URSUMW,UZSUMW,
*          UTSUMW,K)

          AURWRE(K)=REAL(URSUMW(K,NPLUS2))
          AURWIM(K)=AIMAG(URSUMW(K,NPLUS2))
          AUZWRE(K)=REAL(UZSUMW(K,NPLUS2))
          AUZWIM(K)=AIMAG(UZSUMW(K,NPLUS2))
          AUTWRE(K)=REAL(UTSUMW(K,NPLUS2))
          AUTWIM(K)=AIMAG(UTSUMW(K,NPLUS2))

C  The displacements are stored in free formatted data files

          WRITE(20,*) F,AURWRE(K)
          WRITE(25,*) F,AURWIM(K)
          WRITE(30,*) F,AUZWRE(K)
          WRITE(35,*) F,AUZWIM(K)
          WRITE(40,*) F,AUTWRE(K)
          WRITE(45,*) F,AUTWIM(K)

C  The displacements are printed into the output data file

```

```

      WRITE(10,100) F,AURWRE(K),AURWIM(K),AUZWRE(K),
*      AUZWIM(K),AUTWRE(K),AUTWIM(K)
100      FORMAT(F8.1,5X,E14.7,4X,E14.7,7X,E14.7,4X,
*      E14.7,7X,E14.7,4X,E14.7)

C The frequency response is now computed

      R=UZSUMW(K,NPLUS2)

      IF ( N .EQ. NMAX ) THEN

          RW=1000

          BW=2.25E+09

          RM=1500

          BM=4.0E+09

          CTW=1/(SQRT(RW*(1/BW+1/MU)))

          CTM=1/(SQRT(RM*(1/BM+1/MU)))

          AMPBC=-(RM*CTM*CTM/MU)*(1-2*(BETA/ALPHA)**2*
*          (1/(1-(CTM/ALPHA)**2)))

C Frequency response for tool in an empty borehole

          VGVE=1/(1-W*W*MASS*R)

C Frequency response in an empty borehole for tool of
C mass M/2

          VGVE2=1/(1-W*W*(MASS/2)*R)

C Frequency response for tool of mass M/2 in a water
C filled borehole

          VGVEW2=1/(1-W*W*(MASS/2)*R+2*I*RW*CTW*AREA*W*R)

C Frequency response for tool in water filled borehole

          VGVEW=1/(1-W*W*MASS*R + 2*I*RW*CTW*AREA*W*R)

```

C Frequency response for tool in mud-filled borehole

$$VGVEM=1/(1-W*W*MASS*R + 2*I*RM*CTM*AREA*W*R)$$

C Frequency response for tool of mass M/2

C in a mud-filled borehole

$$VGVEM2=1/(1-W*W*(MASS/2)*R+2*I*RM*CTM*AREA*W*R)$$

C Frequency response for tool in a water-filled borehole

C with the borehole coupling force included

$$* \quad VGVEWB=(1 + I*W*RHO*AREA*ZO*R) / (1-W*W*MASS*R + 2*I*RW*CTW*AREA*W*R)$$

C Frequency response for tool in a mud-filled borehole

C with the borehole coupling force included

$$* \quad VGVEMB=(1 + I*W*RHO*AREA*ZO*R) / (1-W*W*MASS*R + 2*I*RM*CTM*AREA*W*R)$$

C Frequency response for tool of mass M/2 in a mud-filled

C borehole with the borehole coupling force included

$$* \quad VGVEMB2=(1 + I*W*RHO*AREA*ZO*R) / (1-W*W*(MASS/2)*R + 2*I*RM*CTM*AREA*W*R)$$

C Frequency response for tool of mass M/2 in a water-filled

C borehole with the borehole coupling force included

$$* \quad VGVEWB2=(1 + I*W*RHO*AREA*ZO*R) / (1-W*W*(MASS/2)*R + 2*I*RW*CTW*AREA*W*R)$$

C The magnitude and phase of the frequency response data

C is stored in free formatted data files

WRITE(70,*) F,CABS(VGVE)

WRITE(71,*) F,CABS(VGVE2)

WRITE(72,*) F,ATAN(AIMAG(VGVE)/REAL(VGVE))

```
        WRITE(80,*) F,CABS(VGVEW)
        WRITE(81,*) F,CABS(VGVEW2)
        WRITE(82,*) F,ATAN(AIMAG(VGVEW)/REAL(VGVEW))
        WRITE(83,*) F,CABS(VGVEWB)
        WRITE(84,*) F,CABS(VGVEWB2)
        WRITE(85,*) F,ATAN(AIMAG(VGVEWB)/REAL(VGVEWB))
        WRITE(90,*) F,CABS(VGVEM)
        WRITE(91,*) F,CABS(VGVEM2)
        WRITE(92,*) F,ATAN(AIMAG(VGVEM)/REAL(VGVEM))
        WRITE(93,*) F,CABS(VGVEMB)
        WRITE(94,*) F,CABS(VGVEMB2)
        WRITE(95,*) F,ATAN(AIMAG(VGVEMB)/REAL(VGVEMW))
    ENDIF
    W=W+DELTAW

10      CONTINUE
        K=0
        IF ( TD .EQ. 1 ) THEN
C      The arrays are now rearranged for suitable inverse FFT.
C      the complex conjugate of the input arrays
C      will then be inputted to the FFT. This will give an
C      output array whose complex conjugate is the inverse FFT.
        NS=31
        DO 40 IN=1,256
            E=IN-5
```

```
URWREA(IN)=0
URWIMA(IN)=0
UZWREA(IN)=0
UZWIMA(IN)=0
UTWREA(IN)=0
UTWIMA(IN)=0
IF ( IN .GT. 5 ) THEN
    URWREA(IN)=AURWRE(E)
    URWIMA(IN)=-AURWIM(E)
    UZWIMA(IN)=-AUZWIM(E)
    UZWREA(IN)=AUZWRE(E)
    UTWREA(IN)=AUTWRE(E)
    UTWIMA(IN)=-AUTWIM(E)
ENDIF
IF ( IN .GT. 36 ) THEN
    URWREA(IN)=0
    URWIMA(IN)=0
    UZWREA(IN)=0
    UZWIMA(IN)=0
    UTWREA(IN)=0
    UTWIMA(IN)=0
ENDIF
IF ( IN .GT. 221 ) THEN
    URWREA(IN)=AURWRE(NS)
```

```
URWIMA(IN)=AURWIM(NS)
UZWREA(IN)=AUZWRE(NS)
UZWIMA(IN)=AUZWIM(NS)
UTWREA(IN)=AUTWRE(NS)
UTWIMA(IN)=AUTWIM(NS)
NS=NS-1
```

```
ENDIF
```

```
IF ( NS .LT. 1 ) THEN
```

```
URWREA(IN)=0
```

```
URWIMA(IN)=0
```

```
UZWREA(IN)=0
```

```
UZWIMA(IN)=0
```

```
UTWREA(IN)=0
```

```
UTWIMA(IN)=0
```

```
ENDIF
```

```
40      CONTINUE
```

```
C now the inverse FFT is calculated
```

```
SS=256
```

```
NU=8
```

```
DELTAT=1/(SS*DELTAF)
```

```
CALL FFT(URWREA,URWIMA,SS,NU)
```

```
CALL FFT(UZWREA,UZWIMA,SS,NU)
```

```
CALL FFT(UTWREA,UTWIMA,SS,NU)
```

```
N2=SS/2
```

```
N21=N2+1
```

```
TMAX=1/(2*DELTA F)
```

```
T=-TMAX
```

```
WRITE(6,*) ' after fft is completed '
```

C The titles for the formatted output are now printed

```
* WRITE(10,140)'TIME', 'Ur(b,z,t)', 'Uz(b,z,t)',
  'Ut(b,z,t)'
```

```
140 FORMAT('1', 3X, A, 21X, A, 30X, A, 30X, A)
```

```
* WRITE(10,150)'(SECONDS)', 'REAL', 'IMAG', 'REAL',
  'IMAG', 'REAL', 'IMAG'
```

```
150 FORMAT(1X, A, 12X, A, 14X, A, 18X, A, 13X, A, 18X, A, 13X, A)
  WRITE(10,30)
```

C Displacements in the time domain are rearranged for

C graphing and for the output file.

```
DO 50 IN=1,SS
```

```
IF ( IN .LT. N21 ) THEN
```

```
INT=IN+N2
```

```
ELSE
```

```
INT=IN-N2
```

```
ENDIF
```

```
IF ( IN .EQ. N21 ) THEN
```

```
T=0.0
```

```
ENDIF
```

```
URTRE=URWREA(INT)*DELTA F
```

```
URTIM=-URWIMA(INT)*DELTA F
```

```
UZTRE=UZWREA(INT)*DELTA F
```

```
UZTIM=-UZWIMA(INT)*DELTA F
```

```
UTTRE=UTWREA(INT)*DELTA F
```

```
UTTIM=-UTWIMA(INT)*DELTA F
```

C Displacements are printed into a formatted data output

```
WRITE(10,160)T,URTRE,URTIM,UZTRE,UZTIM,UTTRE,UTTIM
```

```
160      FORMAT(' ',E11.3,5X,E14.7,4X,E14.7,7X,E14.7,
*        4X,E14.7,7X,E14.7,4X,E14.7)
```

C Displacements in the time domain are stored in data files

```
WRITE(50,*) T,URTRE
```

```
WRITE(55,*) T,URTIM
```

```
WRITE(60,*) T,UZTRE
```

```
WRITE(65,*) T,UZTIM
```

```
WRITE(67,*) T,UTTRE
```

```
WRITE(68,*) T,UTTIM
```

```
T=T+DELTAT
```

```
50      CONTINUE
```

```
ENDIF
```

```
555     CONTINUE
```

```
STOP
```

```
END
```

C The subroutines

C This subroutine computes MC and KC and determines if they

C are real or pure imaginary.

```
SUBROUTINE MKTEST(L,W,ALPHA,BETA,M2,MC,K2,KC,DELTAL)
REAL L,W,ALPHA,BETA,DELTAL
DOUBLE PRECISION M2,K2,M,K,AM2,LWA,AK2,LWB
DOUBLE COMPLEX MC,KC
COMPLEX I
```

```
I=(0,1)
M2=L*L-(W*W/(ALPHA*ALPHA))
M=SQRT(ABS(M2))
AM2=ABS(M2)
LWA=DELTA*(W/(100*ALPHA))

IF ( AM2 .LT. LWA ) THEN

M2=(L+DELTA/5)**2-(W*W)/(ALPHA*ALPHA)

ENDIF

M=SQRT(ABS(M2))

IF (M2 .LT. 0) THEN

    MC=I*M

ELSE

    MC=M

ENDIF

K2=L**2-W**2/BETA**2

AK2=ABS(K2)
LWB=DELTA*W/(100*BETA)

IF ( AK2 .LT. LWB ) THEN

    K2=(L+DELTA/5)*(L+DELTA/5)-(W*W)/(BETA*BETA)

ENDIF

K=SQRT(ABS(K2))

IF (K2 .LT. 0) THEN

    KC=I*K

ELSE

    KC=K

ENDIF

RETURN
END
```

C This subroutine computes $G(1)$, the
 C spatial source distribution

```

SUBROUTINE COGOF(L,LO,GOFL,ZO)
REAL L,LO,PI,GOFL,ZO
DOUBLE PRECISION MMBSJO,ARG
PI=3.14159265

IF ( L .EQ. 0 ) THEN

    GOFL=1.0

ELSE

    ARG=(ZO/2)*L
    GOFL=MMBSJO(ARG,IER)

ENDIF

RETURN

END
  
```

C This subroutine computes $F(w)$, which corresponds to a
 C time transient $f(t)$.

```

SUBROUTINE COFOFW(W,WO,WC,FOFW)
REAL PI,SIPI,W,WO,WC,FOFW
PI=3.14159265
SIPI=1.8516

IF (ABS(ABS((W-WO)/WC)-1.0) .LT. 0.0001) THEN

    FOFW=0.0

ELSE

    FOFW=PI**2*SIN(PI*(W-WO)/WC)/(2*WC*SIPI*PI*(W-WO)
*   /WC)

ENDIF

RETURN

END
  
```

C This subroutine computes the Bessel functions $Wk_b(12)$

```

SUBROUTINE WKBN(KB,PI,I,N,WKB)
DOUBLE PRECISION ARG, YN(12),JN(12),KN(12),B(12),
* YNB(12),BK(12)
INTEGER N,NPLUS1,NPLUS2
REAL ORDER,PI
COMPLEX I,COMPACO(12)
DOUBLE COMPLEX KB,WKB(12),KBS
ORDER=0.0
NPLUS1=N+1
NPLUS2=N+2
COMPACO(1)=(0,1)
COMPACO(2)=(1,0)
COMPACO(3)=(0,1)
COMPACO(4)=(-1,0)
COMPACO(5)=(0,-1)
COMPACO(6)=(1,0)
COMPACO(7)=(0,1)
COMPACO(8)=(-1,0)
COMPACO(9)=(0,-1)
COMPACO(10)=(1,0)
COMPACO(11)=(0,1)
COMPACO(12)=(-1,0)

```

```

IF ( REAL(KB) .EQ. 0.0 ) THEN

```

```

    KBS=-I*KB
    ARG=REAL(KBS)

```

C The Bessel functions Jn and Yn are computed using the

C IMSL library subroutines

```

CALL MMBSJN(ARG,NPLUS2,B,IER)
CALL MMBSYN(ARG,ORDER,NPLUS2,YNB,IER)

```

```

JN(NPLUS2)=B(NPLUS1)
YN(NPLUS2)=YNB(NPLUS1)

```

```

IF ( N .EQ. 0 ) THEN

```

```

    JN(NPLUS1)=B(NPLUS2)
    YN(NPLUS1)=YNB(NPLUS2)

```

```

ELSE

```

```

    JN(NPLUS1)=B(N)
    YN(NPLUS1)=YNB(N)

```

```

      ENDIF

      WKB(NPLUS2)=(PI/2)*I*COMPCO(NPLUS2)*(-(-1)**N)*
*      (JN(NPLUS2)-I*YN(NPLUS2))

      WKB(NPLUS1)=(PI/2)*I*COMPCO(NPLUS1)*(-(-1)**(N-1))
*      *(JN(NPLUS1)-I*YN(NPLUS1))

```

```

ELSE

```

```

  ARG=REAL(KB)

```

```

C The Bessel function Kn is computed using the
C IMSL library subroutines

```

```

  CALL MMBSKR(ARG,ORDER,NPLUS2,BK,IER)

```

```

  KN(NPLUS2)=BK(NPLUS1)*EXP(ARG)

```

```

  IF ( N .EQ. 0 ) THEN

```

```

    KN(NPLUS1)=BK(2)*EXP(ARG)

```

```

  ELSE

```

```

    KN(NPLUS1)=BK(N)*EXP(ARG)

```

```

  ENDIF

```

```

    WKB(NPLUS2)=KN(NPLUS2)

```

```

    WKB(NPLUS1)=KN(NPLUS1)

```

```

  ENDIF

```

```

  RETURN

```

```

  END

```

```

C This subroutine computes the Bessel functions WMB(12)

```

```

SUBROUTINE WMBN(MB,PI,I,N,WMB)
DOUBLE PRECISION ARG, YN(12),JN(12),KN(12),B(12),
* YNB(12),BK(12)
REAL ORDER,PI
COMPLEX COMPCO(12),I
INTEGER N,NPLUS1,NPLUS2
DOUBLE COMPLEX MB,WMB(12),MBS
ORDER=0.0

```

```

NPLUS1=N+1
NPLUS2=N+2
COMPCO(1)=(0,1)
COMPCO(2)=(1,0)
COMPCO(3)=(0,1)
COMPCO(4)=(-1,0)
COMPCO(5)=(0,-1)
COMPCO(6)=(1,0)
COMPCO(7)=(0,1)
COMPCO(8)=(-1,0)
COMPCO(9)=(0,-1)
COMPCO(10)=(1,0)
COMPCO(11)=(0,1)
COMPCO(12)=(-1,0)

```

```

IF ( REAL(MB) .EQ. 0.0 ) THEN

```

```

    MBS=-I*MB
    ARG=REAL(MBS)

```

C The Bessel functions J_n and Y_n are computed

C using the IMSL library subroutines

```

    CALL MMBSJN(ARG,NPLUS2,B,IER)
    CALL MMBSYN(ARG,ORDER,NPLUS2,YNB,IER)

```

```

    JN(NPLUS2)=B(NPLUS1)
    YN(NPLUS2)=YNB(NPLUS1)

```

```

IF ( N .EQ. 0 ) THEN

```

```

    JN(NPLUS1)=B(2)
    YN(NPLUS1)=YNB(2)

```

```

ELSE

```

```

    JN(NPLUS1)=B(N)
    YN(NPLUS1)=YNB(N)

```

```

ENDIF

```

```

WMB(NPLUS2)=(PI/2)*I*COMPCO(NPLUS2)*(-(-1)**N)*
* (JN(NPLUS2)-I*YN(NPLUS2))
WMB(NPLUS1)=(PI/2)*I*COMPCO(NPLUS1)*(-(-1)**(N-1))
* (JN(NPLUS1)- I*YN(NPLUS1))

```

```

ELSE

```

```

      ARG=REAL(MB)
C The Bessel function Kn is computed using the
C IMSL library subroutine

      CALL MMBSKR(ARG,ORDER,NPLUS2,BK,IER)

      KN(NPLUS2)=BK(NPLUS1)*EXP(ARG)

      IF ( N .EQ. 0 ) THEN

          KN(NPLUS1)=BK(2)*EXP(ARG)

      ELSE

          KN(NPLUS1)=BK(N)*EXP(ARG)

      ENDIF

      WMB(NPLUS2)=KN(NPLUS2)
      WMB(NPLUS1)=KN(NPLUS1)

      ENDIF

      RETURN

      END

C This subroutine performs all fft's for this program.
C From Bracewell ( 1978 ).

```

```

      SUBROUTINE FFT(XREAL,XIMAG,N,NU)
      DIMENSION XREAL(N),XIMAG(N)
      N2=N/2
      NU1=NU-1
      K=0
      DO 100 L=1,NU
102      DO 101 I=1,N2
          P=IBITR(K/2**NU1,NU)
          ARG=6.283185*P/FLOAT(N)
          C=COS(ARG)
          S=SIN(ARG)
          K1=K+1
          K1N2=K1+N2
          TREAL=XREAL(K1N2)*C+XIMAG(K1N2)*S
          TIMAG=XIMAG(K1N2)*C-XREAL(K1N2)*S
          XREAL(K1N2)=XREAL(K1)-TREAL
          XIMAG(K1N2)=XIMAG(K1)-TIMAG
      
```

```

XREAL(K1)=XREAL(K1)+TREAL
XIMAG(K1)=XIMAG(K1)+TIMAG
101 K=K+1
    K=K+N2
    IF ( K .LT. N ) GOTO 102
    K=0
100 N1=NU1-1
    N2=N2/2
    DO 103 K=1,N
    I=IBITR(K-1,NU)+1
    IF ( I .LT. K ) GOTO 103
    TREAL=XREAL(K)
    TIMAG=XIMAG(K)
    XREAL(K)=XREAL(I)
    XIMAG(K)=XIMAG(I)
    XREAL(I)=TREAL
    XIMAG(I)=TIMAG
103 CONTINUE
    RETURN
    END

```

```

FUNCTION IBITR(J,NU)
J1=J
IBITR=0
DO 200 I=1,NU
J2=J1/2
IBITR=IBITR*2+(J1-2*J2)
200 J1=J2
    RETURN
    END

```

C This subroutine prints out the title page for the data
C printout

```

SUBROUTINE TITLE(ZO,Z,ALPHA,BETA,RHO,DELTAL,DELTA F
* ,FO,FC,BOR RAD,LAMDA,MU,XX,THETA)
REAL ZO,Z,ALPHA,BETA,RHO,DELTAL,DELTA F,FO,FC,
* BOR RAD,LAMDA,MU,XX
WRITE(10,200)'THE DATA IN THIS PRINTOUT ARE FOR AN
* ISOTROPIC'
200 FORMAT('1',5X,A)
WRITE(10,205)'MATERIAL WITH THE FOLLOWING
* PARAMETERS:'
205 FORMAT('0',5X,A)
WRITE(10,210)'ZO=',ZO,'m.s'
WRITE(10,210)'Theta=',THETA,'radians'
210 FORMAT('0',10X,A,F5.2,1X,A)

```

```

WRITE(10,215)'Z=',Z,'m.s'
215  FORMAT('0',10X,A,F5.2,1X,A)
WRITE(10,220)'ALPHA=',ALPHA,'m/sec'
220  FORMAT('0',10X,A,E9.2,1X,A)
WRITE(10,220)'BETA=',BETA,'m/sec'
WRITE(10,230)'RHO=',RHO,'kg/m2'
WRITE(10,235)'DELTAL=',DELTAL,'1/m.s'
235  FORMAT('0',10X,A,E14.7,1X,A)
WRITE(10,230)'DELTA F=',DELTA F,'hertz'
WRITE(10,230)'FO=',FO,'hertz'
WRITE(10,230)'FC=',FC,'hertz'
WRITE(10,230)'BOR RAD=',BOR RAD,'m.s'
230  FORMAT('0',10X,A,F7.2,1X,A)
WRITE(10,260)'LAMDA=',LAMDA,'Newtons/m2'
WRITE(10,260)'MU=',MU,'Newtons/m2'
260  FORMAT('0',10X,A,E12.5,1X,A)
WRITE(10,201)'THE STRESS IS HIGHER AT THE GEOPHONE
*  ENDS'
201  FORMAT('0',A)
RETURN
END

```

```

SUBROUTINE PARAM(FO,FC,BORRAD,RHO,ALPHA,BETA
*  ,DELTAL,DELTA F,THETA,MASS,AREA)
REAL FO,FC,BOR RAD,RHO,ALPHA,BETA,DELTAL,MASS,AREA
500  WRITE(6,300)'1.) fo=',FO,'hertz','2.) fc=',FC,
*  'hertz','3.) bor rad=',BOR RAD,'m'
WRITE(6,310)'4.) rho=',RHO,'kg/m2','5.)
*  alpha=',ALPHA,'m/sec'
WRITE(6,320)'6.) beta=',BETA,'m/sec','7.)
*  deltal=',DELTAL,'1/m'
WRITE(6,325)'8.) DELTA F=',DELTA F,'HERTZ','9.)
*  theta=',THETA,'rd'
WRITE(6,320)'10.) MASS=',MASS,'KG','11.)
*  AREA=',AREA,'m^2'
WRITE(6,330)'do you wish to change any of the
*  parameters?'
WRITE(6,330)'if so, enter the integer
*  ( 1 thru 11 ) in'
WRITE(6,330)'front of the parameter you
*  wish to change'
WRITE(6,330)'if you do not wish to change
*  anything, enter a 0'

READ(5,*)IP

IF ( IP .EQ. 0 ) THEN

```

```
        GOTO 600

ENDIF

IF ( IP .EQ. 1 ) THEN

    WRITE(6,*)'input the new value for fo (in hertz)'
    READ(5,*)FO
    GOTO 500

ENDIF

IF ( IP .EQ. 2 ) THEN

    WRITE(6,*)'input the new value for fc
*   ( in hertz )'
    READ(5,*)FC
    GOTO 500

ENDIF

IF ( IP .EQ. 3 ) THEN

    WRITE(6,*)'input the new value for bor rad
*   ( in m )'
    READ(5,*)BOR RAD
    GOTO 500

ENDIF

IF ( IP .EQ. 4 ) THEN

    WRITE(6,*)'input the new value for rho
*   ( in kg/m2 )'
    READ(5,*)RHO
    GOTO 500

ENDIF

IF ( IP .EQ. 5 ) THEN

    WRITE(6,*)'input the new value for alpha
*   ( in m/sec )'
    READ(5,*)ALPHA
    GOTO 500

ENDIF
```

```
IF ( IP .EQ. 6 ) THEN

    WRITE(6,*)'input the new value for beta
    ( in m/sec )'
    *   READ(5,*)BETA
        GOTO 500

ENDIF

IF ( IP .EQ. 7 ) THEN

    WRITE(6,*)'input the new value for delta1'
    READ(5,*)DELTAL
    GOTO 500

ENDIF

IF ( IP .EQ. 8 ) THEN

    WRITE(6,*)'INPUT THE NEW VALUE FOR DELTAF'
    READ(5,*)DELTAF
    GOTO 500

ENDIF

IF ( IP .EQ. 9 ) THEN

    WRITE(6,*)'INPUT THE NEW VALUE FOR theta'
    READ(5,*)THETA
    GOTO 500

ENDIF

IF ( IP .EQ. 10 ) THEN

    WRITE(6,*)'INPUT THE NEW VALUE FOR MASS'
    READ(5,*)MASS
    GOTO 500

ENDIF

IF ( IP .EQ. 11 ) THEN

    WRITE(6,*)'INPUT THE NEW VALUE FOR AREA'
    READ(5,*)AREA
    GOTO 500

ELSE
```

```

      WRITE(6,*)'invalid entry. enter only
*      INTEGER values 1 thru 11'
      GOTO 500

```

```

      ENDIF

```

```

300  FORMAT('0',A,F6.1,1X,A,3X,A,F6.1,1X,A,3X,A,F4.1
*      ,1X,A)
310  FORMAT('0',A,E10.3,1X,A,6X,A,E10.3,1X,A)
320  FORMAT('0',A,E10.3,1X,A,6X,A,E10.3,1X,A)
325  FORMAT('0',A,F5.1,1X,A,6X,A,F4.1,1X,A)
330  FORMAT('0',A)

600  RETURN

```

```

      END

```

C This subroutine computes the coefficients A, B, and C

```

      SUBROUTINE ABC(LAMDA,MU,BORRAD,L,W,MC,M2,MB,KC,K2,KB
*      ,FOFW,GOFL,WMB,WKB,A,B,C,I,PI,N,THETA,SOURCE,F,DCF)
      REAL LAMDA,MU,BORRAD,L,W,FOFW,GOFL,PI,THETA,SOURCE,
*      DCF(12)
      INTEGER N,NPLUS1,NPLUS2
      DOUBLE PRECISION M2,K2,SCALE
      DOUBLE
      COMPLEX MC,MB,KC,KB,WMB(12),WKB(12),A,B,C,DETERM
      COMPLEX I
      DOUBLE COMPLEX PRRAT,PRRBT,PRRCT,PRZAT,PRZBT,PRZCT,
*      PRTAT,PRTBT,PRTCT
      SCALE=1.0D-9

      IF ( N . GT. 4 ) THEN

          SCALE=1.0D-12

      ENDIF

      IF ( N .GT. 7 ) THEN

          SCALE=1.0D-23

      ENDIF

      IF ( N .GT. 7 ) THEN

          SCALE=1.0D-23

```

ENDIF

NPLUS2=N+2
NPLUS1=N+1

```

PRRAT=((((LAMDA+2*MU)*M2)-LAMDA*L**2)*WMB(NPLUS2)+
* (2*MU*MC/BORRAD)*(N*(N+1)/(MB))*WMB(NPLUS2)
* +WMB(NPLUS1))*SCALE

PRRBT=(2*MU*I*L*K2*WKB(NPLUS2)+(2*MU*KC*I*L/BORRAD)*
* ((N*(N+1))/KB)*WKB(NPLUS2)+WKB(NPLUS1))*SCALE

PRRCT=(-2*MU*N*K2*((N+1)/(KB**2))*WKB(NPLUS2)+(1/KB)
* *WKB(NPLUS1))*SCALE

PRTAT=((2*MU*N*MC/BORRAD)*(WMB(NPLUS1)+((N+1)/MB)
* *WMB(NPLUS2))*SCALE

PRTBT=((2*MU*N*KC*I*L/BORRAD)*(WKB(NPLUS1)+
* ((N+1)/KB)*WKB(NPLUS2))*SCALE

PRTCT=(-MU*K2*((2/KB)*WKB(NPLUS1)+(1+2*N*(N+1)/
* (KB**2))*WKB(NPLUS2))*SCALE

PRZAT=(-MU*MC*2*I*L*(WMB(NPLUS1)+(N/MB)
* *WMB(NPLUS2))*SCALE

PRZBT=(MU*KC*(L**2+K2)*(WKB(NPLUS1)+
* (W/KB)*WKB(NPLUS2))*SCALE

PRZCT=(I*L*N*MU/BORRAD)*WKB(NPLUS2)*SCALE

DETERM = PRRAT*PRTBT*PRZCT + PRRBT*PRTCT*PRZAT
DETERM = DETERM + PRRCT*PRTAT*PRZBT
DETERM = DETERM - PRRAT*PRZBT*PRTCT
DETERM = DETERM - PRTAT*PRRBT*PRZCT
DETERM = DETERM - PRZAT*PRTBT*PRRCT

SOURCE=SCALE*DCF(NPLUS1)*(-FOFW*GOFL)/(2*PI*BOR RAD)

A=SOURCE*((PRRBT*PRTCT)-(PRTBT*PRRCT))/DETERM

B=SOURCE*(PRTAT*PRRCT-PRRAT*PRTCT)/DETERM

C=SOURCE*(PRRAT*PRTBT-PRTAT*PRRBT)/DETERM

RETURN

```

END

C This subroutine computes the displacements in the

C frequency and axial wavenumber domains

```

SUBROUTINE CURZTL(L,MC,M2,MB,KC,K2,KB,WMB,WKB,UROFL
* ,UZOFL,UTOFL,I,N,NPLUS1,NPLUS2,THETA,BORRAD,A,B,C)
DOUBLE PRECISION M2,K2
REAL L,THETA, BORRAD
INTEGER N,NPLUS1,NPLUS2
COMPLEX I,UROFL,UTOFL,UZOFL
DOUBLE COMPLEX MC,MB,KC,KB,WMB(12),WKB(12),A,B,C

UROFL=(-MC*(WMB(NPLUS1)+(N/MB)*WMB(NPLUS2))*A+
* (N/BORRAD)*WKB(NPLUS2)*C-I*L*KC*(WKB(NPLUS1)
* +(N/KB)*WKB(NPLUS2))*B)*COS(N*THETA)

UTOFL=((-N/BORRAD)*WMB(NPLUS2)*A
* +KC*(WKB(NPLUS1)+(N/KB)*WKB(NPLUS2))*C
* -(I*L*N/BORRAD)*WKB(NPLUS2)*B)*SIN(N*THETA)

UZOFL=(I*L*WMB(NPLUS2)*A-K2*WKB(NPLUS2)*B)*
* COS(N*THETA)

RETURN

END

```

C This subroutine sums over axial wavenumber L

C to give the displacements in the frequency

C and spatial domains

```

SUBROUTINE SUM(PI,DELTAL,UROFL,UZOFL,UTOFL,I,Z
* ,L,UROFW,UZOFW,UTOFW)
COMPLEX UROFL,UZOFL,UTOFL,I,UROFW,UZOFW,UTOFW
REAL PI,L,Z,DELTAL
DOUBLE COMPLEX URSUM,UTSUM,UZSUM

IF ( L .EQ. 0 ) THEN
    URSUM=(0,0)
    UZSUM=UZOFL*(DELTAL/(2*PI))
    UTSUM=UTOFL*(DELTAL/(2*PI))

ELSE

```

```

    URSUM=(DELTAL/PI)*UROFL*(I*SIN(L*Z))
    UZSUM=(DELTAL/PI)*UZOFL*(COS(L*Z))
    UTSUM=(DELTAL/PI)*UTOFL*(I*SIN(L*Z))

```

```

ENDIF

```

```

    UROFW=UROFW+URSUM
    UZOFW=UZOFW+UZSUM
    UTOFW=UTOFW+UTSUM

```

```

RETURN

```

```

END

```

C This subroutine sums over the variable N

```

SUBROUTINE SUMN(N,UROFW,UZOFW,UTOFW,URSUMW,
* UZSUMW,UTSUMW,GG)
COMPLEX UROFW,UZOFW,UTOFW,URSUMW(256,12),
* UZSUMW(256,12),UTSUMW(256,12)
INTEGER GG,N,NPLUS1,NPLUS2
NPLUS1=N+1
NPLUS2=N+2

```

```

IF ( N .EQ. 0 ) THEN

```

```

    URSUMW(GG,NPLUS2)=UROFW
    UZSUMW(GG,NPLUS2)=UZOFW
    UTSUMW(GG,NPLUS2)=UTOFW

```

```

ELSE

```

```

    URSUMW(GG,NPLUS2)=UROFW+URSUMW(GG,NPLUS1)
    UZSUMW(GG,NPLUS2)=UZOFW+UZSUMW(GG,NPLUS1)
    UTSUMW(GG,NPLUS2)=UTOFW+UTSUMW(GG,NPLUS1)

```

```

ENDIF

```

```

RETURN

```

```

END

```